NASA TECHNICAL NOTE

NASA TN D-7416

NASA TN D-7416

MEASUREMENTS AND A MODEL FOR CONVECTIVE VELOCITIES IN THE TURBULENT BOUNDARY LAYER

by William C. Cliff and Virgil A. Sandborn

George C. Marshall Space Flight Center
Marshall Space Flight Center, Ala. 35812

NATIONAL AERONAUTICS AND SPACE ADMINISTRATION • WASHINGTON, D. C. • OCTOBER 1973

TECHNICAL REPORT STANDARD TITLE PAGE

1. REPORT NO.	2. GOVERNMENT ACCESSION NO.	3. RECIPIENT'S CATALOG NO.
NASA TN D-7416		

4. TITLE AND SUBTITLE	5. REPORT DATE
Measurements and a Model for Convective Velocities in the Turbulent Boundary Layer	October 1973
	6. PERFORMING ORGANIZATION CODE
7. AUTHOR(S)	8. PERFORMING ORGANIZATION REPORT #
William C. Cliff and Virgil A. Sandborn*	
9. PERFORMING ORGANIZATION NAME AND ADDRESS	10. WORK UNIT NO.
George C. Marshall Space Flight Center Marshall Space Flight Center, Alabama 35812	11. CONTRACT OR GRANT NO.
	13. TYPE OF REPORT & PERIOD COVERED
12. SPONSORING AGENCY NAME AND ADDRESS	Technical Note
National Aeronautics and Space Administration Washington, D.C. 20546	14. SPONSORING AGENCY CODE

15. SUPPLEMENTARY NOTES

Prepared by Aero-Astrodynamics Laboratory, Science and Engineering
*Professor of Fluid Mechanics, Colorado State University

16. ABSTRACT

A physical model is presented which describes convective velocities within a flat plate turbulent boundary layer. A production zone concept similar to that which Kline has reported with his visualization techniques is used as a basis for the physical model. The production zone concept employs the idea that packets of turbulent fluid are generated near the viscous sublayer. These packets are found to be discernible from the mean motion and may move either outward from the production zone or inward depending on their circulation relative to the fluid surrounding the packet. The packets are predicted to travel with a convective velocity different from the local mean velocity throughout most of the boundary layer. The model also predicts that the convective velocities will be functions of wave number outside the production zone.

The model predicts that the convective velocity profile approaches the mean velocity profile after a finite length or time period. After the finite length, the convective velocities are predicted to become independent of wave number. The model predicts that the asymptotic growth of the boundary layer will be a linear function of distance. Experimental results are presented which agree with the predictions of the model.

Correlation concepts are used to measure the convective velocity. Convective velocity as a function of frequency indicates Taylor's hypothesis to be invalid for the turbulent boundary layer.

17. KEY WORDS	18. DISTRIBUTION STATEMENT

19. SECURITY CLASSIF. (of this report)	20. SECURITY CLASSIF. (of this page)	21. NO. OF PAGES	22. PRICE
Unclassified	Unclassified	143	Domestic, $4.50 Foreign, $7.00

For sale by National Technical Information Service, Springfield, Virginia 22151

ACKNOWLEDGMENTS

The authors wish to express their appreciation to Dr. H. J. Koloseus, Dr. R. N. Meroney, Dr. B. R. Bean, and Dr. H. G. Krause for their advice and review.

Special thanks is given to the George C. Marshall Space Flight Center of the National Aeronautics and Space Administration for support and preparation of this document. The authors wish to express their gratitude to the Aero-Astrodynamics laboratory of the Marshall Space Flight Center under whom the work was accomplished.

TABLE OF CONTENTS

LIST OF ILLUSTRATIONS

LIST OF ILLUSTRATIONS (Concluded)

LIST OF TABLES

LIST OF SYMBOLS

Symbol	Definition	Dimension
A_n	Fourier coefficient of nth harmonic cosine function	
A_x	Acceleration of fluid structure in the X-direction	L/T^2
A_y	Acceleration of fluid structure in the Y-direction	L/T^2
A_n	Denotes a new value for A_n for a functional time shift	
a	Constant	
B_n	Fourier coefficient for nth harmonic sine function	
b	Constant	
C_1	Shape constant	
C_d	Coefficient of drag	
C_n	Fourier coefficient of nth harmonic	
C_v	Constant	
$C_{v\xi}$	Convective velocity using a variable ξ	L/T
$C_{v\tau}$	Convective velocity using a variable τ	L/T
$C_{ff}(\tau)$	Auto-covariance of f(t)	
$c_{fg}(\tau)$	Cross-covariance of f(t) and g(t)	
$C_{fg}(\tau)$	Normalized cross-covariance of f(t) and g(t)	
E	Emf	volts
e_{ij}	Direction cosines	
F_x	Force in X-direction	F
f	Frequency	Hz (cycles/second)
f(t)	Function of t	

LIST OF SYMBOLS (Continued)

Symbol	Definition	Dimension
$f(x,t)$	Function of two variables, x and t	
Hz	Hertz	cycles/second
$h(t)$	Function of t	
K_f	Wave number of frequency f	radians/L
$k_{f(t)}$	Kurtosis of f(t)	
n	Integer value	
$R_{ff}(\tau)$	Auto-correlation of f(t)	
$R_{fg}(\tau)$	Cross-correlation of f(t) and g(t)	
$S_{f(t)}$	Skewness of f(t)	
t	Time	T
T	Total time of record	T
u', v', w'	Velocity fluctuations in the X, Y, and Z directions, respectively	L/T
u_τ	Shear velocity	L/T
V_b	Instantaneous velocity of fluid structure in the X-direction	L/T
V_c	Identical with $C_{v\tau}$	L/T
V_f	Convective velocity as a function of frequency	L/T
V_i	Initial velocity in the X-direction	L/T
V_m	Mean velocity in the X-direction	L/T
V_x	Velocity of packet in the X-direction	L/T
V_y	Velocity of packet in the Y-direction	L/T
V_{yi}	Initial velocity in the Y-direction	L/T
X,Y,Z	Orthogonal cartesian coordinates	L

LIST OF SYMBOLS (Concluded)

Symbol	Definition	Dimension
α	Constant	
$\propto$	Proportional	
β	Constant	
δ	Boundary layer thickness	L
δ^*	Displacement thickness	L
$\Delta\tau$	Incremental step in time delay	T
ΔW	Sensor separation	L
θ	Momentum thickness	L
$\theta_{x,n}$	Phase of the nth harmonic of the function x	
$\lambda_1, \lambda_2, \lambda_3$	Characteristic lengths of fluid structure in the X, Y, and Z directions, respectively	L
μ	Dimensional damping factor	FT/L^2
ρ	Density	FT^2/L^4
$\sigma_{f(t)}$	rms of f(t)	
τ	Time delay	T
τ_m	Upper time delay	T
ξ	Separation distance	L
ϕ	Velocity function	
ω	Angular velocity	radians/second
$( )'$	Denotes differentiation with respect to time	1/T
$\overline{( )}$	Time average of ( )	

MEASUREMENTS AND A MODEL FOR CONVECTIVE VELOCITIES IN THE TURBULENT BOUNDARY LAYER

I. INTRODUCTION

The extraction of an exact solution from the equations of motion for the turbulent boundary layer has proven to be difficult because of the lack of an adequate physical model for the turbulence and because of mathematical complexities. A basic step forward would be an understanding of the fundamental physical structure of the flow. The examination of organized fluid structures within the boundary layer would give valuable insight into the understanding of the physical flow structures. The velocities of such organized structures will be designated as convective velocities.

Klebanoff [1], Kline et al., [2], and Grant [3] give some insight into the turbulent structure. G. I. Taylor [4] with what is now called "Taylor's Hypothesis" gave perhaps the first physical model for the motion of eddies embedded within a flow. Taylor stated, "If the velocity of the air stream which carries the eddies is very much greater than the turbulent velocity, one may assume that the sequence of changes in u' at the fixed point are simply due to the passage of an unchanging pattern of turbulent motion over the point, i.e., one may assume that $u' = \phi(t) = \phi(X/V_m)$ where X is measured upstream at time $t = 0$ from the fixed point where u' is measured." Taylor requires that the turbulent structure of the flow is convected or transported at the same rate as the mean flow, when the above conditions are met. One statistical method by which to evaluate the rate at which turbulent structures are convected within a flow is the space-time correlation of signals originating at spatially separated sensors. The space-time correlation comparing the signature identification of turbulent structures sensed at one location with signatures sensed at a downstream location yields a most probable transit time for structures to be convected between the sensors. The rate at which turbulent structures are convected can be evaluated by dividing the probe separation by the most probable transit time evaluated from the space-time correlation. In this work the term convective velocity is defined as being the rate at which the turbulent structures are convected.

The convective motion of the embedded eddies has been studied in grid-generated turbulence. The most recent study is that of Comte-Bellot and Corrsin [5], 1971, where the grid flow was found to be consistent with the constraints of Taylor's hypothesis. The experimental results were also consistent with the hypothesis.

Fluid motions with high turbulence intensities, or those where velocity gradients allow the mixing of fluids of different velocities, cannot be considered to fall within the constraints of Taylor's hypothesis. Thus, convective motions in shear flows, such as jet flow and the turbulent boundary layer, become somewhat more complex. Wills [6-9], Favre, Gaviglio, and Dumas [10-15] have shown that convective velocities in the turbulent boundary layer may be much different from the pointwise mean velocities.

This report presents a physical model which describes the convective velocity processes for the flat plate turbulent boundary layer. Analytical inferences and restrictions are derived from the physical model. Finally, experimental evidence is presented to justify the model.

The model predicts convective velocities greater than the mean flow near the wall of a turbulent boundary layer, below the formation zone. Convective velocities less than the mean flow are predicted for the outer portion of the layer, above the formation zone. In special instances the convective velocity may be greater than the mean velocity throughout the layer.

II. BACKGROUND

Osborn Reynolds [16] gives the best history of fluid mechanics before 1900. Reynolds notes the original accomplishments of Navier in 1822 with updating by Venant in 1846 and Stokes in 1845, with Stokes making mention of the term "eddies." Osborn Reynolds introduced what is now termed the Reynolds Number in 1883, and expanded on it in 1895 [16]. This work laid the foundation for the understanding of the general effect of eddies in fluid motions. In 1915, G. I. Taylor examined eddy motion in the atmosphere and made the first documented statement about the convective transport ability of the eddy, when he said, "It seems natural to suppose that eddies will transfer not only the heat and water vapour, but also the momentum of the layer in which they originated to the layer with which they mix" [17].

In 1917 Taylor performed experiments to map the shape of eddies in the atmosphere [18]. Taylor found that the eddy shape is dependent upon the elevation above the ground. He expanded further on the eddy in 1918 [19], and in 1921, he introduced the idea of a random migration (walk), and with it the ability of the turbulent fluid to diffuse fluid properties [20]. In 1923 he introduced the concept of the eddy cascade [21]; that is, that the large eddies lose their energy by forming smaller eddies, and at last the smallest eddies are dissipated by viscosity. In 1931, he examined the motion of eddies near an instability [22]. Taylor's microscale and macroscale were defined in 1935 to give insight into eddy size as well as a statistical approach to the problem of turbulence [23-27]. He published the relationship between correlation measurements and spectra in 1938 [4]. This study laid the foundation for future work using correlation measurements to describe particular motions of selected portions of the spectrum. It is here that Taylor gave insight into the motions of eddy structures as compared with mean fluid motions. Taylor states, "If the velocity of the air stream which carries the eddies is very much greater than the turbulent velocity, one may assume that the sequence of changes in u' at the fixed point are simply due to the passage of an unchanging pattern of turbulent motion over the point, i.e., one may assume that

$$u' = \phi(t) = \phi(X/V_m) \quad , \quad (7)$$

where x is measured upstream at time $t = 0$ from the fixed point where u is measured. In the limit when $u'/V_m \to 0$ (7) is certainly true. Assuming that (7) is still true when u'/V_m is small but not zero, R_x is defined as

$$R_x = \frac{\overline{\phi(t)\,\phi(t + X/V_m)}}{\bar{u}'^2} \text{ ."}$$

This quote was later to become known as Taylor's hypothesis. Taylor referenced work by Dryden [28] where correlations were measured with band filtered circuits. Dryden's test was performed in grid-generated turbulence and was held within the constraints of Taylor's hypothesis. Since Dryden's experimental results which supported Taylor's hypothesis were published, many others have examined convection in grid-generated turbulence [29-32]. A comprehensive study is reported by Comte-Bellot and Corrsin [5], and their experiments are shown to support Taylor's hypothesis.

Since it does not fall within the constraints of Taylor's hypothesis, the turbulent boundary layer does not have a simple space-time relationship with which to speculate on the turbulent structure. Visualization and analytical techniques have been used in an attempt to understand the boundary layer's physical structure. Numerous papers which delve into the structure of turbulence have been written. The most important studies with regard to the background and development of this paper are given in References 1, 2, 3, and 33 through 47.

Insight into the flow structure has been obtained by studying the structure of the turbulent pressure field on the floor of a boundary layer [48-52]. Corcos [48], Bradshaw [49], Blake [50], Willmarth and Roos [51], and Willmarth and Wooldridge [52] note that the convective velocity of the pressure fluctuations is a function of wave number. Willmarth and Wooldridge [52] note, "The lower convection speeds are measured when the spatial separation of the pressure transducers is small, or when only the pressure fluctuations at high frequencies are correlated." This observation also agrees with Corcos [48]. Willmarth also notes that the pressure fluctuations are produced by eddies convecting at the same rate, intimating that the convection velocities of eddies near the wall are a monotonically decreasing function of frequency.

The use of correlations for resolving the structure of the turbulent boundary layer has not been limited to pressure measurements [10, 11]. The use of such techniques to establish convective properties of the flow is of prime interest for this report. Favre et al. [10-15], Wills [6-9], and others [53-58] have approached the problem of convection with the use of space-time correlation concepts. The constraints, limitations, and use of these techniques are presented in Section IV to give physical and analytical insight into a simple model to predict gross characteristics of the convection processes in the turbulent boundary layer. These concepts are also used for constructing an experimental test procedure to check the model's predictions.

Kline et al. [2], presented extensive visual studies of the turbulent boundary layer near the wall, where the major portion of the turbulent production occurs. It was observed that well organized spatially and temporally dependent motions in the viscous sublayer formed low speed streaks in the region near the wall. These streaks begin a gradual "lift-up" process, which finally oscillates and ejects fluid into the outer portion of the boundary layer. Kline used a hydrogen bubble technique which showed details of the trajectory away

from the wall. He attributes the streak breakup to the dominant transfer of momentum between the inner and outer region. These concepts appear consistent with the findings of Sandborn [38], who observed that the high frequency components are intermittent throughout the layer.

Laufer and Narayanan [59] gave reasons to believe that these inner streaks and their final breakdown may be correlated with the undulating outer edge of the flow. Kibens and Kovasznay [34] also noted that the streaky structure near the wall was closely associated with the undulating outer edge of the boundary layer. Grant [3] mentions that stress relieving motions very near the wall would cause an outward migration originating near the wall. When Kline and Lahey [54] later used short time averaging to better examine the migrations, the spectra of the migrations seemed to peak away from zero. One is now tempted to speculate about whether the migration results from fluid being driven upward from an instantaneous localized separation.

III. THE PHYSICAL MODEL

Based on the observations of Kline et al. [2], Laufer and Narayanan [59], and others, we may hypothesize a physical model for the turbulent boundary layer. A portion of the model relies on the concept that a relationship exists between the external potential flow and turbulent production near the wall of a turbulent boundary layer. This concept comes from Laufer and Narayanan [59] who showed that processes occurring near the viscous sublayer scaled with outer flow parameters of a boundary layer.

The scaling may be a result of strong localized pressure gradients created in the valleys of the convoluting (intermittent) outer edge of the boundary layer [34, 54]. These strong localized pressure gradients in the outer portion may create either small jets or pressure pulses which travel through the boundary layer and result in an instability near the surface. Directly above the viscous subregion near the wall is the layer where the effect is observed. The subsequent instability becomes the streaks noticed by Kline which form packets of vorticity. The packet of vorticity, with its circulation, is then acted upon by the surrounding velocity field. The direction of circulation coupled with the surrounding fluid velocity then creates a pressure gradient across the packet, causing the packet to be driven either upward or downward toward the wall. If the surrounding fluid's velocity coupled with the circulation velocity on the top is greater than it is on the bottom, the packet will be forced upward. Conversely, if the surrounding fluid's velocity coupled with the circulation velocity on the bottom of the packet is greater than the top velocity, the packet will move downward toward the wall.

A model allowing turbulence to enter the viscous subregion tends to be in agreement with Klebanoff [1], who notes that the dissipation is greater than the production in a very thin region next to the wall. (The above model allows the packets of vorticity to enter the viscous sublayer where they may be quickly dissipated.) After the packets of vorticity have been formed, they may be identified by the structure of their oscillations. The velocity of the packets is termed "convective velocity" because the mean flow becomes the forcing or driving function on the packets and convects the packets in a downstream direction.

Corcos [48], Bradshaw [49], Blake [50], Willmarth and Roos [51], Willmarth and Wooldridge [52] and Wills [6-9] all observe that the convection processes near the wall are faster than the mean motion. Experimentation by Kline et al. [2, 33, 54] shows mainly the motion away from the sublayer. Favre et al. [10-15] found that the convective motion in the outer portions of the layer is slower than the mean motion.

The input of energy from the highly intermittent outer edge of the boundary layer will be a rapid process. The packet of vorticity is formed and moves approximately with the mean velocity of the layer in which it is formed. The packet of vorticity moves both upward into the main body of the boundary layer and downward into the viscous subregion. The region directly above the viscous subregion is where Kline [2] and Kovasznay [42] both observe the apparent formation of the vorticity.

The present experimental study will show that the convective velocity is equal to the mean (ensemble average) velocity in the region where the packets are formed. Below the formation region (viscous sublayer), the convective velocity is greater than the mean velocity; and above the formation region, the convective velocity is less than or equal to the mean velocity. (The relative positions of the various regions are shown in Figure 1.)

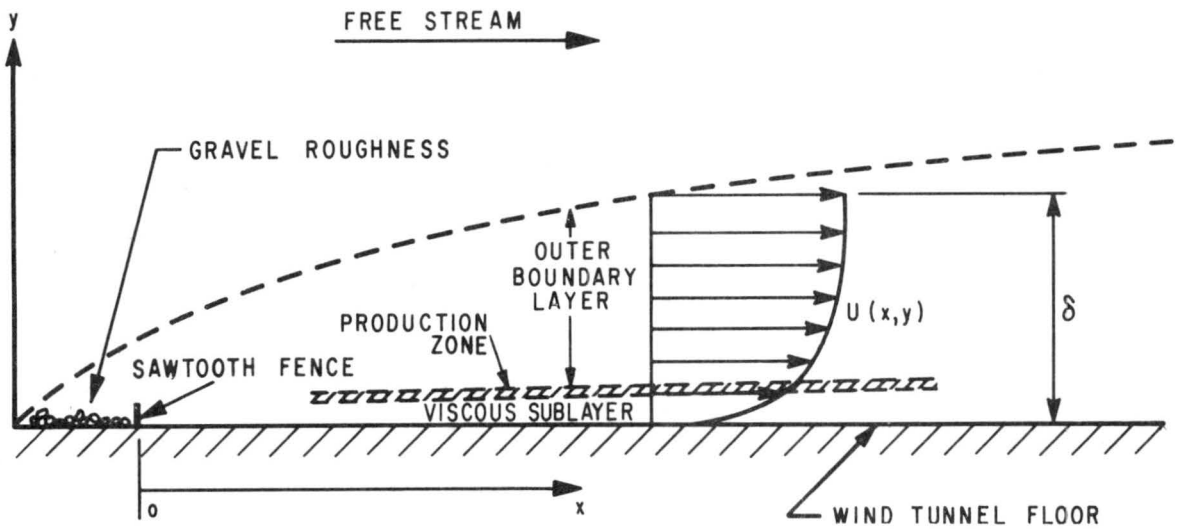

Figure 1. Sketch of the boundary layer.

The packet of vorticity, now an integral part of the boundary layer, is traceable because of the packet's organized wave pattern. The high degree of orderliness of the structure makes it identifiable for distances of two orders of magnitude greater than its length scales [60]. This characteristic suggests that once the packets are formed they tend to be entities within themselves. The present mathematical analysis of the proposed model will show that the intermittent outer edge of the boundary layer is controlled by the packets, which are shown to control the asymptotic growth of the boundary layer. Insight into the question of when a flow is fully established is also gained through the present mathematical study.

The derivations for the equations of motion of the packets of vorticity will be presented later, and will be inspected to obtain inferences regarding the motion of the packet.

A. Vertical Direction of Motion

The following assumptions are made so that an analytical derivation can be performed:

1. Once the packet leaves the layer in which it was formed only its translational motion need be considered.

2. Since the analysis starts only after migration from the production zone, it may be assumed that the packet has an instantaneous velocity at time $t = 0$.

3. Once the packet has moved away from the production zone the only accelerational influence on the packet in the vertical direction will be opposite to its velocity, such as a pressure drag or viscous drag.

Consider a packet of vorticity that is three dimensional. Three characteristic lengths or scales, λ_1, λ_2 and λ_3, are used to describe the packet. The mass of the packet is represented by $C_1\lambda_1\lambda_2\lambda_3\rho$. ($C_1 = \pi/4$, if the packet were considered a cylinder.) Subscripts 1, 2, and 3 denote directions parallel to the mean flow, vertical to the mean flow away from the wall, and parallel to the wall and perpendicular to the mean flow, respectively.

When the previous assumptions for the physics of the packet's vertical motion are used, the only force acting on the packet will be in a direction opposite its velocity. The effect of drag is introduced by using a viscous damping term, μ, with the dimensions FT/L^2. If the flow were completely viscous, μ would be some constant times the dynamic viscosity. In dimensionally forming Newton's second law, a characteristic length is necessary. The characteristic length perpendicular to the direction of motion was selected for the following analysis. However, the conclusions derived from the following analysis do not depend upon which characteristic length is selected. This is because the analysis considers all packets to have similar geometrical configurations; thus each characteristic length is directly proportional to the other characteristic lengths. The reason we use λ_1 for the characteristic length is because Cliff [60] used this characteristic length to formulate an empirical formula describing radial motion of turbulent packets in an axisymmetrical jet. The motion was successfully used to predict the intermittency factor as a function of radial direction in the axisymmetrical jet. Noting that the acceleration is in a direction opposite to that of the velocity, we see that Newton's second law becomes

$$C_1\rho\lambda_1\lambda_2\lambda_3 \frac{d^2y(t)}{dt^2} + \mu\lambda_1 \frac{dy(t)}{dt} = 0 \qquad (1)$$

or

$$\frac{d^2 y(t)}{dt^2} + \frac{\mu}{C_1 \rho \lambda_2 \lambda_3} \frac{dy(t)}{dt} = 0 \quad . \tag{2}$$

The physical restrictions placed on the model require that at time, t , equal to zero, an initial velocity exists, V_i, and the original location may be some vertical distance above the flat plate; i.e., $y(0) = Y_i$. A reasonable assumption for the region of formation might be $y^* = 50$ [61], where $y^* = yu_\tau/\eta$. Here, u_τ = shear velocity = $\sqrt{\tau_{wall}/\rho}$ and η = kinematic viscosity. The initial conditions may be expressed as follows:

$$dy(t)/dt = V_{yi}$$

and (3)

$$y(0) = Y_i \,,$$

at $t = 0$.

Integrating equation (1) and using $y(0) = Y_i$ yields

$$\frac{dy(t)}{dt} = -\frac{\mu}{C_1 \rho \lambda_2 \lambda_3} y(t) + V_{yi} + \frac{50\mu^2}{C_1 \lambda_2 \lambda_3} \sqrt{\tau_w \rho} \quad . \tag{4}$$

Using the translated coordinate system with $y = 0$ at $y^* = 50$, equation (4) becomes

$$\frac{dy(t)}{dt} = -\frac{\mu}{C_1 \rho \lambda_2 \lambda_3} y(t) + V_{yi} \quad . \tag{5}$$

Equation (5) is now the equation for the velocity of the packet of vorticity in the vertical direction, the left-hand side of the equation being the vertical velocity of the packet. The first term on the right is the dissipative term which retards the motion of the packet.

A direct solution of equation (2) with $y(0) = 0$, $dy(0)/dt = V_{yi}$, at $t = 0$ gives

$$y(t) = -V_{yi}\frac{C_1\rho\lambda_2\lambda_3}{\mu} e^{-\int\frac{\mu}{C_1\rho\lambda_2\lambda_3}dt} + V_{yi}\frac{C_1\rho\lambda_2\lambda_3}{\mu} \tag{6}$$

or

$$y(t) = V_{yi}\frac{C_1\rho\lambda_2\lambda_3}{\mu}\left(1 - e^{-\int\frac{\mu}{C_1\rho\lambda_2\lambda_3}dt}\right) \tag{7}$$

Because

$$V_{yi}\, e^{-\int\frac{\mu}{C_1\rho\lambda_2\lambda_3}dt} = -\frac{\mu y(t)}{C_1\rho\lambda_2\lambda_3} + V_{yi} \quad , \tag{8}$$

differentiation of equation (6) produces equation (5).

B. X-Direction of Motion

Once a packet of vorticity has been formed and is injected into the surrounding boundary layer, the vertical position may be described by equation (7).

The horizontal motion of the packet may be examined by assuming that the only external force in the X-direction is caused by the mean motion of the surrounding fluid. That is, whenever the packet velocity is different from the mean velocity, the mean motion becomes the driving force to either accelerate or decelerate the packet in question.

A first approximation might be that the force on the packet would be equal to the rate of change of momentum incurred by the mean fluid because of the presence of the packet of vorticity. The mass of fluid that must be deflected in some manner as it passes over the packet is $C_1\lambda_2\lambda_3\rho(V_m - V_x)dt$. A moving reference frame is used for convenience [62].

The force on the packet must be equal to the mass times the acceleration of the surrounding fluid as a result of the packet. This force must in turn accelerate the packet of vorticity, the total force on the fluid being

$$F_x = C_1 \lambda_2 \lambda_3 \rho (V_m - V_x) dt \frac{dV_m}{dt} \cdot \quad ,$$

where V_x = convective velocity of packet and V_m = velocity of mean motion. Since the actual acceleration may not be known because of the uncertainty of the shape and other related processes (i.e., pressure drag, etc.), a coefficient of drag C_d is introduced such that

$$C_d(V_m - V_x) = dV_m$$

Thus, setting F_x equal to mass times acceleration yields

$$C_d C_1 \lambda_2 \lambda_3 \rho (V_m - V_x)^2 = C_1 \rho \lambda_1 \lambda_2 \lambda_3 \frac{dV_x}{dt} \tag{9}$$

or

$$\frac{dV_x}{dt} = \frac{C_d (V_m - V_x)^2}{\lambda_1} = \frac{C_d}{\lambda_1} [V_x^2 - 2V_m V_x + V_m^2] \quad . \tag{10}$$

In terms of displacement in the X-direction:

$$\frac{d^2 x}{dt^2} - \frac{C_d}{\lambda_1} \left(\frac{dx}{dt}\right)^2 + 2V_m \frac{C_d}{\lambda_1} \frac{dx}{dt} - \frac{C_d V_m^2}{\lambda_1} = 0 \quad . \tag{11}$$

Solutions of these differential equations are given in Appendix A [63, 64], when the functional forms for C_d, λ_1 and V_m are known. When C_d, λ_1, and V_m are essentially constant, the exact solution to equations (10) and (11) are given (Appendix A). The solutions for constant C_d, λ_1, V_m are

$$V_x(t) = V_m - \frac{\lambda_1 (V_m - V_i)}{t C_d (V_m - V_i) + \lambda_1} \quad , \tag{12}$$

where V_i is the initial value of V_x at time $t = 0$ and

$$x(t) = V_m t - \frac{\lambda_1}{C_d} \ell n[\lambda_1 + tC_d(V_m - V_i)] + \frac{\lambda_1 \ell n \lambda_1}{C_d} \quad . \tag{13}$$

The assumption that the rate of change of λ_1 may be considered small can be justified by Kline's [2, Fig. 15] picture of the lift-off phenomena near the wall. Cliff [60] presents pictures showing shape changes in the outer portion of a free shear flow. Both of the above references indicate that the length scale in the X-direction may be considered constant for short periods of time. The rate of change of C_d for cylinders and spheres is not greatly affected by small changes in Reynolds number, as shown by Schlichting [65] and Sabersky and Acosta [62]. It is shown that C_d may vary approximately 30 percent over two orders of Reynolds number. The rate of change of V_m may be considered small in the outer portions of the boundary layer, or where there is little shear. One could also develop the equations and use small increments of time to allow the equations to be used in high shear regions; that is, assume that the velocity takes step increases, and use the equations for each step.

Once the packet of vorticity is removed from the region of high shear, the above simplifying assumptions are reasonable.

The equation for the Y-direction of motion of the packet indicates that the packet moves most quickly away from its origin in the high shear region, and will spend most of its time in the outer portions of the boundary layer. Thus the above solutions should give good first approximations, and are exact solutions for the case where the simplifying assumptions are met. The limiting case where the packet is in the extreme outer portion of the boundary layer and is not subject to great shears should give the best results.

C. Evaluation of the Motion of the Packet of Vorticity

The motion of the packet of vorticity gives direct insight into the structure of the turbulence and the turbulent bounday layer. First, some of the packets will eventually become the turbulence at the intermittent outer edge of the boundary layer. Second, the boundary layer growth is eventually controlled by the motion of the packets, the limiting case occurring when the packets force the boundary layer to grow as a linear function of the X-direction. Third, the turbulent flow may not be considered in equilibrium as long as there are accelerations of the packets within the flow; however, the following analysis shows that within a finite distance the packets become very close to equilibrium with the surrounding flow.

The equations to be examined are as follows.

The acceleration of the packet in the Y-direction;

$$A_y(t) = \frac{-\mu}{C_1\rho\lambda_2\lambda_3} V_y(t) = \frac{-\mu}{C_1\rho\lambda_2\lambda_3} V_{yi}\, e^{-\int \frac{\mu}{C_1\rho\lambda_2\lambda_3} dt} \quad .$$

$$= \frac{\mu^2}{(C_1\rho\lambda_2\lambda_3)^2} y(t) - \frac{\mu V_{yi}}{C_1\rho\lambda_2\lambda_3} \quad . \tag{14}$$

The Y-direction of velocity;

$$V_y(t) = V_{yi}\, e^{-\int \frac{\mu}{C_1\rho\lambda_2\lambda_3} dt} = V_{yi} - \frac{\mu y(t)}{C_1\rho\lambda_2\lambda_3} \quad . \tag{15}$$

The Y-direction of displacement;

$$y(t) = V_{yi} \frac{C_1\rho\lambda_2\lambda_3}{\mu} \left(1 - e^{-\int \frac{\mu}{C_1\rho\lambda_2\lambda_3} dt}\right) \quad . \tag{16}$$

The X-direction of acceleration;

$$A_x(t) = \frac{C_d[V_m - V_x(t)]^2}{\lambda_1} = \frac{\lambda_1 C_d (V_m - V_i)^2}{[tC_d(V_m - V_i) + \lambda_1]^2}$$

$$= \frac{C_d\, \lambda_1 (V_m - V_i)^2}{\left[\left\{ x(t) + \frac{\lambda_1}{C_d} \ell n[\lambda_1 + tC_d(V_m - V_i)] - \frac{\lambda_1 \ell n \lambda_1}{C_d} \right\} \frac{C_d}{V_m}(V_m - V_i) + \lambda_1\right]^2} \quad . \tag{17}$$

The X-direction of velocity;

$$V_x(t) = V_m - \frac{\lambda_1 (V_m - V_i)}{tC_d(V_m - V_i) + \lambda_1}$$

$$= V_m - [\lambda_1 V_m(V_m - V_i)] / \left\{ C_d(V_m - V_i) \left[x(t) \right.\right.$$

$$\left.\left. + \frac{\lambda_1}{C_d} \ell n[\lambda_1 + tC_d(V_m - V_i)] - \frac{\lambda_1 \ell n \lambda_1}{C_d} \right] + \lambda_1 \right\} \tag{18}$$

The X-direction of displacement;

$$x(t) = V_m t - \frac{\lambda_1}{C_d} \ell n[\lambda_1 + tC_d(V_m - V_i)] + \frac{\lambda_1 \ell n \lambda_1}{C_d} \quad . \tag{19}$$

The equations of motion for the packet of vorticity in the Y-direction, equations (14), (15), and (16), will be discussed first.

Equation (14) requires that the deceleration of the packet be inversely proportional to $\lambda_2 \lambda_3$. This inverse ratio means that larger packets are decelerated at a slower rate than the smaller packets. Consider the limiting case:

$$\text{limit}_{t \to \infty} \; A_y(t) = 0 \quad .$$

The acceleration becomes equal to zero when $y(t) = V_{yi} \frac{C_1 \rho \lambda_2 \lambda_3}{\mu}$. A longer distance is required for the larger packets to reach a constant velocity.

Equation (15) shows that the velocity of the packet decreases exponentially with time. It also requires that the vertical velocity of the packet become equal to zero at a distance $y = V_{yi} \frac{C_1 \rho \lambda_2 \lambda_3}{\mu}$. Thus, the penetration of the packet into the flow is proportional to $\lambda_2 \lambda_3$. For the same initial vertical velocity, a larger packet will move farther into the flow than a small packet. Similar results were obtained by Cliff [60] for jet flow. One may infer from this that the spectral content of the flow should change such that there must be more high wave number structures near the wall where the packet forms than farther away. That is, the spectral roll-off must be somewhat less close to the formation

zone, which Tieleman [66] has shown using the CSU-Army wind tunnel. Since the equations are not limited to the positive y axis, the same effect should occur below the formation zone as well. Thus, as one moves away from the production zone, the high frequency must disappear.

Equation (16) is the general relation for the vertical displacement of the packet. At time $t = 0$, the packet is at the axis of the coordinate system; i.e., $t = 0$ and $y = 0$ where $y = 0$ is the formation zone, $y^* = 50$. The most interesting case is the asymptotic values for t very large,

$$y(\infty) = V_{yi} \frac{C_1 \rho \lambda_2 \lambda_3}{\mu} \quad . \tag{20}$$

This equation implies that, if the outer edge of the boundary layer is formed by packets generated near the wall, only the largest structure would have propagated to this area. If V_{yi}, μ, C_1, ρ are the same for two different packets, the final distance in the Y-direction to which they may propagate is proportional to $\lambda_2 \lambda_3$. If λ_2 and λ_3 are each proportional to some basic characteristic length, λ, the migration distance the packet will attain is proportional to λ^2. The larger packets are decelerated at a lower rate than the smaller packets. Thus, the outer edge of the boundary layer will be composed primarily of the larger structures. Photographs, as well as experimental results, indicate that this is true [33, 34, 37, 60]. The height of the boundary layer, δ, becomes the value of $y(\infty)$ or

$$\delta = V_{yi} \frac{C_1 \rho \lambda_2 \lambda_3}{\mu} \quad . \tag{21}$$

The clumping of smaller packets could increase their basic size to allow the packet to penetrate the flow to a greater distance. Fiedler and Head [37] suggest the possibility that the transition zone is a breakdown of small randomly distributed patches of turbulence which finally coalesce. This is found to be consistent with the proposed model. For boundary layers, an increase in the energy of the power spectrum at lower wave numbers with increasing distance from the wall could indicate the occurrence of clumping, However, other phenomena such as dissipation and slower migration rates of smaller packets will also cause a decrease in the power spectrum at large wave numbers. Tieleman [66] indicates a gain in power in the low frequencies with increasing distance from the wall.

Equation (15) should also be valid in the transition region. This suggests that the transition region must develop much more rapidly than the turbulent boundary layer. This may be deduced from the fact that the packets move out more quickly from the region of their point of formation.

Cliff [60] noted for jet flow that, since the equation for the vertical motion is exponential in nature, the intermittency of the outer edge should also have an exponential form. The present analysis for the boundary layer will lead to the exponential form for the variation of intermittency. Fiedler and Head [37] obtained an exponential variation of the outer edge intermittence for a number of turbulent boundary layers.

The limiting case for large time gives

$$\text{limit}_{T\to\infty}\, y(t) = \delta \propto \lambda_2\lambda_3 \quad . \tag{22}$$

(Note: $\text{limit}_{T\to\infty} y(t)$ + distance from the wall to the formation zone = δ . However $\text{limit}_{T\to\infty} y(t) \gg$ distance from the wall to the formation zone.) The boundary layer thickness will be proportional to $\lambda_2\lambda_3$. Taylor [20] found that the growth of a length scale will be proportional to the square root of time. Thus,

$$\text{limit}_{T\to\infty}\, y(t) = \delta \propto t^{1/2} t^{1/2} \propto t \quad .$$

Therefore, for a constant V_∞ , $t^{1/2} = \left(\frac{x}{V_\infty}\right)^{1/2}$; thus,

$$\delta \propto x \quad . \tag{23}$$

Thus, for the limiting case of long times, the boundary layer growth becomes a linear function of distance. Zoric [67] points out that this is a requirement for similarity solutions to exist in the turbulent boundary layer. That is, one of the requirements for the boundary layer to have a nondimensional velocity profile that is invariant with respect to downstream distance is that the boundary layer have a linear growth in the streamwise direction.

Equation (17) gives the acceleration of the packet in the X-direction. At time $t = 0$, the acceleration is inversely proportional to its characteristic wavelength in the mean flow direction. As time becomes larger, such that $tC_d(V_m - V_i) \gg \lambda_1$, the acceleration of the packet becomes proportional to λ_1 and inversely proportional to time and C_d . Thus, the smaller the packets are, the more quickly they are initially accelerated; that is, the smaller packets are the most affected by the initial conditions. Since the acceleration is also a function of the square of the difference in velocity from that of the mean flow, there comes a point where the smaller packets are moving faster than the larger ones. Thus at some time the larger packets (moving more slowly) are accelerated at a greater rate than the smaller ones. This point occurs when the finer structure has approached the mean velocity and the

velocity of the larger structure is still significantly different from the mean. The velocity equation for the X-direction is equation (18), which shows that, at time $t = 0$, the convective velocity is not a function of wavelength or characteristic length. The zero time limit corresponds to the formation zone. As time becomes a factor, the velocity of the packet of vorticity in the X-direction is negatively proportional to λ_1, the characteristic wavelength in the mean flow direction; i.e.,

$$tC_d(V_m - V_i) \gg \lambda_1 \quad ,$$

$$V_x = V_m - \frac{\lambda_1}{tC_d} \quad . \tag{24}$$

Thus, the smaller the packet is, the closer its velocity is to the mean velocity. Likewise, the larger the packet is, the greater the difference its velocity is to the mean velocity.

Equation (24) also indicates that for t very large, the convective velocity of the packet once again becomes independent of wave number. At some finite time, velocities of all packets, which had been generated for that length of time, should travel at approximately the same rate.

A simple calculation can be made for the time needed for the convective velocities to approach their asymptotic value. Consider that the fluid impinging on the packet is deflected entirely in the Y-direction. Here, then, $C_d = 1$. Also, when the convective velocity is approximately equal to the mean velocity, λ_1 would be equal to $\frac{V_m}{2\pi f}$, or the inverse of the wave number. The flow will be considered stable (i.e., a similarity solution for the velocity profile will exist) when the convective velocity is equal to $0.99\,V_m$, where V_m is the mean velocity of the outer flow.

Equation (24) may be written as

$$1 - \frac{V_x}{V_m} = \frac{\lambda_1}{tV_mC_d} \quad . \tag{25}$$

For the outer regions,

$$\lambda_1 = \frac{V_m}{2\pi f} \quad ,$$

thus,

$$1 - \frac{V_x}{V_m} = \frac{1}{2\pi f t C_d} \quad .$$

Applying the above requirement on the convective velocity (0.99 V_m),

$$0.01 = \frac{1}{2\pi f t} \quad .$$

Thus the time for flow stability becomes

$$t = \frac{1}{0.063f} \qquad \text{for} \qquad \frac{V_m - V_x}{V_m} = 0.01 \quad , \tag{26}$$

the general relation being

$$t = \frac{V_m/(V_m - V_x)}{2\pi f} \quad . \tag{27}$$

Example 1: Consider that the freestream velocity is $V_\infty = 20$ ft/sec (6.1 m/sec) and that the initial velocity of the packet is $V_i = 5$ ft/sec (1.525 m/sec). Consider also that the minimum frequency content of concern is 10 Hz. Therefore,

$$\lambda_1 = \frac{20}{63} = 0.318 \text{ ft } (0.097 \text{ m})$$

and

$$t = \frac{1}{0.63} \text{ sec} = 1.59 \text{ sec.}$$

Equation (19) gives the distance the packet must travel before a similarity solution could be expected:

$$x(t) = V_m t - \frac{\lambda_1}{C_d} \ell n[\lambda_1 + C_d(V_m - V_i)] + \lambda_1 \frac{\ell n \lambda_1}{C_d}$$

$$x = (20)(1.59) - 0.318\, \ell n[0.318 + 1.59\,(15)] + 0.318(-1.15)$$

$$= 31.8 - 3.2 - 0.4 = 28.2 \text{ ft } (8.6 \text{ m}) \quad .$$

For the same initial conditions, for a frequency content of 20 Hz, we see that only approximately one-half of this distance would be required. Equation (27) shows that the time required for the convective velocity to approach the mean velocity is a linear function of the percent difference that may be allowed.

Example 2:

$V_\infty = 80$ ft/sec (24.4 m/sec) ,

$V_i = 1/4\ V_\infty = 20$ ft/sec (6.1 m/sec),

Minimum frequency of concern = 10 Hz,

Experimental error ~ 4 percent (agreement between mean and convective velocity),

and $\lambda_1 \frac{V_\infty}{2\pi f} = \frac{80}{20\pi} = 1.273$ ft (0.338 m).

Thus, equation (25) becomes

$$1 - \frac{V_x}{V_m} = 0.04 = \frac{1}{2\pi f t C_d} = \frac{0.1}{2\pi t} \quad ,$$

$$t = \frac{0.1}{(0.04)2\pi} = 0.398 \text{ sec} \quad ,$$

and

$$x(t) = V_m(t) - \frac{\lambda_1}{C_d}\ell n[\lambda_1 + tC_d(V_m - V_i)] + \frac{\lambda_1 \ell n\lambda_1}{C_d}$$

$$= (80)(0.398) - 1.273\,\ell n[1.273 + (0.398)(60)] + 1.273\,\ell n\,1.273$$

$$= 27.4 \text{ ft } (8.35 \text{ m}) \quad .$$

This result agrees well with Zoric's work taken in the CSU-Army wind tunnel [67]. Zoric finds that for $V_\infty = 80$ ft/sec (24.4 m/sec), the boundary layer thickness, δ, displacement thickness, δ^*, and momentum thickness, θ, all begin to grow linearly at $x = 30$ ft (9.15 m). Our model is presently concerned with the linear growth of the boundary layer thickness. That is, when the internal flow structure comes into equilibrium with the mean flow, the growth of the boundary layer is predicted to be linear.

Equation (19) gives the X-direction of motion for the packet. The larger particles are found to travel the least distance because their acceleration is originally somewhat slower than that of a smaller particle. Examples 1 and 2 show the importance of this equation. With the knowledge of the difference between the convective velocity and mean velocity, one can estimate the length required for similarity solutions to exist. The mean velocity profile used in the derivations may be slightly modified; however, since the nature of the vertical direction of motion demands that the packet will expend most of its life in the outer portion of the flow, equation (19) should be useable with little or no modification.

A more detailed approach to evaluating equation (10) would be to assume a specific velocity distribution through the boundary layer rather than a characteristic velocity, V_m. As an example, consider $V_m = [C_v y + V_i]$, where C_v is a constant and V_i is the velocity in the X-direction at $y = 0$.

Using a first order approximation for y(t) (i.e., $V_m = C_v V_{yi} t + V_i$), equation (10) becomes

$$\frac{dV_x}{dt} = \frac{C_d}{\lambda_1} V_x^2 - 2\frac{C_d}{\lambda_1}[C_v V_{yi} t + V_i] V_x + \frac{C_d}{\lambda_1}[C_v V_{yi} t + V_i]^2 \quad . \qquad (28)$$

Equation (28) is of the same form as that considered in Appendix A. The method of approach given for the general case in Appendix A is, however, not well suited for this particular differential equation. Thus, a slightly different transformation is used, as outlined in Appendix B, to solve equation (28).

The solution of equation (28) in Appendix B, gives the following X-direction relation for the motion of the vorticity packet. A flow of the form $V_m = C_v y$, where C_v is some constant, is assumed. The velocity in the X-direction is given by

$$V_x = \frac{-C_v C_{yi}}{(C_d C_v V_{yi}/\lambda_1)^{1/2}} \tanh\left(\frac{C_d C_v V_{yi}}{\lambda_1}\right)^{1/2} t + C_v V_{yi} t + V_i$$

$$= V_m - \left(\frac{\lambda_1}{C_d}\right)^{1/2} \left(\frac{V_m - V_i}{t}\right)^{1/2} \tanh\left[\frac{C_d}{\lambda_1}(V_m - V_i)t\right]^{1/2} , \tag{29}$$

while the motion in the X-direction is given by

$$x(t) = C_v V_{yi} \frac{t^2}{t} + V_i t - \frac{\lambda_1}{C_d} \ell n \cosh\left(\frac{C_d C_v V_{yi}}{\lambda_1}\right)^{1/2} t$$

$$= \frac{V_m + V_i}{2} t - \frac{\lambda_1}{C_d} \ell n \cosh\left[\frac{C_d}{\lambda_1}(V_m - V_i)t\right] . \tag{30}$$

Equations (29) and (30) are approximations to the governing equations for the conditions when the packet is near the floor. The velocity profile of the turbulent boundary layer might be examined in two parts, A and B. A is the linear fit to the portion near the formation zone, and B is the linear fit to the outer region. Equations (17), (18), (19), (28), (29), and (30) could be used to describe the motion of the packet throughout the layer. The asymptotic solutions would still be governed by equations (17), (18), and (19) which have previously been discussed.

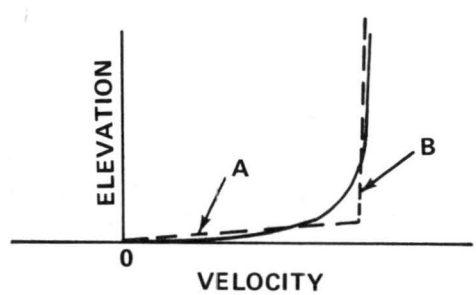

A general form $V_m = (C_v Y)^{1/7}$ [62, page 229], where C_v is a dimensional constant, may also be used for the velocity profile. Using again a first order approximation for the Y-direction of motion; i.e., $y(t) = V_{yi}t$, gives $V_m = (C_v V_{yi} t)^{1/7}$.

The differential equation governing the motion is still equation (10). The solution given in Appendix C is

$$V_x = V_m - \frac{V_m(V_m - V_i)}{\frac{C_d}{\lambda_1}(V_m - V_i)\left[\frac{7}{8} C_v V_{yi} t^{8/7} + V_i t\right] + V_m} \tag{31}$$

where

$$V_m = (C_v V_{yi} t)^{1/7} + V_i = (C_v y)^{1/7} + V_i$$

and

$$\alpha = 2 \quad .$$

Equation (31) would be difficult to work with, since the velocity profile increases to infinity as time goes to infinity. However, the expansion of the velocity profile, $V = Cy^{1/7}$, in a Taylor series yields

$$V(y) = V(y_c) + (y - y_c)\frac{C}{7} y^{-6/7} - \frac{3}{49}(y - y_c)^2 \, Cy^{-13/17} + \ldots \quad .$$

Thus in regions where y is large, the velocity profile may be considered constant for large increments of elevation, implying that the equations for convective velocity in a flow with no velocity gradient could be used. The simple case of allowing the mean velocity to approach some asymptotic value and using the equations for a constant mean motion would be realistic.

The velocity of the packets in the formation region should be independent of wave number, because at this location all packets move with the local mean velocity of the fluid. Thus, a direct transformation between wave number and size may be determined for this region. When the velocity of the packets approaches the mean velocity, once again a unique relationship will exist between wave number and size.

From the previous analysis one may infer that the boundary layer must grow rapidly through the laminar to the turbulent transition region. The boundary layer growth rate must then decrease with the limiting case being when the growth rate has decreased to a linear function of X. The shape of the undulating outer edge may be examined in the light of the model. The outer edge will contain, primarily, large scale structures. If the boundary layer goes to separation, the formation zone would be raised suddenly, and the outer edge would contain a greater number of smaller scale structures. One might expect that the outer edge would, thus, be somewhat less intermittent than upstream. (This was observed by Fiedler and Head [37].)

At the point in time where the convective processes travel at nearly the mean flow rate, correlation measurements should more nearly indicate a near frozen flow. The width of the correlation curve should not change greatly with separation distance, because the spreading of the covariance with distance is partially attributed to the fact that various frequencies traveling at different rates will not allow all frequencies to be in phase at separations other than zero. It may be shown that spatial weighting of individual harmonies will not decrease the magnitude of the normalized cross covariance (Appendix D, paragraph E). This leads to an interesting speculation that the majority of spreading or diffusion processes in a boundary layer may be caused by varying convective velocities of structures or frequencies of various sizes.

IV. EVALUATION OF CONVECTIVE VELOCITIES

This section concerns the use of the statistical concept of space-time covariance computation to obtain the magnitude of the convective velocity. The convective velocity is most easily obtained by either holding time constant and varying the separation distance until the cross-covariance becomes a maximum, or holding the separation distance constant and varying the time delay until the cross-covariance becomes a maximum. In both cases, the convective velocity is obtained by dividing the appropriate separation distance by the appropriate time delay. The special case of Taylor's frozen flow theory is covered, along with the case in which the flow may not be considered frozen.

A. Convective Velocity for Time Invariant Covariance

The relationship between time and space in shear flows has, for the most part, been avoided in the past by assuming that Taylor's hypothesis [4] was valid. That is, for flows in which the turbulent intensity is low, the flow pattern is assumed frozen. Thus, an observer moving with the mean motion of the flow would detect an unchanging spatial pattern in the

flow. A shift in space could be represented solely by an appropriate time displacement. A function of space and time, $f(x,t)$, would be equally represented by $f(x + U\tau, t + \tau)$. For this special case, the correlation or covariance function would be invariant in time for a statistically stationary set of data: that is,

$$\frac{\partial}{\partial t} \overline{f(x,t)\, f(x + U\tau, t + \tau)} = 0 \quad . \tag{32}$$

This result follows the analysis given in Appendix D, which requires that

$$\frac{\partial}{\partial t} \overline{f(x,t)\, f(x + U\tau, t + \tau)} = \frac{\partial}{\partial t} \overline{f(x,t)\, f(x,t)} = 0 \quad . \tag{33}$$

The covariance may also be expressed as

$$\overline{f(x,t)\, f(x + \xi, t + \tau)} = \overline{f(x,t)\, f(x + \xi + U\tau_1, t + \tau + \tau_1)} \quad . \tag{34}$$

Wills [49] noted that temporal invariance of the covariance may be obtained if it is assumed that the change in the turbulence pattern between the two measuring points is statistically independent of the instantaneous velocity fluctuation at the initial point. Wills obtained the relation

$$\overline{\frac{\partial^n f(x,t)}{\partial t^n} \frac{\partial^m [f(x,t) - f(x + \xi, t + \tau)]}{\partial t^m}} = 0 \tag{35}$$

for some ξ/τ and for all N and M. For $n = m = 0$,

$$\overline{f(x,t)^2} = \overline{f(x,t)\, f(x + \xi, t + \tau)} \quad . \tag{36}$$

Frozen flow requires that $f(x + \xi, t + \tau)$ reduce to $f(x,t)$ when considered at the point $x + \xi$ and at time $t + \tau$, where ξ is in the direction of the flow. Thus, for frozen flow, the covariance is invariant. For the frozen flow, the convective velocity may be uniquely defined by

$$\left.\frac{d\xi}{d\tau}\right)_{C_{xy}(\xi,\tau) = \text{constant}} = C_v = \text{Convective Velocity.} \qquad (37)$$

This relation is shown schematically in Figure 2. Here the spatial pattern is convecting at a velocity identical to the mean flow rate.

B. Convective Velocity for Noninvariant Covariance

The real world presents a somewhat more complicated picture in that the flow is not frozen, and the covariance is not invariant. Turbulent decay, for example, is a condition that will cause the turbulent velocity to change its nature and the covariance to decrease in the streamwise direction. However, turbulent decay may or may not change the value of the normalized covariance (Appendix D, paragraph F).

Figure 3 shows how the isocovariance curves may appear in nature. Dumas, Favre, and Gaviglio [14] present similar curves for velocity fluctuations in a flat-plate turbulent boundary layer.

Two separate convective velocities may now be obtained. The first is defined by a two-point measurement separated by a given distance, ξ, where the time delay between sensors (located at each point) is allowed to vary. The convective velocity is equal to the separation distance divided by the time delay which gives the largest covariance amplitude.

This convective velocity is represented in Figure 3 by holding ξ constant at ξ_1, and varying τ until $C_{xy}(\xi,\tau)$ becomes a maximum; that is at the point

$$\frac{\partial}{\partial\tau} C_{xy}(\xi,\tau) = 0 \quad ,$$

which is the case τ_2 in Figure 3. Thus, the convective velocity becomes $C_{v\tau} = \xi_1/\tau_2$, where $C_{v\tau}$ is the convective velocity obtained by holding ξ constant and varying τ.

A second convective velocity may be obtained in a similar manner by holding τ constant and varying ξ. This is represented in Figure 3 by holding τ_2 constant and moving in the ξ direction until $C_{xy}(\xi,\tau)$ becomes a maximum; that is,

$$\frac{\partial C_{xy}(\xi,\tau)}{\partial\xi} = 0 \quad .$$

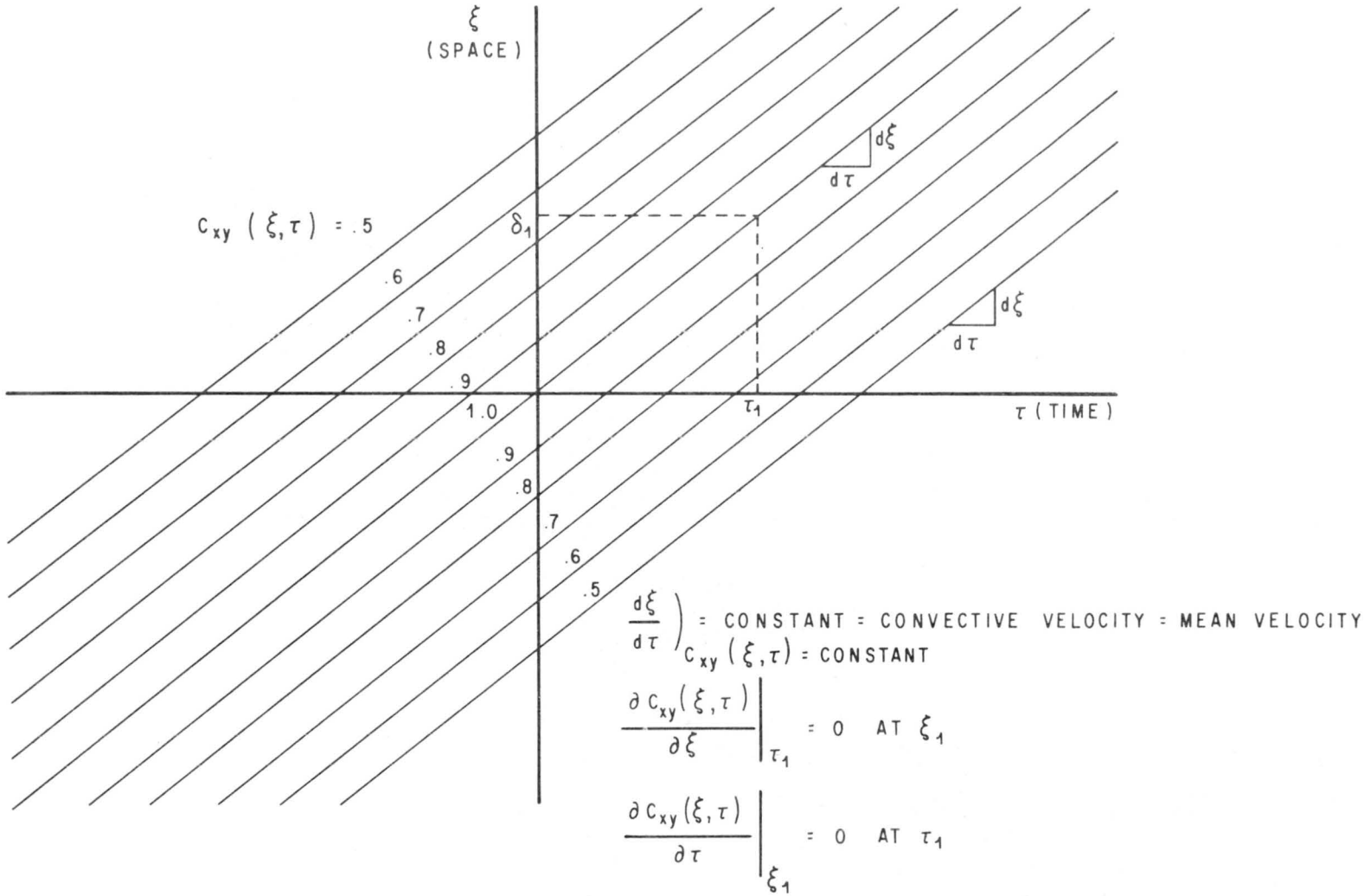

Figure 2. Iso-correlation lines for frozen flow.

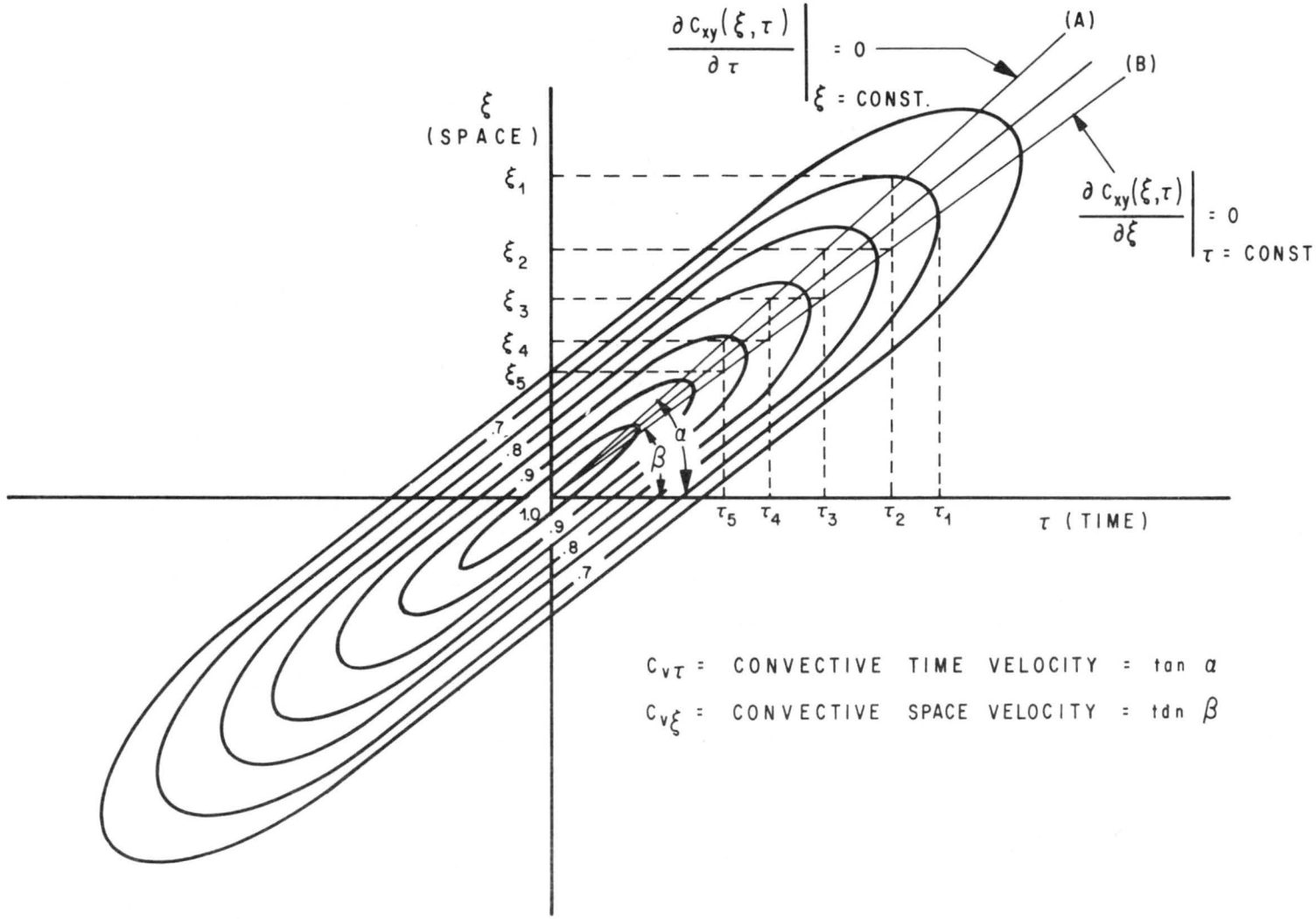

Figure 3. Iso-correlation lines for nonfrozen flow.

For this case, Figure 3 gives $C_{v\xi} = \xi_2/\tau_2$, where $C_{v\xi}$ is the convective velocity defined by holding τ constant and varying ξ.

Line A (Fig. 3) passes through all points of

$$\frac{\partial C_{xy}(\xi,\tau)}{\partial \tau} = 0 \quad .$$

Therefore, the slope of line A is $C_{v\tau}$. Line B passes through all points where

$$\frac{\partial C_{xy}(\xi,\tau)}{\partial \xi} = 0 \quad .$$

Therefore, the slope of Line B is $C_{v\xi}$. Figure 3 shows that the two convective velocities are different for nonfrozen flows.

To demonstrate that the convective velocity measured using a constant spatial separation and varying the time delay is the more useful for the present analysis, a signal representative of a particular packet of fluid at several locations was considered (Fig. 4). Another aid is the examination of the interactions of the two separate correlations. Assume that the time-varying covariance between points 1 and 3 of Figure 4 is that of Figure 5. Let $\xi = \xi_1$, of Figure 2, where Figure 2 gives the maximum of the curve occurring at time delay, τ_2 . For this case, $C_{xy}(\xi,\tau) = 0.7$. From Figure 2 we see that, for the same time delay, we are able to get a higher correlation, approximately 0.74, if the separation distance was only ξ_2, $(\xi_2 < \xi_1)$. This point is represented on Figure 5 by point A. Examining Figure 2 again, it is seen that for ξ_2 , an even larger correlation occurs at τ_3 ,$(\tau_3 < \tau_2)$. This point is plotted as point B on Figure 5.

Applying the same procedure we see that for τ_3 there occurs a greater correlation at an even shorter separation, ξ_3 . This correlation is point C on Figure 5. For ξ_3 there is a greater correlation at τ_4 , point D of Figure 5.

This process may be repeated over and over again until the origin is reached. Thus, the peak of a time covariance must lie within the time covariance curve for a slightly smaller separation distance. The maximum time covariance value for a given time delay (note that this is not the peak) is the true maximum of the space covariance for that time delay and corresponds to the separation distance for the curve on which it lies. For Figure 4, the time covariance of points 1 and 3 would give a maximum at some delay; e.g., τ_i . At this same time delay, the covariance of points 1 and 2 could have a larger value.

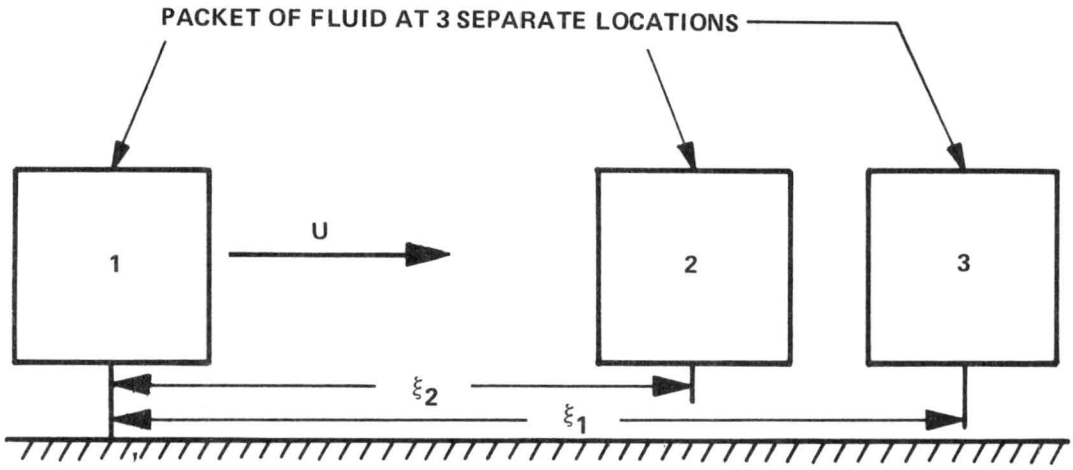

Figure 4. Schematic for correlation analysis.

Figure 6 may be examined in the same manner as Figure 5. For a given time delay, τ_2 , a peak will occur at ξ_2 (point A, Fig. 6). However, at ξ_2 a higher covariance is obtained at τ_3 , $\tau_3 < \tau_2$ (point B). At τ_3 a larger covariance is found at ξ_3 (point C). At ξ_3 the maximum covariance occurs at τ_4 , $\tau_4 < \tau_3$ (point D) and so on as in the above case.

Statistically, the peak of the space-time covariance curve with varying time delay occurs when the signals are most closely matched; that is, the optimum time delay is the time delay where the wave shapes are the most alike. The space-varying, space-time covariance curve indicates that a slight decrease in separation will give a higher covariance amplitude for the same time delay. The difference between the two convections gives a measure of the degree to which the flow is not frozen.

The present analysis deals primarily with the passage of fluid packets and the signal produced as a result of them. A transit time needed for the packet to best reproduce itself is desired. Thus, the time-varying scale was selected. That is, the convective velocity will be obtained as the given separation distance divided by the time delay at which the covariance becomes a maximum. (This is consistent with the work of Favre, Gaviglio, and Dumas.)

$$\left.\frac{\xi}{\tau_m}\right|_{\frac{\partial C_{xy}(\xi,\tau)}{\partial \tau} = 0} = C_{v\tau} \tag{38}$$

A typical covariance curve is shown in Figure 7. Unless otherwise stated, the covariance will henceforth be written as $C_{xy}(\tau)$. The above chosen convective velocity, $C_{v\tau}$, will be written V_c for the overall convective velocity. To this point, nothing has been said about whether the convective velocity is a function of wave number or characteristic lengths.

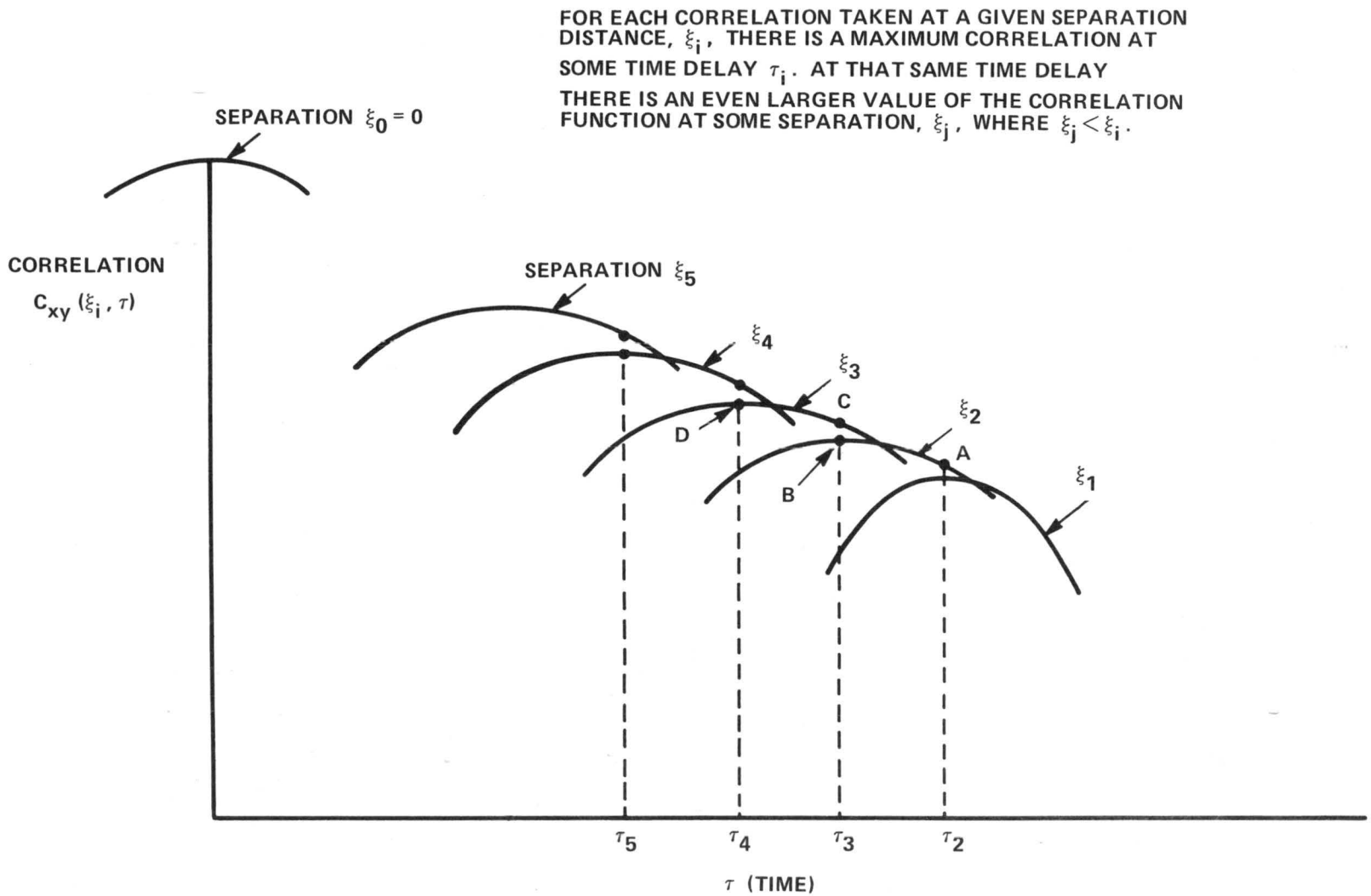

Figure 5. Correlation in time domain as function of space.

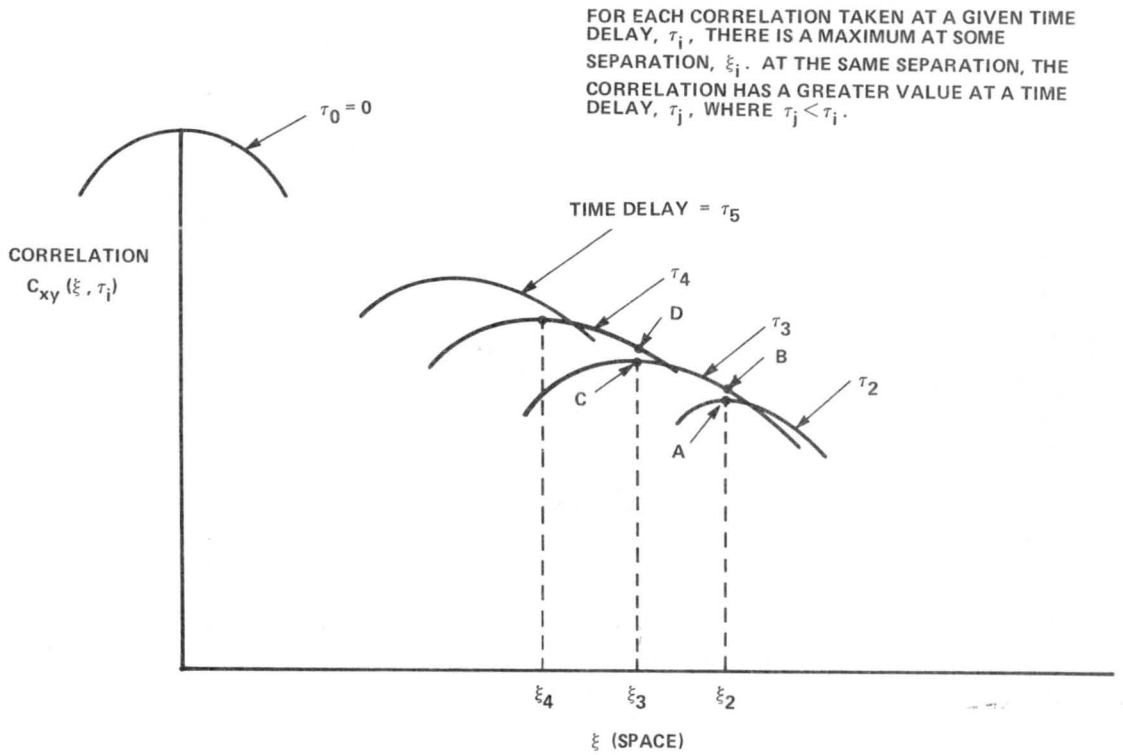

Figure 6. Correlation in space domain as function of time.

The convective velocity of specific frequencies will be denoted by V_f, where the subscript f will be replaced by the frequency in question.

C. Evaluation of Convective Velocities

The following paragraphs on concepts and experimental procedures deal primarily with correlation, spectra, and statistical signal analyses. A short outline on signal analysis and correlation concepts is given in Appendix D, which includes the spectral relationships for the correlations discussed in the preceding section, using both stationary and nonstationary series. Also included are restrictions imposed on the correlation and spectra by physical limitations, such as records of finite time and stationarity of the original signals through the nth and mth moments, respectively. The effect of correlating derivatives, a physical meaning for the cross phase spectrum, effects of space and frequency weighting functions on covariance computations, as well as the interrelationship of correlation and probability density, are examined. Although the fluid model presented in this report does not rely on these statistical tools, advances have been made which give more insight into statistical processing and are presented in the appendices to aid future studies.

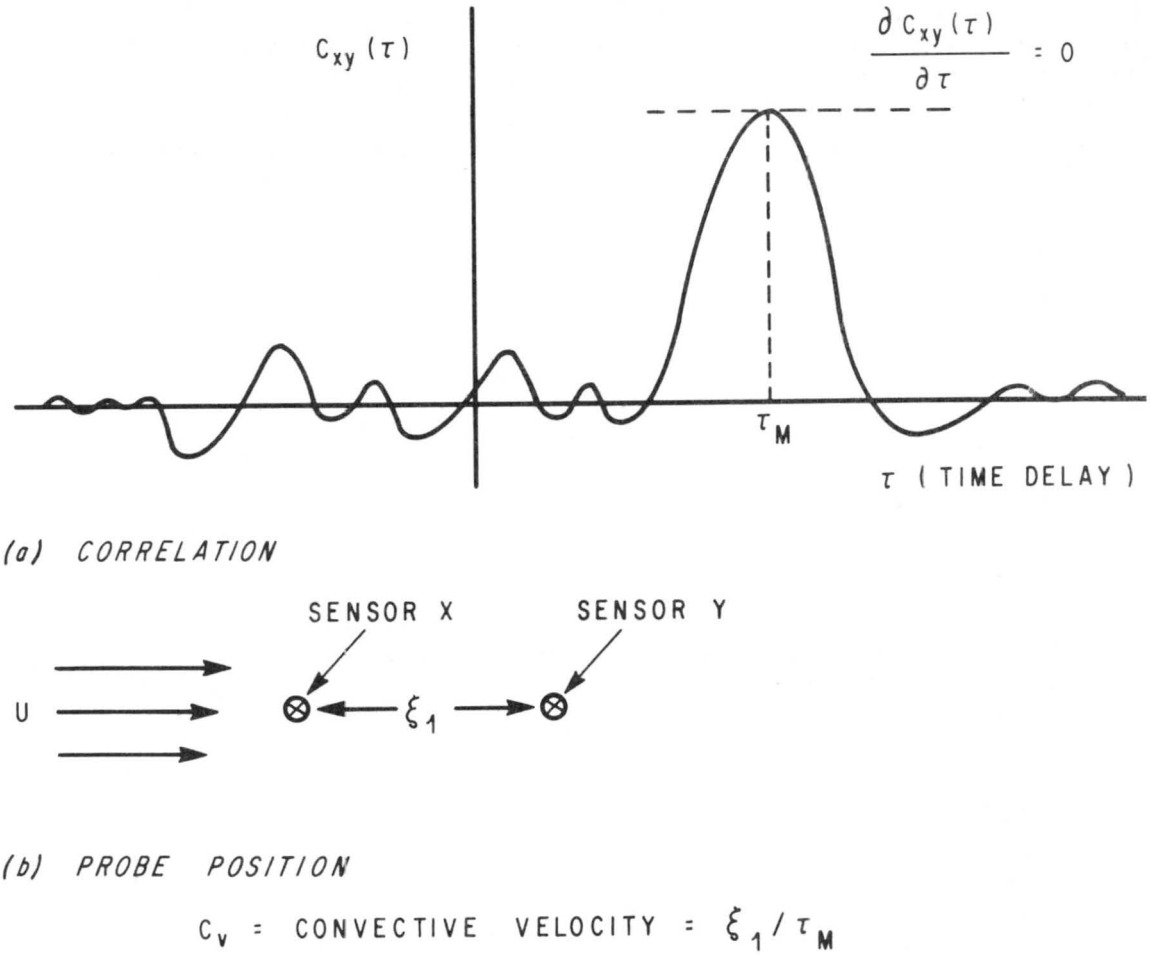

Figure 7. Convective velocity evaluation.

D. Concepts

This section outlines the necessary physical and statistical tools used to check the physical model presented in Section III. The model requires a correlation of the undulating outer edge of the boundary layer with the region directly above the viscous sublayer. Packets of vorticity are formed which migrate from a region called the "production zone." The model predicts that the boundary layer acts as a filter to separate sizes or wave number components; that is, the convective velocity becomes a function of wave number.

Finally, an asymptotic approach of all sizes of packets to the local mean velocity is predicted. Thus, after a finite residence time, the convective velocity will become independent of frequency. Methods by which to analyze each of the above hypotheses are presented.

1. Correlation of the Outer Edge of the Boundary Layer with the Internal Flow. The model assumes that the convoluting outer edge of the boundary layer will create strong local pressure gradients, which affect what transpires near the wall of the boundary layer. However, it is not crucial to know exactly what produces the packet for the major contribution of the present report. When the flow near the wall is affected by occurrences in the convoluting outer edge, a packet is formed. One may speculate about whether a stress-relieving phenomenon [3] may cause localized separation to occur that initiates the onset of turbulence.

A measure of the phenomena proposed is the cross-correlation of the local pressure gradients at the two locations in question, such as

$$\overline{\left(\frac{\partial P}{\partial x_i}\right)_{\text{outer}} \left(\frac{\partial P}{\partial x_j}\right)_{\text{inner}}} \quad ,$$

where $i = 1, 2$; $j = 1, 2$; x_1 = X-direction; and x_2 = Y-direction.

Since the local pressure gradients are difficult to measure, one may wish to use local accelerations of the fluid particles which are related to the local pressure gradients. Thus, the correlation

$$\overline{\left(\frac{\partial u_i}{\partial t}\right)_{\text{outer}} \left(\frac{\partial u_j}{\partial t}\right)_{\text{inner}}}$$

might be considered. For covariance computations, only the fluctuations need be considered:

$$\overline{\left(\frac{\partial u_i'}{\partial t}\right)_{\text{outer}} \left(\frac{\partial u_j'}{\partial t}\right)_{\text{inner}}} \quad ; \; i = 1,2; \; j = 1,2; \; u_1' = u'; \text{and } u_2' = v' \quad . \tag{39}$$

Appendix D, equation (D-82), gives the relationship between

$$\overline{\left(\frac{\partial u_i'}{\partial t}\right)_{\text{outer}} \left(\frac{\partial u_j'}{\partial t}\right)_{\text{inner}}}$$

and

$$\overline{u_i'\Big)_{\text{outer}} \quad u_j'\Big)_{\text{inner}}} \ .$$

The correlation of the velocity fluctuation may be used to evaluate the inner-outer correlation described by the model. When only the fluctuating portions of the signals are correlated, the product is often referred to as the "covariance."

The covariance deals only with the fluctuations. The dc or mean values give no insight into convective transport rates, and, thus, only covariance computations will be examined for the present applications. "Correlation" will be used interchangeably with "covariance," and, unless otherwise stated, correlation will refer to ac-coupled signals (i.e., the means are zero).

2. Production Zone. The main requirement for this region of the boundary layer is that the convective velocity equal the mean velocity; that is, the convective velocity of all size structures is the same.

Evaluation in this zone will be the measure of the convective transport rate for various frequencies. If all frequencies travel at the same rate, one can infer the structure's size from the wave number concept. The space time correlation concept discussed in the preceding chapter is used to evaluate the convective velocities.

3. Filtering Action of the Boundary Layer. Filtering of the boundary layer implies an ability of the boundary layer to separate frequencies in some prescribed fashion. The physical model predicts that varying frequencies will be convected at different speeds in certain portions of the boundary layer. The separation in speed will occur in both the vertical and horizontal directions.

Spatially separated sensors are used to measure the convective speeds of the different wave numbers. The convective velocity is used, together with the frequency, to determine the wave number. The packet size is related to the wave number.

4. Convective Velocity Profile Independent of Frequency. The model predicts that packets of all sizes will asymptotically approach the mean flow velocity after a finite length of time. The example previously given indicates that lengths of the order of 25 to 30 ft (7.6 to 9.15 m) are required for the convective velocities in a turbulent boundary layer to equal the mean velocity. The convective velocities are measured by the spatially separated hot wires.

V. EXPERIMENTAL SETUP AND PROCEDURES

The experimental portion of this investigation was performed at the Engineering Research Center of Colorado State University. Two wind tunnels were used to study the

convective velocities: a large meteorological wind tunnel and the entrance portion of a small separation tunnel.

As defined in Section IV, the convective velocity is a time-average quantity, much like the concept of mean velocity. Figure 7b is a schematic of the hot wire configuration used to define a convective velocity. First, signals from two spatially separated hot wires are selectively filtered to obtain desired frequency components. (The wires are separated in the X-direction of motion – the mean flow direction.) The signals are then fed into the correlator, which produces the signal's temporal cross-correlation and integrates this value for a desired length of time. Integration times of approximately 5 minutes were used for this experiment. The cross-correlation is then plotted by an X-Y plotter on graph paper.

The instrumentaiton involved for this measurement includes the hot wire anemometers, filters, a correlator, an X-Y plotter, and a tape transport.

A. Wind Tunnels

1. The Meteorological Wind Tunnel. The meteorological wind tunnel test section has a cross section that is 6 ft (1.83 m) by 6 ft (1.83 m) and has a 95-ft (29-m) long test floor over which the boundary layer may develop. The wind tunnel is of the recirculating type with the air speed controlled by a variable speed, variable pitch aircraft propeller. Plate and Cermak [68] describe the facility in detail. Figure 1 shows a sketch of the boundary layer's development along the tunnel test floor, and Figure 8 shows a top view of the tunnel.

Tieleman [66] has shown that damping screens and a 9:1 entrance contraction produce extremely low free-stream turbulence, and his results showed that the turbulence intensity ranges from 0.00015 at 20 ft/sec (6.1 m/sec) to 0.00027 at 80 ft/sec (24.4 m/sec). The boundary layer along the floor of the tunnel is artificially tripped by a saw-toothed fence preceded by a 4-ft (1.22-m) section of gravel (Fig. 7).

The first 30 ft (9.15 m) of the floor were used for the present experiment. A boundary layer thickness of approximately 18 in. (0.457 m) [69] is attained in the 30 ft (9.15 m). The measurements were made in the vertical plane along the centerline of the tunnel behind the tripped section at distances downstream of 1, 2, 4, 8, 18, and 30 ft (0.305, 0.61, 1.22, 2.44, and 9.15 m). The X-axis was taken along the centerline of the tunnel floor, the Y-axis is vertical to the floor, and the Z-axis is parallel to the floor and perpendicular to the flow direction.

2. Separation Tunnel. The separation tunnel is of the open return type. A honeycomb, which is located in a large circular inlet, is used to straighten the inlet flow and break up any large scale disturbances. From the inlet the flow passes through a settling chamber and is then accelerated into the test section, where the cross section narrows to 18 by 18 in. (0.457 m by 0.457 m). The entire test section is made of plexiglass for visual observations. A 54-in. (1.37-m) fan which governs the flow rate by a variable speed motor is located downstream of the test section. Figure 9a is a photograph of the flow facility.

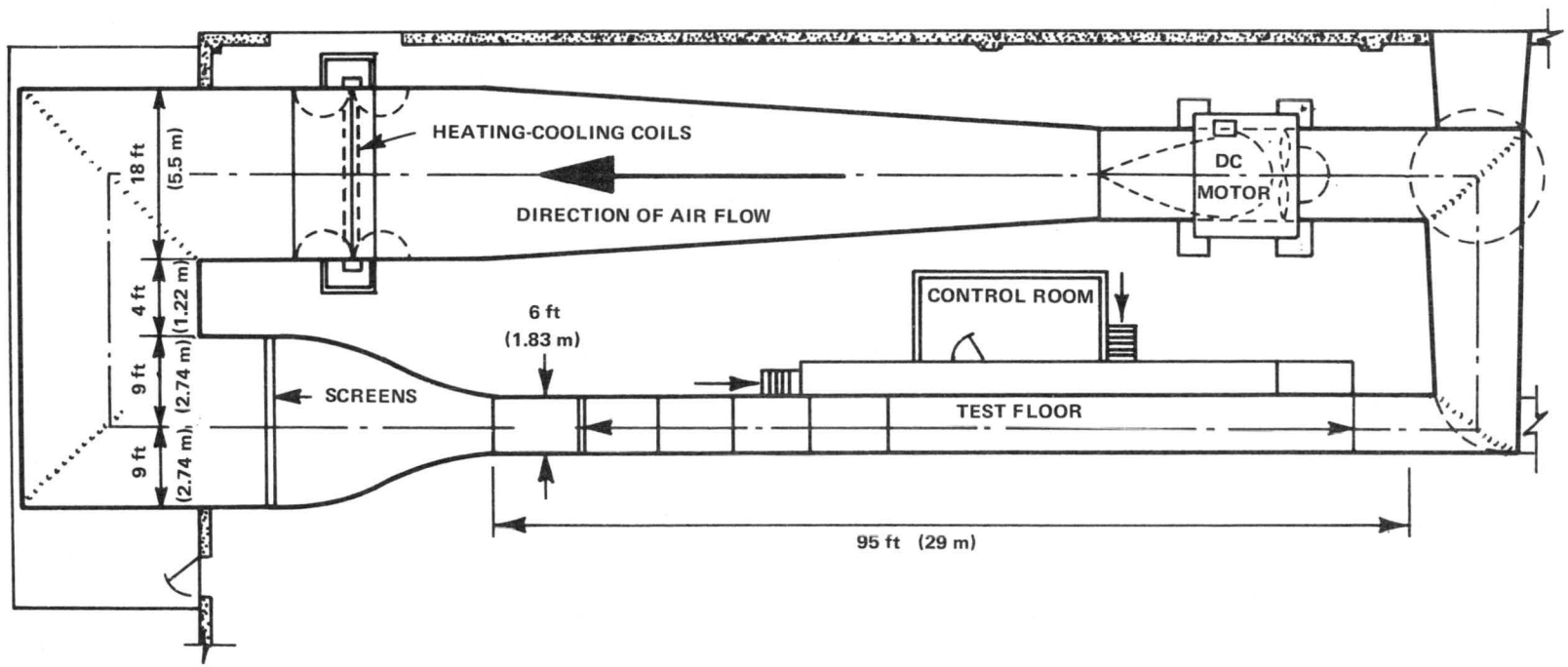

Figure 8. Plan view of meteorological wind tunnel.

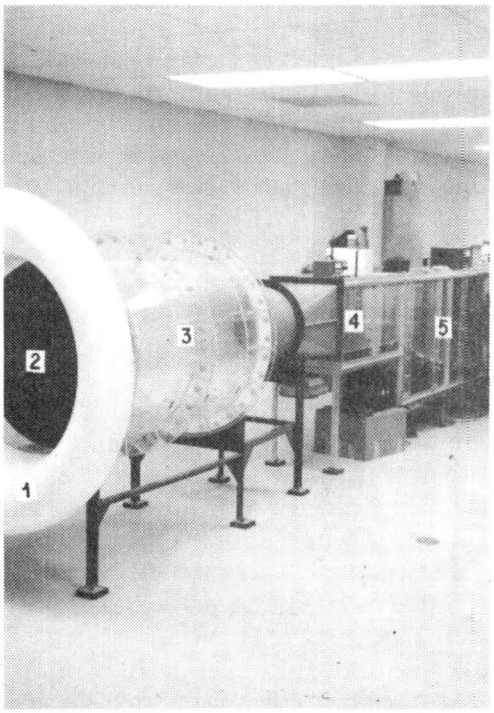

(a) WIND TUNNEL/FLOW FACILITY

1. ENTRANCE
2. HONEYCOMB
3. SETTLING CHAMBER
4. BOUNDARY LAYER DEVELOPMENT SECTION
5. SEPARATION SECTION

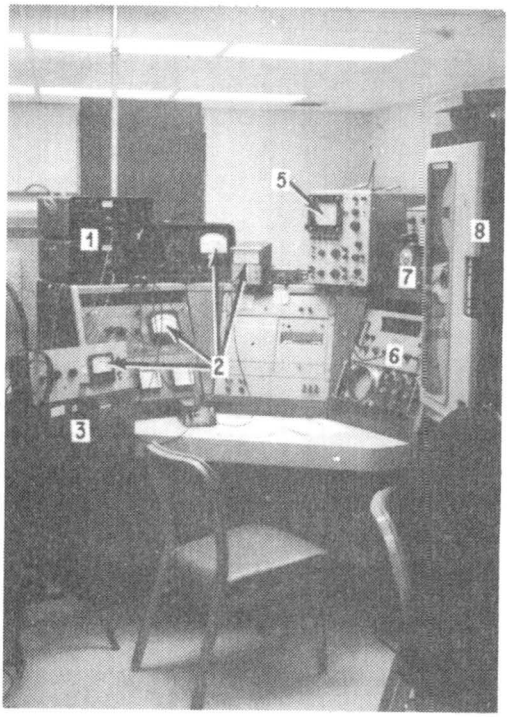

(b) INSTRUMENTATION

1. CSU HOT WIRE ANEMOMETERS
2. TRUE RMS METERS
3. SINE WAVE GENERATOR
4. TRUE RMS METER
5. SCOPE
6. DIGITAL VOLTMETERS
7. FILTERS
8. 14 CHANNEL TAPE RECORDER

Figure 9. Wind tunnel and instrumentation.

The entrance portion of the separation tunnel was used for the initial convective velocity measurements. The tests were run at 2 ft, 2 in. (0.66 m) and 4 ft (1.22 m) from the start of the test section. The ceiling of the tunnel was adjusted so as to develop a near zero pressure gradient flat-plate boundary layer. The boundary layers were approximately an order of magnitude smaller than those of the large wind tunnel. Probes were traversed vertically through the boundary layer by an external actuator. The X-axis was parallel to the ceiling in the flow direction, the Y-axis was perpendicular to the ceiling in the flow direction, and the Z-axis was parallel to the ceiling and perpendicular to the flow direction.

B. Instrumentation

1. Hot Wire Probes. The hot wire was used as the basic sensing element for all correlation measurements and turbulence measurements. The material for the hot wires was 80 percent platinum, 20 percent iridium, 0.0004-in. (0.01-mm) diameter wire. The wires

were operated by constant temperature hot wire anemometers designed at Colorado State University by Finn and Sandborn [70]. Figure 9b1 is a photograph of the anemometers. Figure 10 shows probes of five different designs which were used during the running of the experiment. The first probe (Fig. 10a1) was used for spatial separation measurements in the Z-direction of the inner-outer correlations. One wire was placed close to the wall and the other in the intermittent outer edge of the boundary layer. The second probe (Fig. 10a2) was a manifold of twelve hot wire elements erected in the Y-Z plane with its major axis in the Z-direction. Nine of the twelve wires were in the Z-direction and were used for inner-outer correlations as well as spatial correlations. The three remaining wires were in the Y-direction for use in space correlations. The next three probes (Fig. 10a) were used in traversing the boundary layer for taking mean, turbulent, and convective velocity profiles. Each of these probes used two wires: the lead wire being used to make mean velocity and turbulence measurements, and the second wire being directly downstream from the lead wire but out of the lead wire's wake. The downstream wire was used to correlate with the lead wire to measure a convection time for the flow to traverse from the lead wire to the second wire. The length of wires used ranged from 0.05 in. (1.3 mm) to 0.16 in. (4.1 mm). The wires ranged from about 3 to 20 ohms cold resistance. Separation distance between the leading wire and the lagging wire ranged from 0.002 ft (0.00061 m) to 0.0275 ft (0.00084 m). Tapered piano wire or jeweler's broaches were used for the hot wire supports. The piano wire or jeweler's broaches were soldered to conventional copper lead wire, which was connected to the anemometer. The hot wire anemometer is comprised of a sensing element and a control unit. The output of a constant temperature hot wire anemometer depends on the temperature difference between the wire and the local fluid temperature, and the velocity of the flowing fluid. There are many different sensing materials which may be used.

The hot wire anemometer is able to sense a number of fluid properties which may in some way transport heat either to or from the sensing element. The temperature of the flow was held constant and the pressure fluctuations were very small. It was thus assumed that the only first order heat transfer effect was produced by the convection properties of the fluid passing over the wire. Therefore, for this case where an overheat ratio of 1:1 is used, the "hot" wire will, in general, sense only velocity fluctuations [71]. For the convective velocity measurements, a calibration of voltage versus velocity is not necessary. Only a measure of the ability of the flow to transport its heat transfer qualities is necessary.

The hot wire is also used for the mean and turbulence measurements. The output voltage of the hot wire is a measure of the velocity of the flow.

To obtain accurate calibration curves, the calibration measurements of the hot wires were taken in the free-stream section of the wind tunnel against a calibrated pitot tube. An averaging circuit, included as an integral part of the anemometer housing, was used to obtain an integrated averaged voltage.

Each hot wire was annealed before its calibration and use. That is, the wire was heated until red hot, and was allowed to "cook" until the hot wire characteristics became stabilized. The hot wires were calibrated before and after each run. A typical calibration curve is given in Figure 11. The slope of the calibration curve $\partial E/\partial U$ is the sensitivity of the hot wire to velocity. Velocity rms values were calculated by measuring the rms and the mean value of the signal, with the local sensitivity, $\partial E/\partial U$, being determined graphically at

(a) VARIOUS HOT WIRES

1. ORIGINAL INNER-OUTER PROBE
2. 12 WIRE MANIFOLD FOR INNER-OUTER CORRELATIONS AND SPACE CORRELATIONS
3. 2 WIRE PROBE FOR CONVECTIVE VELOCITIES
4. 2 WIRE PROBE FOR CONVECTIVE VELOCITIES
5. 2 WIRE PROBE FOR CONVECTIVE VELOCITIES

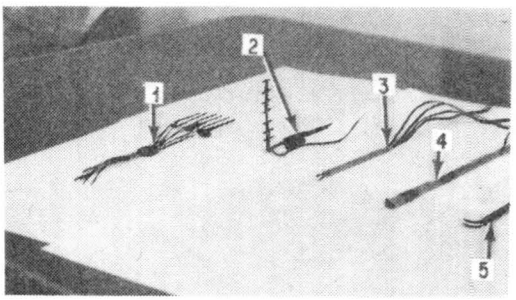

(b) PRINCETON CORRELATOR

1. GAIN CONTROLS
2. COUPLING CONTROL
3. SIGNAL DELAY CONTROL
4. READOUT RATE
5. INPUT CHANNELS
6. OUTPUT OF TIME BASE
7. OUTPUT OF CORRELATION

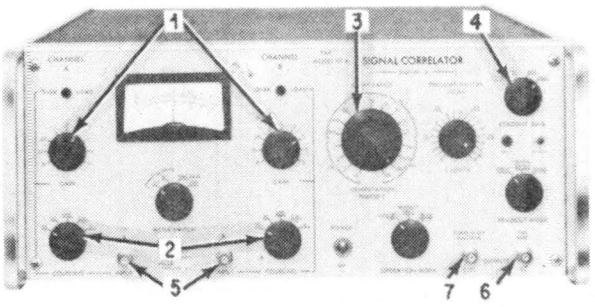

Figure 10. Instrumentation.

the mean value of the signal, E. Multiplying $\partial U/\partial E$ with the rms of voltage, $\sqrt{e^2}$, gives the rms of the velocity, $\sqrt{u^2}$. An error could arise in this evaluation if the turbulence intensity becomes too great, although this is not a problem for turbulence intensities below approximately 15 to 20 percent [71]. High turbulent intensities are encountered near the boundary, and these measurements are therefore less accurate. The sensitivity of a hot wire to flow direction and an empirical solution for the hot wire evaluation are given by Zoric [67]. Sources of error such as solid boundary effects, wire length, velocity gradient, and turbulent intensity are covered by Tieleman [66] and Zoric [67].

For convective velocity measurements, a new source of error may be a phase or time-delay mismatch of the anemometer electronics. The convective velocity measurement relies on the fact that time-delay separation of leading and lagging wires is dependent only upon the convective flow velocity. The two hot wire anemometers used in the research were checked for differences in time delay or phase shift. By placing both of the hot wire sensing elements very close together in a turbulent flow, and cross-correlating the output of the two systems, any time-delay errors would be seen as a difference between the auto- and cross-correlations. Figure 12 shows the result of one such test. The units were found to be identical for the purposes of this experiment.

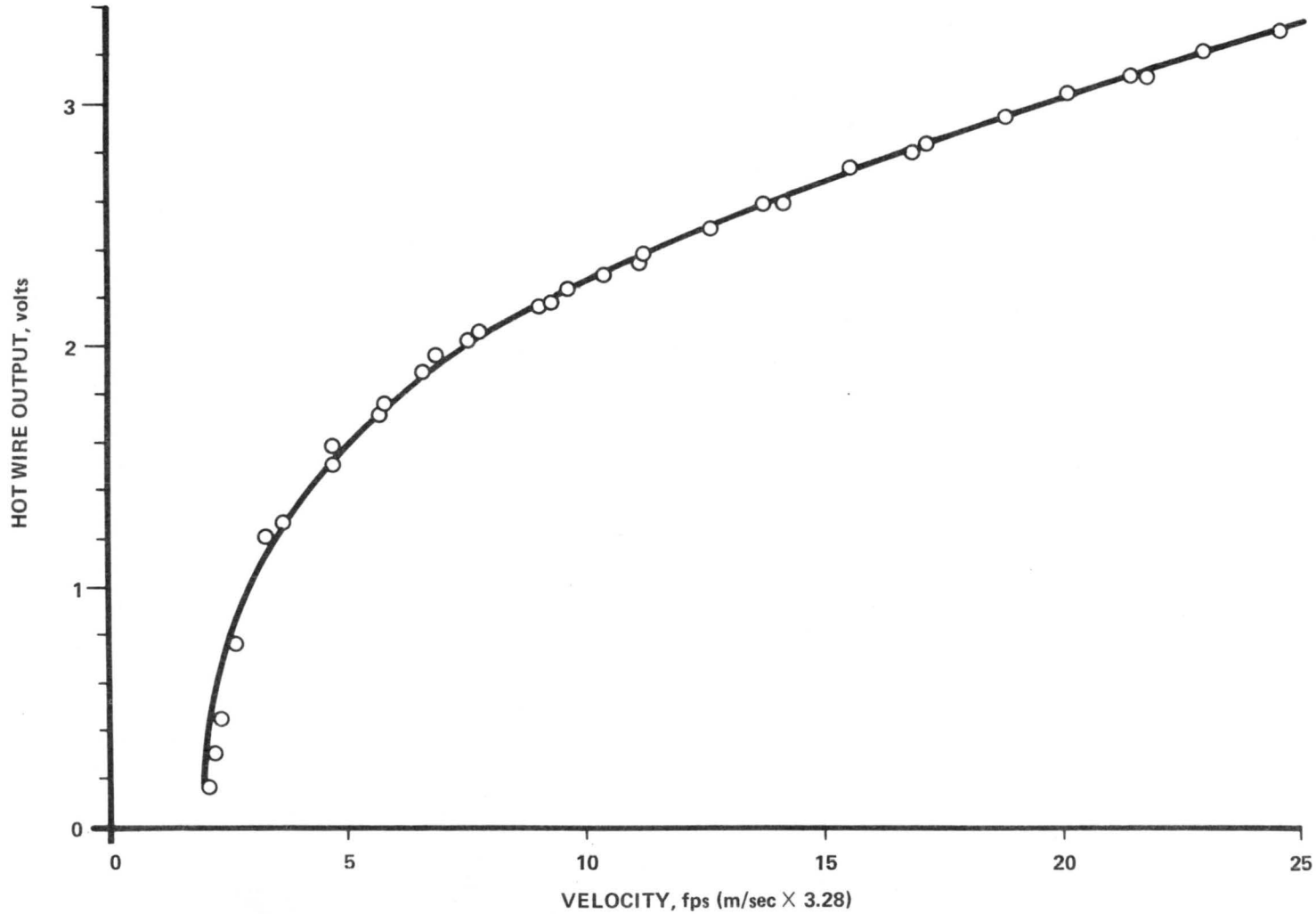

Figure 11. Hot wire calibration curve.

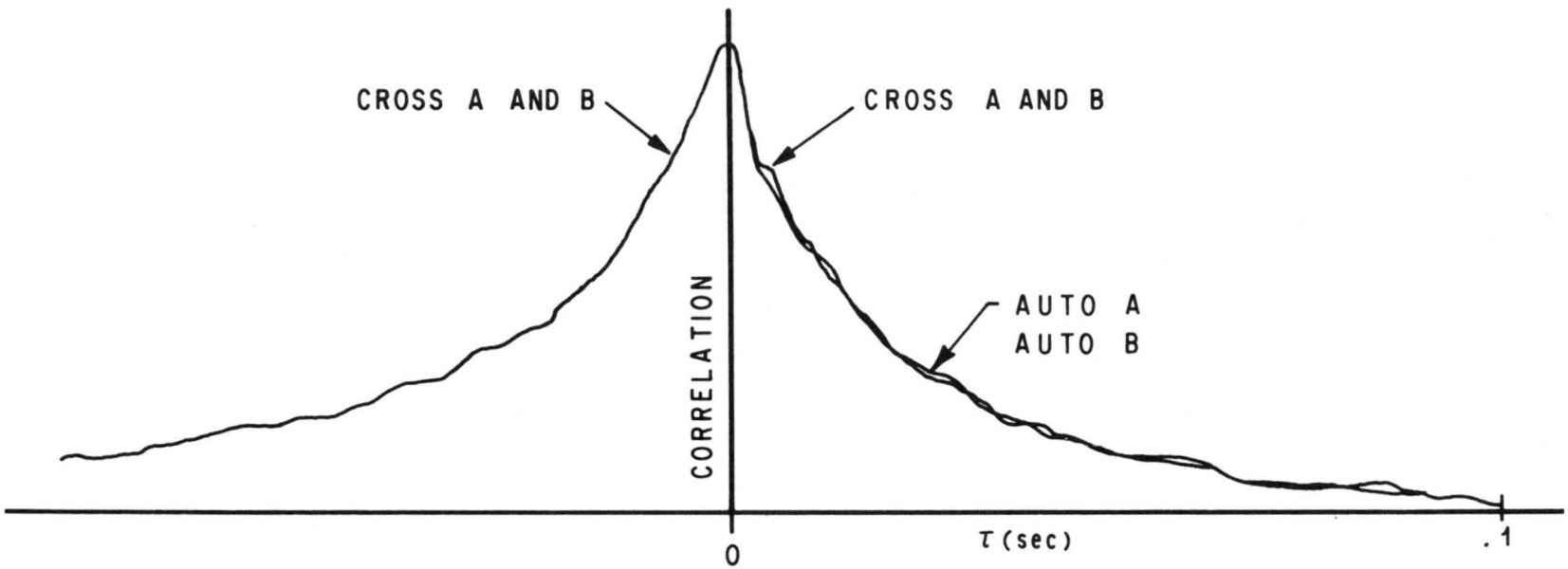

Figure 12. Phase check of hot wire units.

2. Pitot-Static Tube. Mean velocity was measured by a standard 1/8-in. (3.18-mm) diameter pitot-static tube. The pitot tube used for mean velocity measurements was calibrated by comparing it with a laboratory standard pitot tube. The standard had previously been calibrated by placing it on a whirling arm, the length of which is known. With this information, along with the number of revolutions made per unit time and correcting for swirl effects, the laboratory standard was calibrated. The pitot pressure from the laboratory standard was read on a water, U-tube micromanometer, as was the case for the test pitot tube. The micromanometer has been calibrated from laboratory standard micromanometers. The possible sources of error for the mean velocity measurement are covered by Zoric [67]. They were found to be negligible for this experiment.

3. Actuator. Two types of actuators were used for precision placing of the sensors in the vertical direction of the boundary layer. The first was a stand-type model, which was set directly on the floor of the meteorological wind tunnel. A small electric motor with a screw-type gear was used to change the probe elevation. A variable potentiometer which changed resistance as the carriage moved up or down was used to determine the elevation of the probes. The second type of actuator extended a rod through the ceiling of the separation wind tunnel. Variations in the external length of the rod gave a direct measure of the probe location in the flow. This actuator was also controlled with an electric motor and a resistance potentiometer with an emf output to measure the elevation of the probe. The first actuator, used in the meteorological tunnel, had a range of approximately 18 in (0.46 m) while the second actuator had a range of about 6 in. (0.15 m). In both cases initial conditions of probe placement were determined with a standard length scale, within an accuracy of 0.005 in. (0.13 mm).

4. Electronic Filters. The filters used in this study were continuously adjustable from 0.2 Hz to 20 kHz in either a low-pass or high-pass mode. Filter attenuation and phase shift as a function of frequency were found to be identical for the two filter banks employed. Attenuation of the filter units shown in Figure 9b, was 24 dB per octave.

Since filters may cause nonlinear phase shifts as a function of frequency, two electronic filtering systems that are not identical would produce what appears to be a time delay between two identical signals after passing through the filters. Thus, a calibration and check procedure was used to determine phase differences as a function of frequency for the filters used in this experiment. All possible types of auto- and cross-correlations of filtered hot wire signals were used to check for phase differences. The same signal was fed through each filter and then correlated. Similarly, identical sine waves were used. Both cases showed the filters to be identical as far as the present study was concerned.

Figures 13 and 14 show the phase checks using a hot wire signal as the emf.

5. Time Correlator. For auto- and cross-correlation of hot wire signals, the Princeton Applied Research Correlation function computer model 101 was used (Fig. 10). The correlator is a hybrid computer which uses both analog and digital techniques. The correlator shifts one signal in time, multiplies the two signals together, and integrates. It performs the operation for 100 discrete points each separated by a time shift of $\Delta\tau$. The time shift $\Delta\tau$ between successive points may be selected. The correlation may be examined from 0 to 100 $\Delta\tau$ in steps of $\Delta\tau$. A precomputation period may also be selected, so that

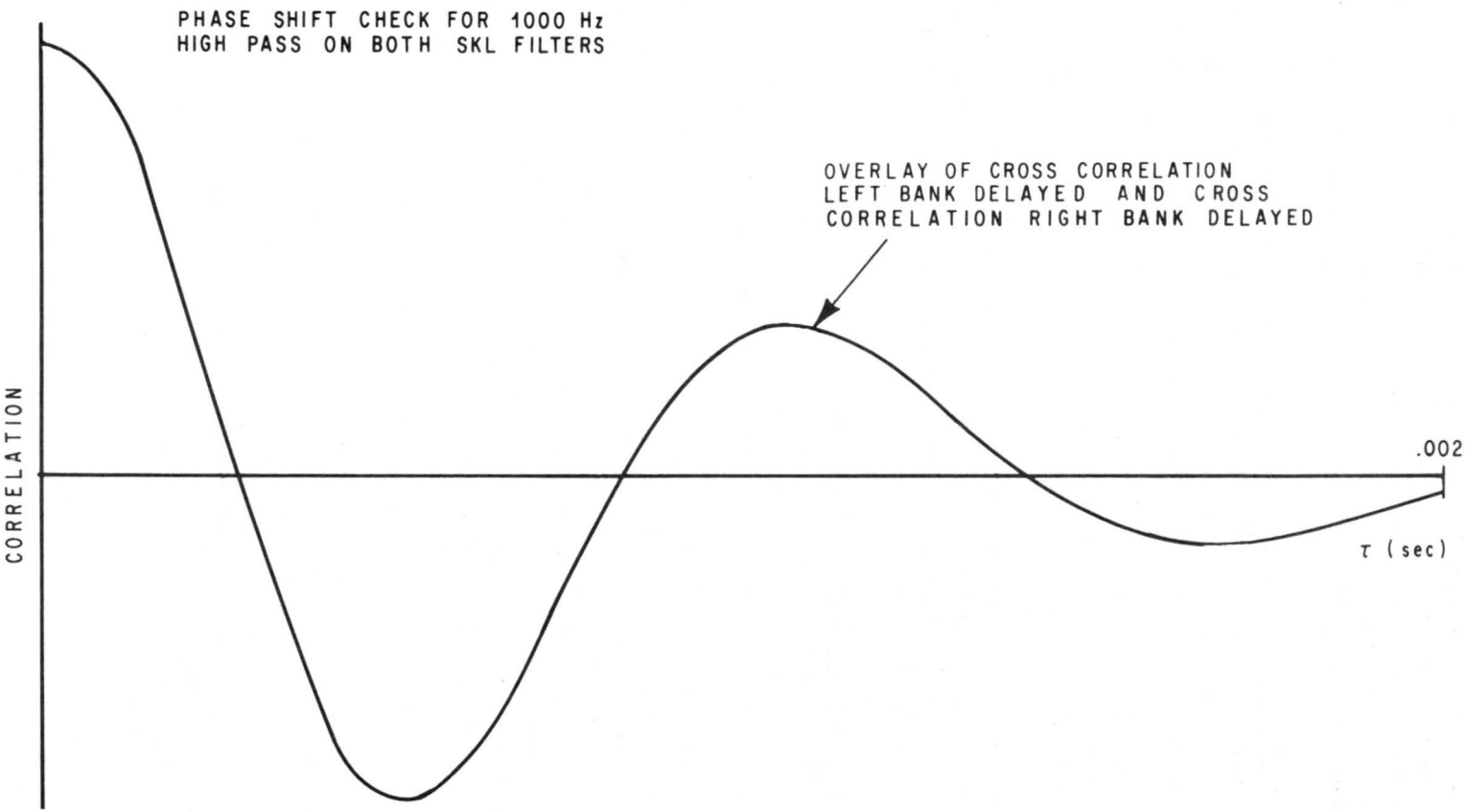

Figure 13. Phase check of filters.

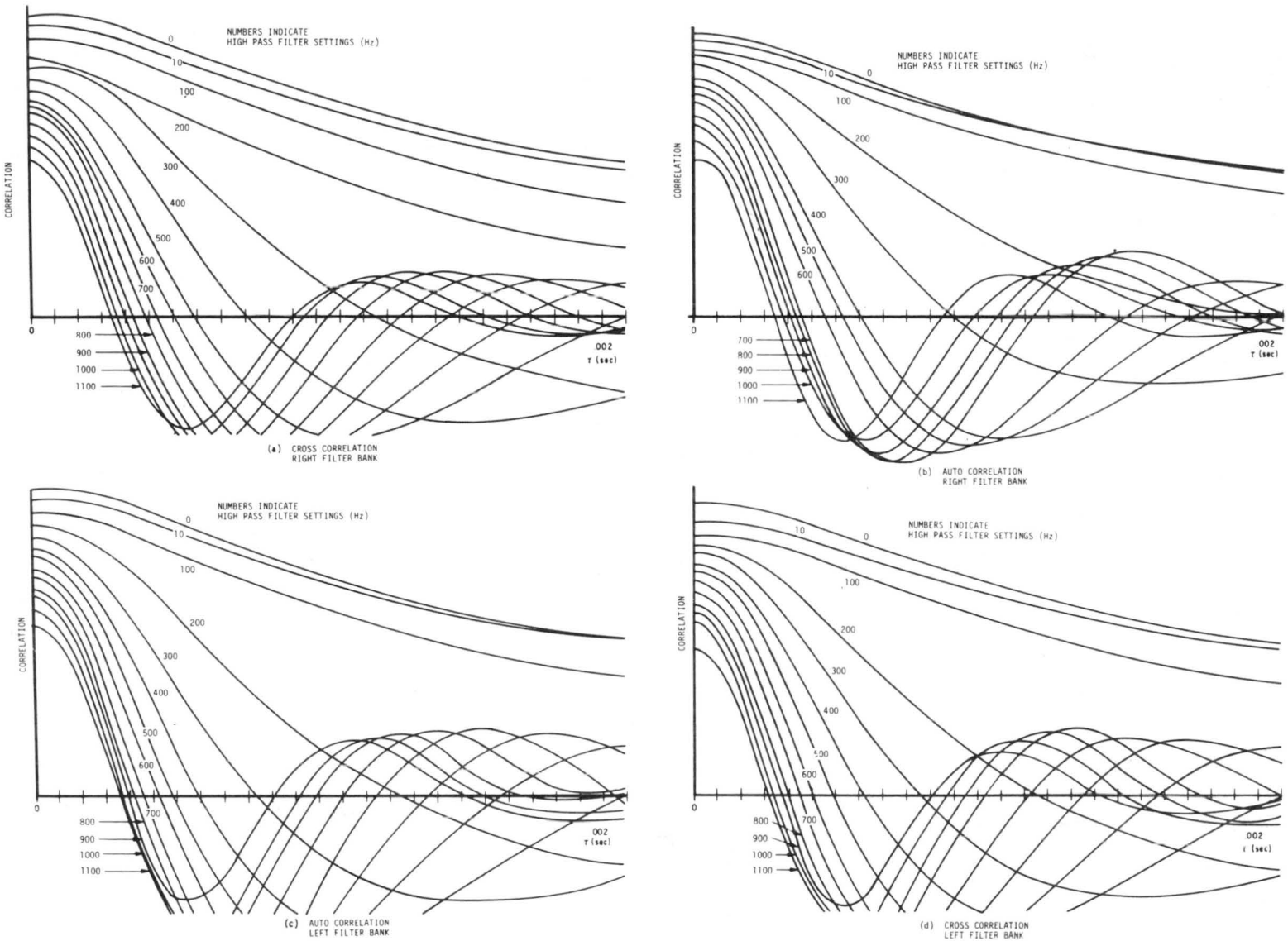

Figure 14. Correlation phase check of filters using typical hot wire signal.

the initial time delay is not 0, but j(100 $\Delta\tau$), where j may be selected from 1 to 10. The term 100 $\Delta\tau$ may be selected from 0.0001 to 10 sec. Readout circuitry allows the continuous monitoring of the function during operation. The correlation function may be either viewed on an oscilloscope or plotted on an X-Y plotter or strip chart recorder. The accuracy of the unit is within 1 percent of the ideal function. Both ac and dc couplings are available.

The correlator was checked for phase shift and time delay within its own dual circuitry by cross-correlating a sine wave from a calibrated function generator. This check is good for both phase shift and time delay calibration. The magnitude of the correlator compared with a calibrated rms meter was found to be in calibration.

6. Tape Transport. The tape transport used in this experiment was a 14-channel standard I-rig (Fig. 9b) recorder. The recorded signals were FM modulated. The carrier frequencies were calibrated with a special commercial unit. The 14 channels are split into two sets of heads, one set for odd numbered channels and one set for even numbered channels. Only odd channels, or only even channels, were used when recording a run to avoid time-displacement errors caused by the physical separation of the heads. Interchannel displacement errors were checked by recording various frequency sine waves and correlating the outputs. Any off-zero peak of the correlation would indicate a time-displacement error in the recorder. For frequencies less than 100 kHz, no error could be detected. Frequencies of interest for this experiment were below 2 kHz. Dynamic interchannel time placement errors in the recorder were also checked and found to be inconsequential.

7. Other Instrumentation. The ordinary types of instrumentation which are common will not be described in detail, but rather are listed so that the reader will have a feeling for the type of instrumentation needed for this type of experiment. They are oscilloscopes, function generators, rms meters, digital voltmeters, and X-Y plotters. The type of transport described above is also desirable, so that the identical signal may be analyzed for all computations, some of which must be done recursively.

The time base of the correlator was used to calibrate the X-component of the X-Y plotter, and a standard cell was used for amplitude calibration.

C. Convective Velocity Computations

The convective velocity was determined by the following procedure:

1. Orient two spatially separated hot wires in the direction of the mean flow.

2. Measure the magnitude of the hot wires' separation.

3. Cross-correlate the output from the two spatially separated sensors.

4. Determine the time delay for which the cross-correlation is a maximum.

5. Now, dividing the separation distance by the time delay for which the correlation was a maximum gives the convective velocity. We see that simultaneous filtering of phase matched systems may be used to describe convective velocities of various frequencies.

D. Inner-Outer Correlation Measurements

The velocity fluctuations in the intermittent outer region were correlated with velocity fluctuations near the wall using two hot wire sensing elements in the respective locations. Signals were put directly into the correlator, which was described previously. The normalized correlation is used to give a relative measure of the similarity of the two signals, and it gives some insight into a possible mechanism for the triggering of turbulent production near the wall. A time delay of the correlation other than zero would indicate the length of time for the production process to acknowledge a stimulus produced at the outer edge.

E. Data Reduction of Time Series

Because of the length of this subject it has been placed in Appendix D. General signal analysis is covered, as well as some extensions which give insight into methods of dealing with convective velocities in Fourier transformation planes. Restrictions imposed upon correlations by either finite time series lengths or certain degrees of nonstationarity of the time series are examined. The effect of space and frequency weighting functions on the normalized cross-covariance is analyzed, and finally the space-time covariance is viewed as to its relationship with the probability density distribution of the original time series.

VI. EXPERIMENTAL RESULTS AND DISCUSSION

The theoretical model presented in Section III predicts the occurrence of several phenomena, some of which have been confirmed by previous investigators.

The objective of this section is to present experimental evidence confirming the physical model presented earlier. Experimental evidence shows correlations of the intermittent outer edge with flow near the wall. Data confirming the existence of a formation zone where the convective velocity is independent of wave number are presented. The convective velocity is seen to be a function of wave number throughout most of the boundary layer. The convective velocity is shown to approach the mean velocity in the outer portion of the boundary layer at a distance downstream, as predicted by the model. Several special cases concerning the convective velocities will also be examined.

A. Outer-Inner Correlation

The correlation between the intermittent outer edge of the boundary layer with flow near the wall was evaluated in the small wind tunnel previously described. The boundary layer thickness was about 3 in. (0.076 m) with a free-stream velocity of approximately 30 ft/sec (9.15 m/sec). The basic principle involved was to determine if a correlation existed between the velocity fluctuations of the undulating outer edge of the boundary layer and the turbulence near the wall.

The outer-inner correlation was performed by placing a hot wire in the highly intermittent outer region of the boundary layer and one very near the surface. Both wires were oriented normal to the flow and parallel to the surface. The size and type of wires used are described in paragraph V.B.1. A sketch of the setup is given in Figure 15b. The signals were ac-coupled and cross-correlated. The normalized cross-covariance was then computed. The experimental values of the correlation obtained were about 0.1. Figure 15a shows a typical experimental curve. It was always found that a time delay existed between the two sensors for the peak of the correlation; that is, the maximum correlation occurred when the signal from the wire near the wall was delayed slightly in time before correlating it with the wire in the intermittent outer region. In an attempt to see if it was possible to get a maximum of the correlation to occur nearer zero time delay, the lower sensor (sensor y in Fig. 15b) was slowly moved upstream. Moving the probe upstream so that the lower probe was either directly under or upstream of the outer probe resulted in the complete elimination of a measurable correlation. A measurable correlation could only be obtained when the sensor near the surface was slightly downstream of the outer probe. This result seems to give support to the assumption that disturbances are transmitted from the outside of the boundary layer to the inside, and not vice versa. The vanishing of the correlation, when the inner probe is moved upstream of the outer probe, gives some confidence that the correlation did not result from large scale circular structures that pass through both probes simultaneously.

Other configurations of wire geometry were also used for this correlation; for example, the outer wire parallel to the mean flow and the inner wire normal to both the mean flow and floor. The configuration where both wires were perpendicular to the flow produced the same result as that above. The manifold-type of probe (Fig. 10b) was also used with the same results. These measurements are in agreement with the physical model presented at the beginning of this report. Laufer and Narayanan [59] have shown that processes occurring near the viscous sublayer scaled with outer flow parameters.

The experimental test run, correlating the inner and outer edge of the boundary layer, tempts one to speculate about the role of the outer edge in the onset of turbulence near the wall. It may be inferred that information is fed into the near surface region of the boundary layer from the undulating intermittent outer edge.

B. The Formation Zone

The physical model required the assumption that there is a region near the surface where the convective velocity is identically equal to that of the local mean velocity. Convective and mean velocity measurements were made simultaneously across the boundary layer to determine if such a condition did exist.

The convective velocity was calculated using two spatially separated hot wires. The wires were spatially separated in the direction of the mean motion. The lead hot wire was used to measure mean velocity as well as the turbulent velocities. The cross-correlation of the ac-coupled lead wire with the ac-coupled second wire was evaluated. A maximum correlation at some finite time delay was obtained. (Figure 16 is a typical example of the correlations that were found.) The spatial separation of the wires divided by the time delay at which the maximum correlation occurred was then considered a measure of the convective velocity; that is,

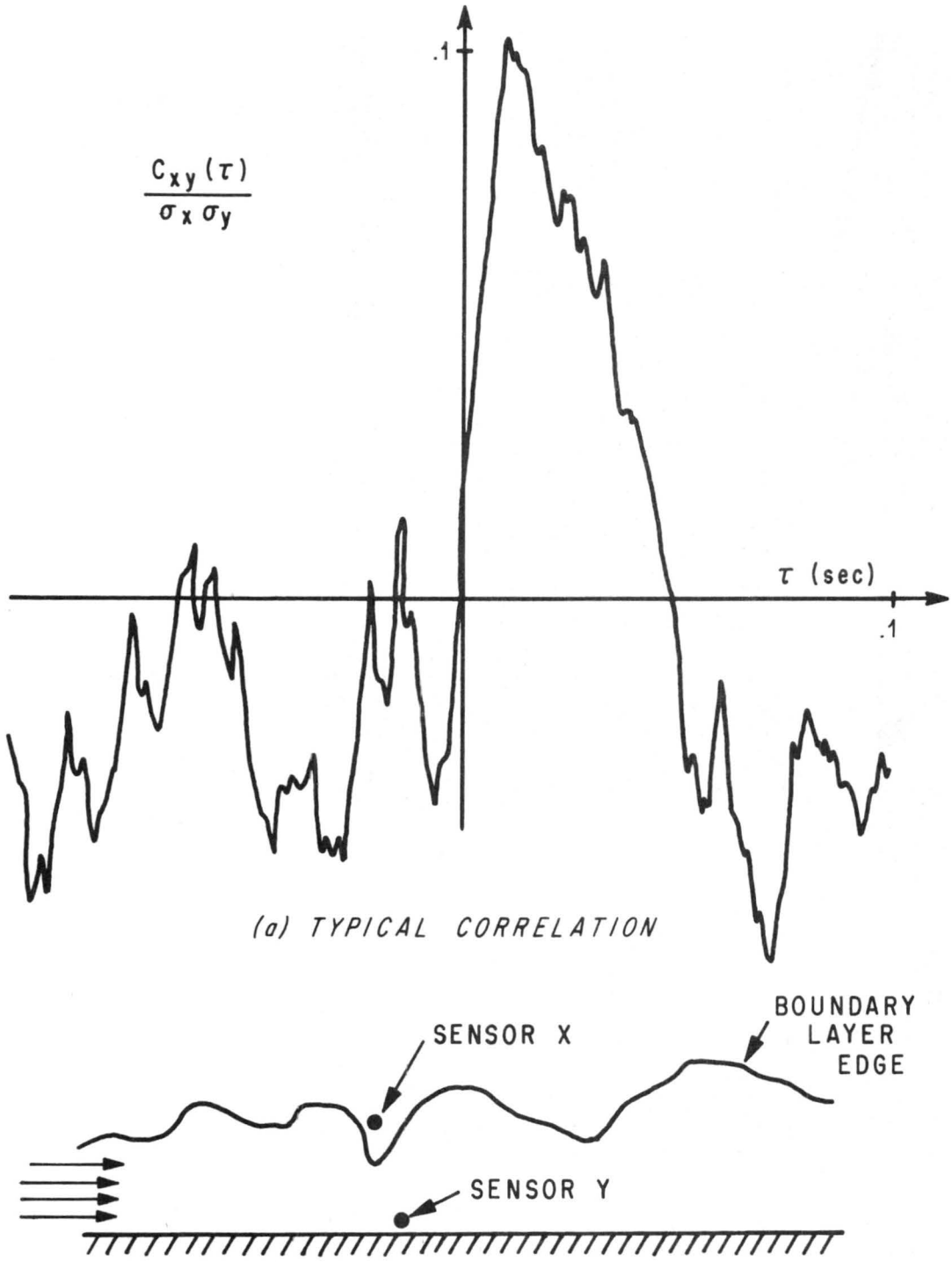

Figure 15. Inner-outer correlation.

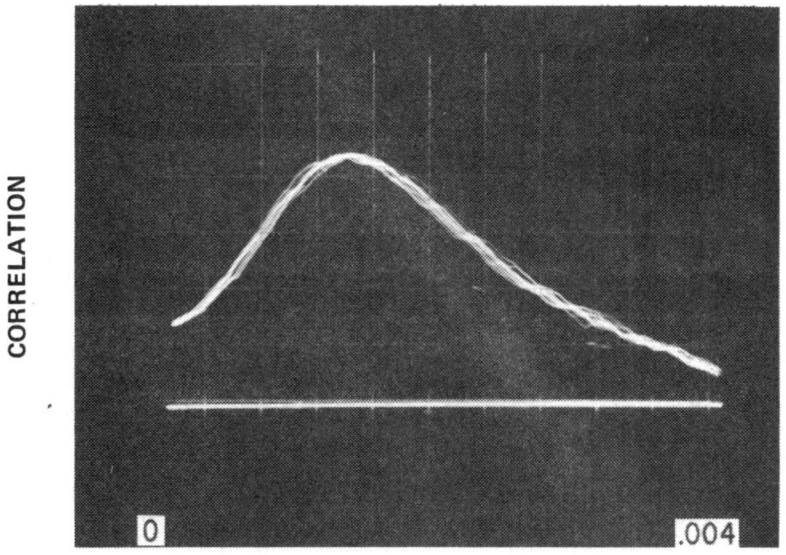

(a) $\tau_M \sim 0.004$ sec

ELEV. = 3.670 in. (9.33 cm)

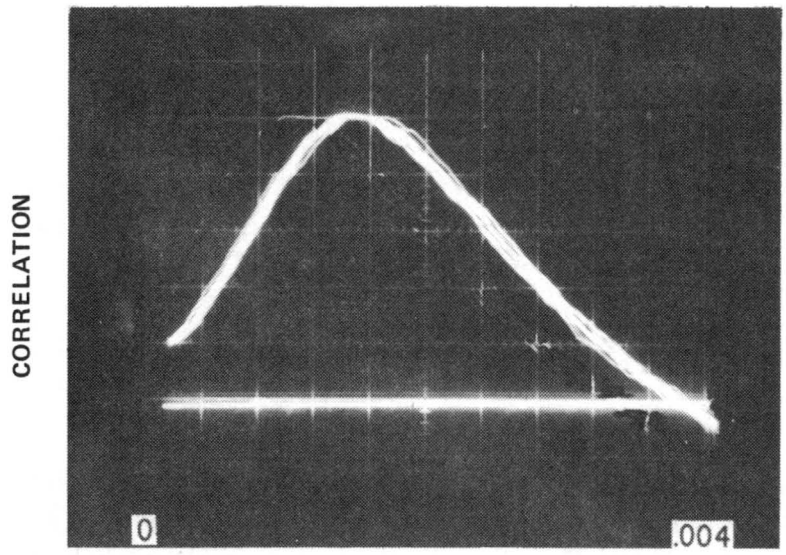

(b) $\tau_M \sim 0.004$ sec

ELEV. = 2.620 in. (6.65 cm)

Figure 16. Correlation curves with no filtering in the outer region.

$$C_v = \frac{\Delta W}{\tau_m} \quad . \tag{40}$$

Figure 6 gives a graphical picture of this process, where C_v is the convective velocity in the direction of the spatial separation, ΔW, and τ_m is the time delay at which the cross-correlation is a maximum. Section IV describes the convective velocity concept in more detail.

Figures 17 and 18 show the experimental results obtained across two different boundary layers. (Note: Two different wire separations were used for these two sets of measurements.) Both of these flat plate velocity profiles give a region where the mean and convective velocities are equivalent. It appears that this may be more likely a region than a point, where the two profiles are very nearly equal. The location of the region corresponds closely with that observed by Kline et al. [2, 33] in the visualization studies. The convective velocity is less than the mean velocity in the outer portion of the boundary layer. At the same time, the convective velocity is higher than the mean velocity profile below the formation zone.

The problems associated with one wire following downstream of another must be evaluated. One must be sure that the trailing wire is not affected by the wake of the upstream wire or probe. This was checked by moving the front probe slightly, and seeing if there was an effect on the dc level of the second wire. That is, if the second wire was in a wake flow caused by the leading wire or probe, the mean velocity recorded by the second wire would be less than if the front wire or probe was not there. The fact that the convective velocity exceeds the mean velocity indicates that the convective velocity is not a probe-interference phenomenon and gives some assurance that the second probe is not in the wake of the first. Closely spaced, large wires would be more prone to interference errors. The rear wire was also shifted up and down to see if a velocity defect region existed. There was no indication that the second wire was in the wake of the first.

The cross-correlations of the longitudinal velocity fluctuations across the boundary layer are seen in Figures 16, 19, and 20. It is interesting to note the sudden decrease in amplitude of the correlation near the wall. The decrease is in part due to the fact that the high frequency spectral components are dissipated in the viscous subregion.

Appendix D, paragraph F, shows the relationship between the probability density distribution and the covariance computation. Equation (D-93) shows that, since the covariance is a squared function of the perturbation size and a linear function of time, the larger excursions from the mean are the most heavily weighted. It is also found that if the turbulent velocities continue to propagate with the velocity indicated at the first sensor, equal perturbations above and below the mean velocity will create correlations of equal magnitude at time delays equally spaced about the time delay that indicated the mean velocity.

It is anticipated that a symmetrical probability density distribution will produce a correlation peak that will indicate the mean velocity. Figure 21 shows the probability density distribution and probability distribution at specific points in the flat plate boundary

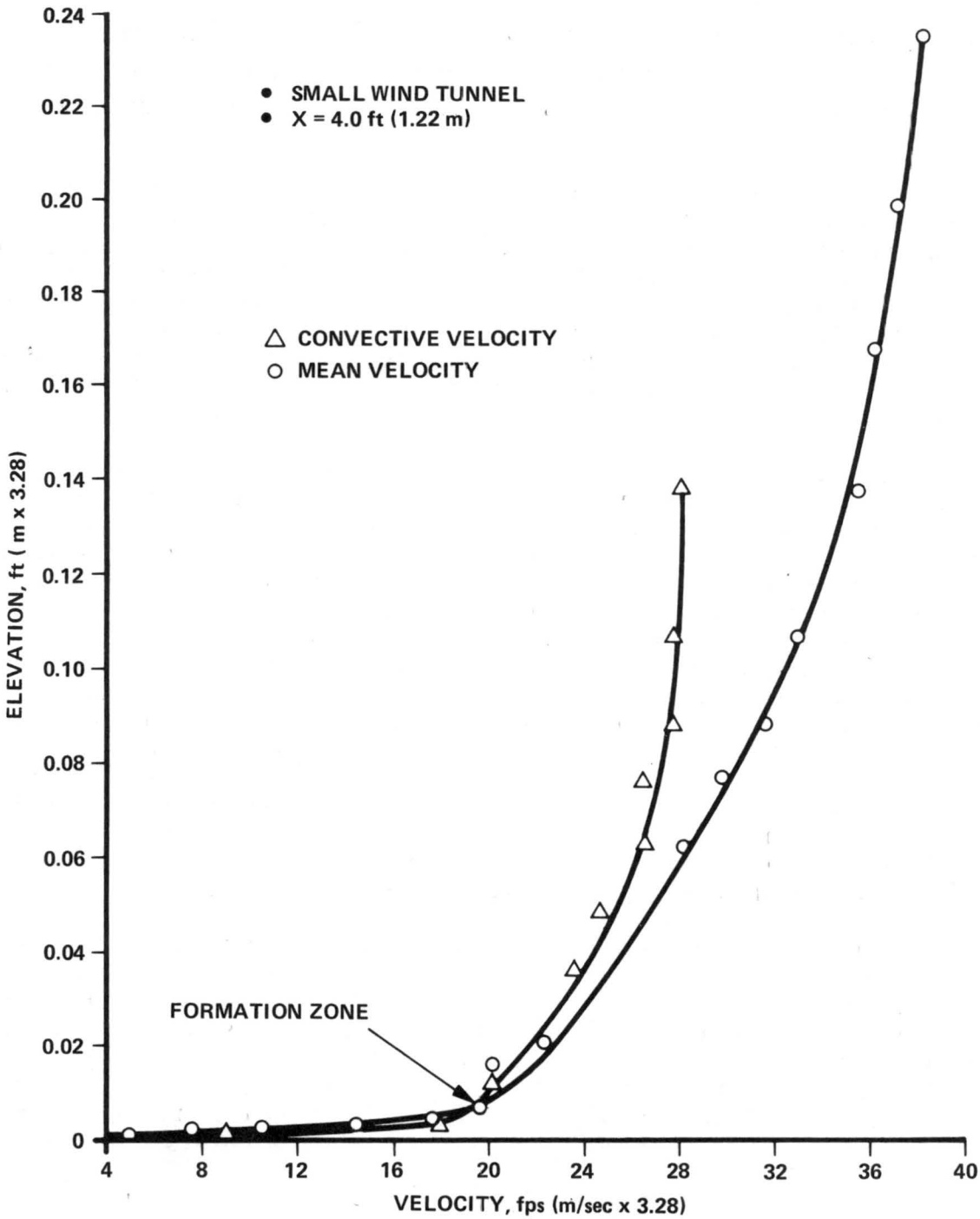

Figure 17. Mean and convective velocity versus elevation, $\Delta W = 0.0233$ ft (7.1 mm).

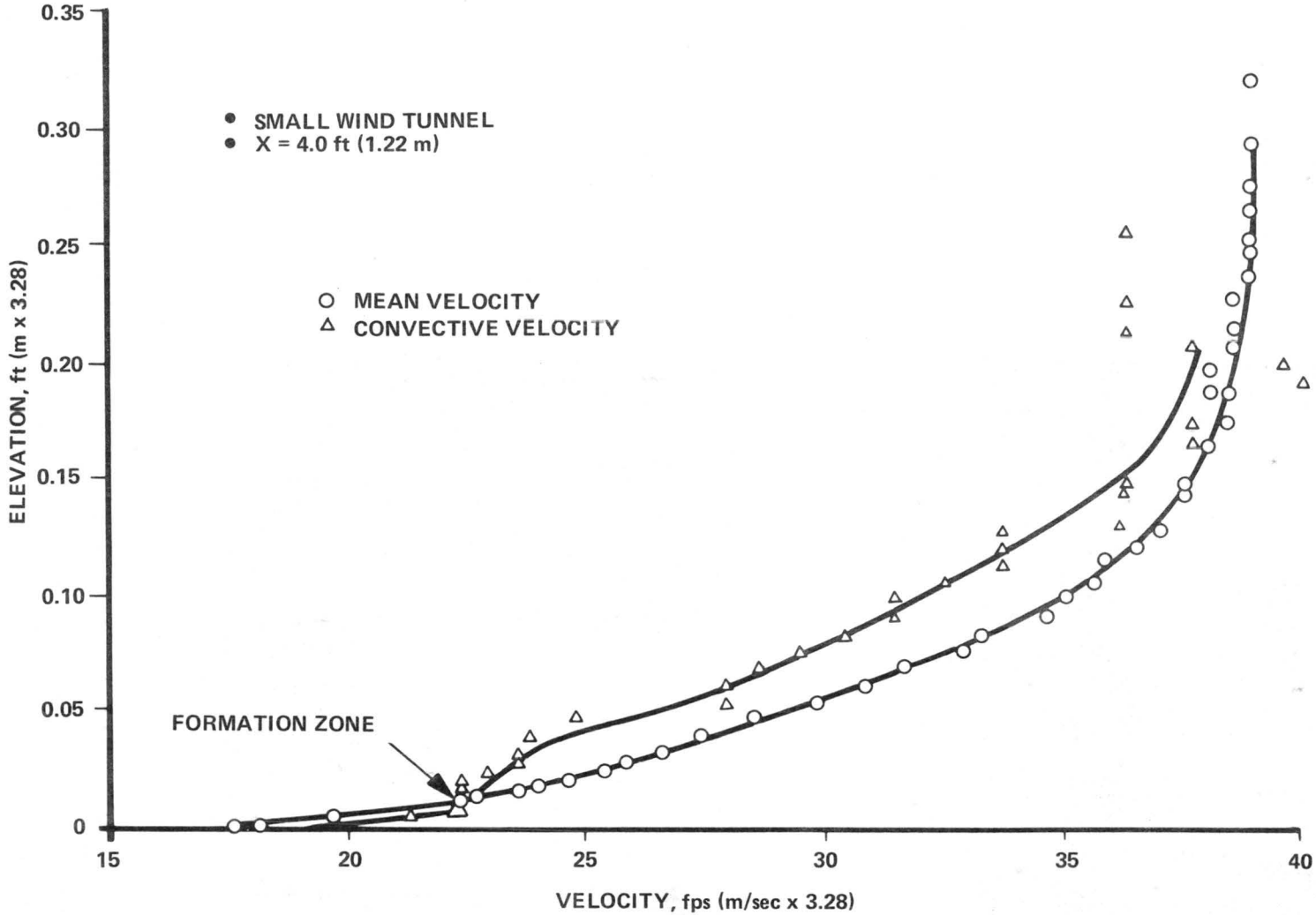

Figure 18. Mean and convective velocity versus elevation, $\Delta W = 0.0183$ ft (5.58 mm).

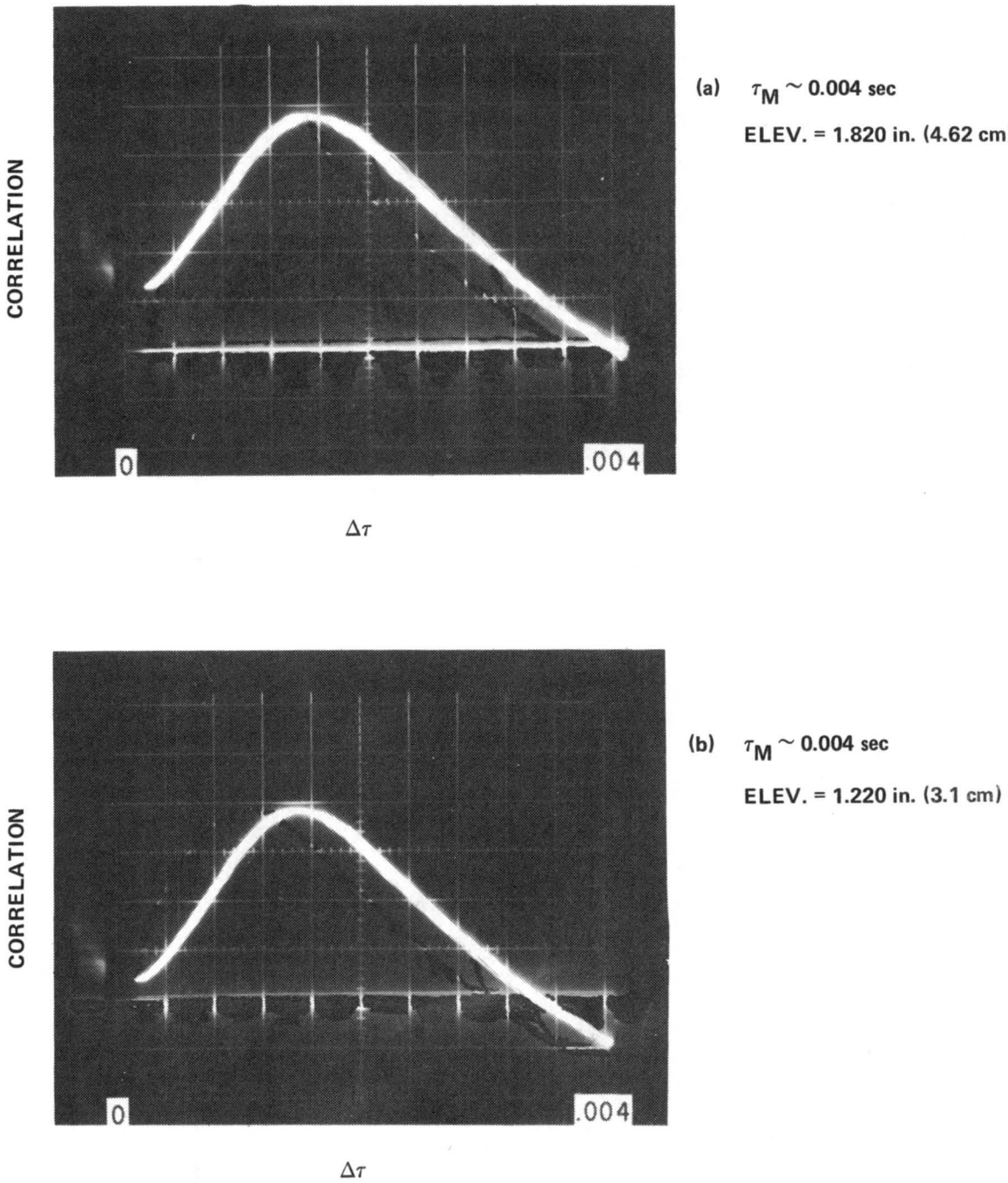

Figure 19. Correlation curves with no filtering.

layer, which was about 2 in. (5.08 cm) thick at the point of measurement. Figures 21, a and b, show the distributions near the outer edge of the boundary layer. The obvious skewing toward the negative side indicates that the convective velocities will be substantially lower

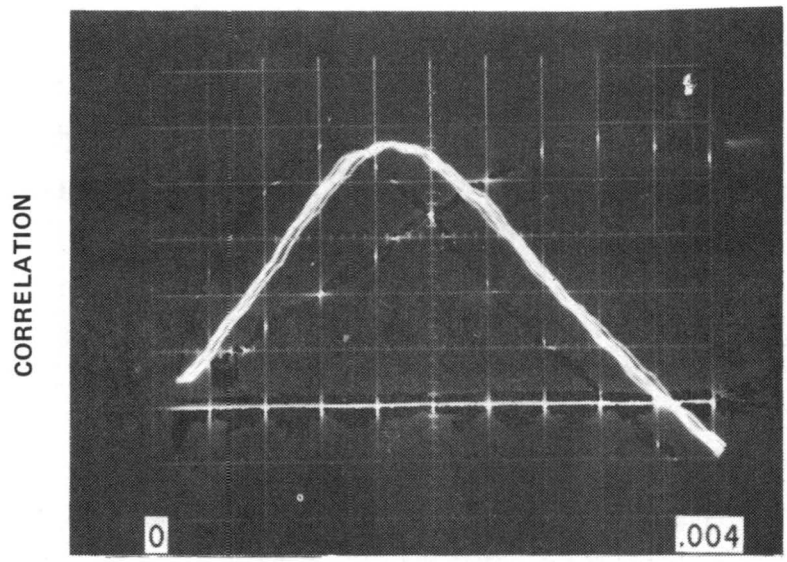

(a) $\tau_M \sim 0.004$ sec

ELEV. = 0.635 in. (1.61 cm)

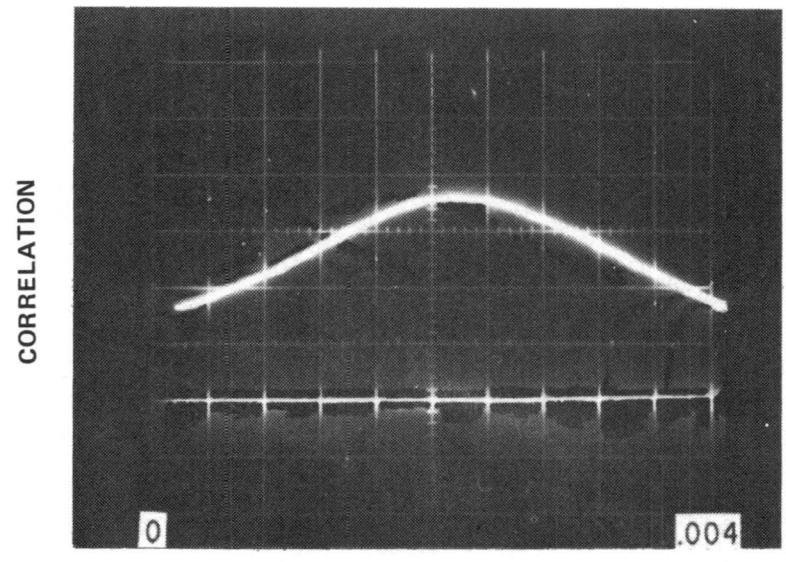

(b) $\tau_M \sim 0.004$ sec

ELEV. = 0.240 in. (0.605 cm)

Figure 20. Correlation curves with no filtering near the surface.

than the mean velocity at these locations. This indication of a lower convective velocity agrees with the actually measured convective velocities. Figures 21, c through f, show the probability densities closer to the wall. The distributions are skewed over a large part of the

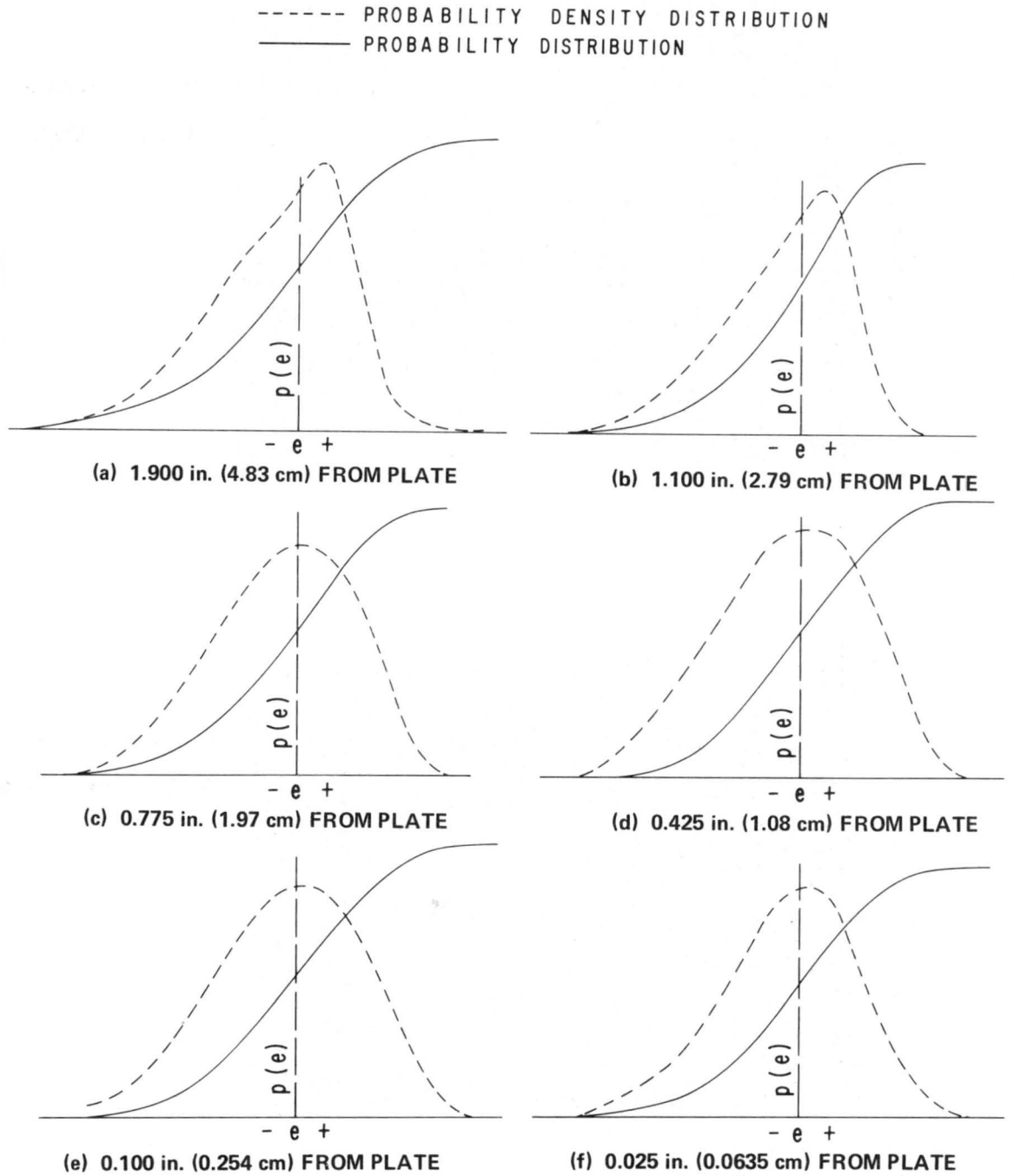

Figure 21. Probability distributions in the flat plate boundary layer, 26 in. (0.66 m) from start of test section, free stream 40 ft/sec (12.2 m/sec).

boundary layer. Only very near the wall does the probability distribution appear symmetrical. A symmetrical probability distribution would indicate that the convective velocity is almost equal to the mean velocity (Appendix D, paragraph F).

As noted in Appendix D, paragraph F, if the probability distribution indicates a skewing toward the positive or negative velocity fluctuations, the convective velocity will likewise be correspondingly higher or lower than the mean velocity. The correlation function is built up by all the velocity contributions of the probability distribution. The wings of the probability distribution are the most heavily weighted. A convective velocity less than the mean would give a time delay greater than the time delay for the mean velocity; a convective velocity greater than the mean would give a time delay less than that for the mean velocity. Appendix D, paragraph F, gives the contribution produced by each turbulent velocity acting over some finite time interval. Thus, a skewing of the probability distribution is propagated into a skewing of the shape of the correlation function. Figures 16, 19, and 20 are photographs of the correlation function for various Y-distances. Note that the correlation curve skews to the right at the outer edge of the boundary layer and becomes more symmetrical nearer the surface. The shapes of the probability distributions and correlation functions are consistent with the proposed physical model. The symmetries of the correlation function and probability density distribution are consistent with the production zone of the model. Here the convective velocity is equal to the mean velocity, so that symmetrical correlations and probability density distributions are observed.

C. Convective Velocity Profiles as Functions of Frequency

This section presents experimental data to support the physical model's hypothesis that the boundary layer will frequency-filter the packets of vorticity that migrate from the production zone; that is, the packets will be separated according to frequency. Also, some support is given to justify associating frequency with size.

The analysis in Section IV required that the boundary layer local velocity separate the various scales as they migrate from the production zone. In general, only at the point of origin, where all scales are moving with the mean velocity, should the convective velocity be independent of frequency. The special case when the convective velocities have reached equilibrium with the mean flow will be discussed later.

Convective velocity measurements were taken across a flat plate, zero pressure gradient boundary layer using various wire separations. Willmarth et al. [51, 52] noticed that the convective velocity of pressure fluctuations on the floor of a flat plate boundary layer were functions of sensor separation. The measurements taken during this experiment also showed that for very closely spaced sensors, the convective velocities are a function of sensor spacing. The convective velocity for closely spaced sensors is lower than convective velocities measured with larger separations for the same frequencies.

Figure 22 shows the measured mean velocity profiles along with convective velocity profiles for various frequencies. Phase-matched filters were used together with the two hot wires, as indicated in paragraph VI.A, to obtain Figure 22. The normal dropoff of the turbulent spectrum acted as a low pass filter, while electronic filtering was used for the high pass filtering. This combination of electronic filtering and turbulent spectral rolloff acts as a notch filter, which allowed the evaluation of convective velocity for narrow bandwidths. Figure 22 represents convective velocities measured with different separations between the sensors. In all cases the farther from the production the measurement is made, the greater

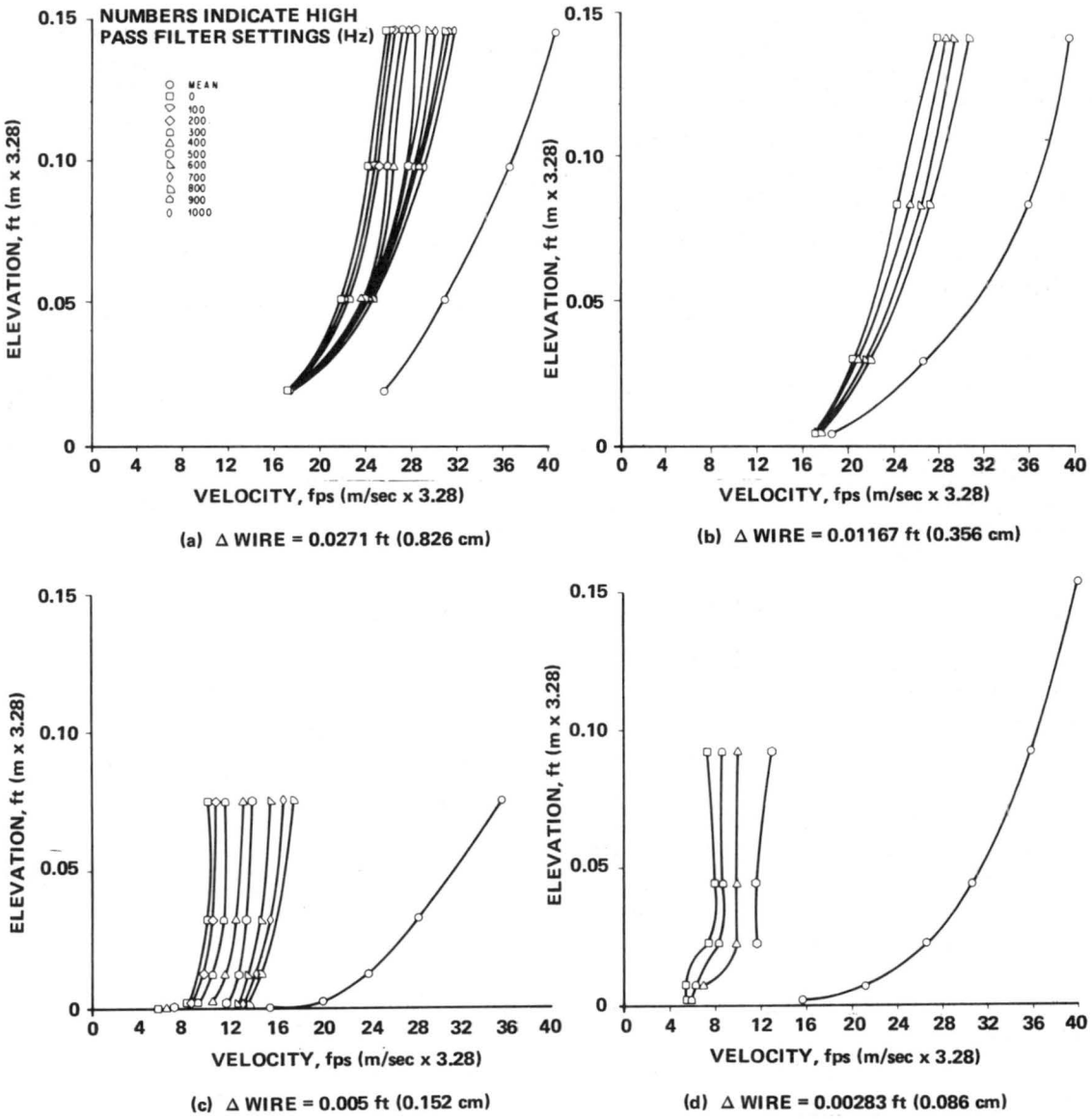

Figure 22. Mean and convection velocity versus elevation for various ΔW.

the spread is of the convective velocities, and, as the profiles get nearer the surface, the spread of the convective velocities decreases and begins to collapse to a single velocity. Another way to view this problem is to plot the ratio of the convective velocity at a given frequency to the convective velocity with notch filtering versus wave number. The wave number is computed by the formula,

$$K_f = \frac{2\pi f}{V_{c_f}} \tag{41}$$

where V_{c_f} is the convective velocity at frequency f (V_{c_f} will sometimes be expressed as V_f for brevity). Figure 23 shows the variation of the data of Figure 22 plotted in convective velocity versus wave number form. In every case the profile of the convective velocity versus wave number which is nearly one for all wave numbers is that of the measurement nearest the production zone (Tables 1 through 4). The spreading or frequency filtering of the convective velocities by the boundary layer was predicted by the physical model. The spreading of all frequencies from a single point supports the belief that this is a formation zone.

Figure 24 shows measurements in the region both above and below the formation zone in a very large boundary layer. The large boundary layer showed the same effects as the small boundary layer. As before, spreading occurs whenever the measurement is made away from the production zone (Table 5); that is, above the production zone the higher frequencies moved faster than the lower frequencies, and below the production zone the higher frequencies move slower than the lower frequencies. However, in both cases the higher frequencies more closely approach the mean velocity than do the lower frequencies. In general, the convective velocities above the production zone are slower than the mean velocity; the convective velocities below the production zone are higher than the mean velocity. The mean velocity obviously is the driving or forcing function on any packet or structure in the flow. The relationship between convective and mean velocities, as indicated above, is consistent with the physical model presented. Figure 25 shows a typical set of cross-correlations for convective velocities in the outer portion of a boundary layer. Note that the skewing is consistent with the analysis of Appendix D, paragraph F. The progression of higher frequencies toward the mean velocity time delay is consistent with the physical model.

The coalescing of all convective velocities at a particular point makes it difficult to accept models which require large eddies with characteristically high velocities protruding into the lower layers of the boundary layer.

Figures 22 and 23 and Tables 1 through 4 represent four separate evaluations of convective velocity with various wire separations. Figures 26 and 27 present the above data in the form of V_{c_f}/V_m versus $K_f \frac{\Delta W}{2\pi}$. Although V_{c_f}, V_m, K_f, and ΔW have previously been defined, $K_f \frac{\Delta W}{2\pi}$ has not in itself been examined. If one considers a time function with an angular frequency of $2\pi f$ convecting with a velocity V_{c_f}, the number of cycles that the function performs while traversing a distance ΔW is

$$\frac{2\pi f}{V_{c_f}} \frac{\Delta W}{2\pi} = K_f \frac{\Delta W}{2\pi} \quad . \tag{42}$$

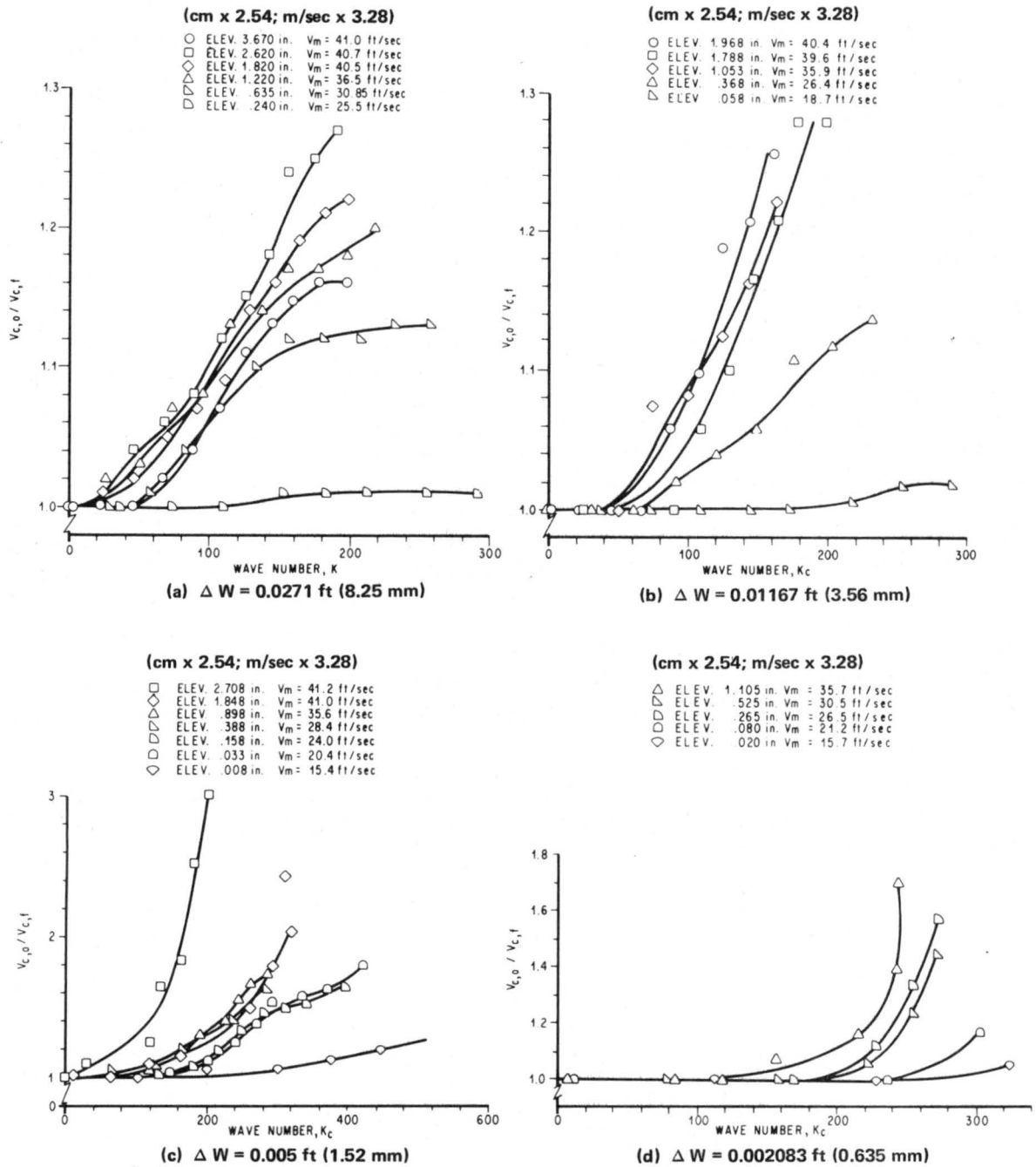

Figure 23. Convective velocity versus wave number.

This dimensionless number is similar to a dimensionless frequency or Strouhal number. However, here the parameter represents the number of oscillations a particular frequency will make between the first and second sensor. Figure 26 shows the individual test results.

TABLE 1. TEST I CONVECTIVE VELOCITY PARAMETERS

Run No. 1
V_m = 40.4 ft/sec (12.3 m/sec)
ΔW = 0.01167 ft (3.56 mm) Elevation = 1.968 in. (4.99 cm)

Convective Frequency	Convective Velocity, fps (m/sec × 3.28)	V_f/V_o	K_f	V_f/V_m	$K_f\Delta W/2\pi$, cycles
All	27.8	1.00	0.00	0.688	0.0000
1	27.8	1.00	0.23	0.688	0.0004
10	27.8	1.00	2.26	0.688	0.0042
100	27.8	1.00	22.60	0.688	0.0419
200	27.8	1.00	45.20	0.688	0.0840
300	27.8	1.00	67.80	0.688	0.1259
400	28.6	1.029	87.88	0.708	0.1632
500	29.15	1.049	107.8	0.722	0.2002
600	30.4	1.094	124.0	0.752	0.2303
700	30.7	1.104	143.3	0.760	0.2261
800	31.35	1.128	160.3	0.776	0.2978

Run No. 2
V_m = 39.6 ft/sec (12.1 m/sec) Elevation = 1.788 in. (4.55 cm)

Convective Frequency	Convective Velocity, fps (m/sec × 3.28)	V_f/V_o	K_f	V_f/V_m	$K_f\Delta W/2\pi$, cycles
All	27.8	1.000	0.000	0.702	0.0000
1	27.8	1.000	0.226	0.702	0.0004
10	27.8	1.000	2.260	0.702	0.0042
100	27.8	1.000	22.60	0.702	0.0420
200	27.8	1.000	45.20	0.702	0.0840
300	27.8	1.000	67.80	0.702	0.1260
400	27.8	1.000	90.40	0.702	0.1680
500	28.6	1.029	109.8	0.722	0.2040
600	29.2	1.050	129.1	0.737	0.2398
700	30.1	1.083	146.1	0.760	0.2714
800	30.7	1.104	163.7	0.775	0.3041
900	31.7	1.140	178.4	0.801	0.3313
1000	31.7	1.140	198.2	0.801	0.3681

TABLE 1. (Continued)

Run No. 3
V_m = 35.9 ft/sec (11.0 m/sec) Elevation = 1.053 in. (2.67 cm)

Convective Frequency	Convective Velocity, fps (m/sec × 3.28)	V_f/V_o	K_f	V_g/V_m	$K_f\Delta W/2\pi$, cycles
All	24.3	1.000	0.000	0.677	0.0000
1	24.3	1.000	0.260	0.677	0.0005
10	24.3	1.000	2.580	0.677	0.0048
100	24.3	1.000	25.86	0.677	0.0480
200	24.3	1.000	51.71	0.677	0.0960
300	25.2	1.037	74.80	0.702	0.1389
400	25.3	1.041	99.34	0.705	0.1845
500	25.8	1.062	121.7	0.719	0.2262
600	26.3	1.082	143.3	0.733	0.2662
700	27.0	1.111	162.9	0.752	0.3026

Run No. 4
V_m = 26.4 ft/sec (8.05 m/sec) Elevation = 0.368 in. (0.935 cm)

Convective Frequency	Convective Velocity, fps (m/sec × 3.28)	V_f/V_o	K_f	V_f/V_m	$K_f\Delta W/2\pi$, cycles
All	20.4	1.000	0.000	0.773	0.0000
1	20.4	1.000	0.308	0.773	0.0006
10	20.4	1.000	3.080	0.773	0.0057
100	20.4	1.000	30.80	0.773	0.0572
200	20.4	1.000	61.60	0.773	0.1144
300	20.6	1.010	91.50	0.780	0.1699
400	20.8	1.020	120.8	0.788	0.2244
500	21.0	1.029	149.6	0.795	0.2779
600	21.5	1.054	175.3	0.814	0.3257
700	21.6	1.059	203.6	0.818	0.3782
800	21.8	1.069	230.6	0.825	0.4283

TABLE 1. (Concluded)

Run No. 5
V_m = 18.7 ft/sec (5.7 m/sec) Elevation = 0.050 in. (0.127 cm)

Convective Frequency	Convective Velocity, fps (m/sec × 3.28)	V_f/V_o	K_f	V_f/V_m	$K_f\Delta W/2\pi$, cycles
All	17.2	1.000	0.00	0.920	0.0000
1	17.2	1.000	0.37	0.920	0.0007
10	17.2	1.000	3.65	0.920	0.0068
100	17.2	1.000	36.53	0.920	0.0678
200	17.2	1.000	73.06	0.920	0.1357
300	17.2	1.000	109.6	0.920	0.2035
400	17.2	1.000	145.1	0.920	0.2695
500	17.2	1.000	172.6	0.920	0.3207
600	17.25	1.003	218.6	0.922	0.4059
700	17.35	1.009	253.5	0.928	0.4708
800	17.35	1.009	289.7	0.928	0.5381

TABLE 2. TEST II CONVECTIVE VELOCITY PARAMETERS

Run No. 1
ΔW = 0.0271 ft (8.25 mm)
V_m = 41.0 ft/sec (12.5 m/sec) Elevation = 3.670 in. (9.33 cm)

Convective Frequency	Convective Velocity, fps (m/sec × 3.28)	V_f/V_o	K_f	V_f/V_m	$K_f\Delta W/2\pi$, cycles
All	27.4	1.00	0.00	0.668	0.0000
10	27.4	1.00	2.29	0.668	0.0099
100	27.4	1.00	22.93	0.668	0.0989
200	27.4	1.00	45.86	0.668	0.1978
300	28.0	1.02	67.32	0.683	0.2904
400	28.6	1.04	87.87	0.698	0.3790
500	29.4	1.07	106.8	0.717	0.4609
600	30.4	1.11	124.0	0.741	0.5349
700	31.0	1.13	141.9	0.756	0.6119
800	31.5	1.15	159.6	0.768	0.6882
900	31.9	1.16	177.3	0.778	0.7646
1000	31.9	1.16	196.9	0.778	0.8496

TABLE 2. (Continued)

Run No. 2
V_m = 40.7 ft/sec (12.4 m/sec) Elevation = 2.62 in. (6.65 cm)

Convective Frequency	Convective Velocity, fps (m/sec × 3.28)	V_f/V_o	K_f	V_f/V_m	$K_f\Delta W/2\pi$, cycles
All	26.0	1.00	0.00	0.639	0.0000
10	26.0	1.00	2.24	0.639	0.0104
100	26.0	1.00	24.17	0.639	0.1042
200	27.1	1.04	46.37	0.639	0.1200
300	27.6	1.06	68.30	0.666	0.2946
400	28.2	1.08	89.12	0.693	0.3844
500	29.0	1.12	108.3	0.713	0.4672
600	30.0	1.15	125.7	0.737	0.5420
700	30.8	1.18	142.8	0.757	0.6159
800	32.2	1.24	156.1	0.791	0.6733
900	32.5	1.25	174.0	0.799	0.7505
1000	33.0	1.27	190.4	0.811	0.8212

Run No. 3
V_m = 40.5 ft/sec (12.4 m/sec) Elevation = 1.820 in. (4.63 cm)

Convective Frequency	Convective Velocity, fps (m/sec × 3.28)	V_f/V_o	K_f	V_f/V_m	$K_f\Delta W/2\pi$, cycles
All	25.8	1.00	0.00	0.636	0.0000
100	26.1	1.01	24.07	0.644	0.1650
200	26.3	1.02	47.78	0.649	0.2061
300	27.1	1.05	69.56	0.669	0.3000
400	27.6	1.07	91.06	0.681	0.3928
500	28.2	1.09	111.4	0.696	0.4805
600	29.4	1.14	128.2	0.726	0.5531
700	30.0	1.16	146.6	0.741	0.6323
800	30.8	1.19	163.2	0.760	0.7039
900	31.2	1.21	181.2	0.770	0.7817
1000	31.6	1.22	198.8	0.780	0.8576

TABLE 2. (Continued)

Run No. 4
V_m = 36.5 ft/sec (11.2 m/sec) Elevation = 1.220 in. (3.1 cm)

Convective Frequency	Convective Velocity, fps (m/sec × 3.28)	V_f/V_o	K_f	V_f/V_m	$K_f\Delta W/2\pi$, cycles
All	24.2	1.00	0.00	0.663	0.0000
10	24.3	1.00	2.59	0.663	0.0111
100	24.8	1.02	25.34	0.666	0.1117
200	25.0	1.03	50.27	0.679	0.2168
300	25.8	1.07	73.06	0.685	0.3151
400	26.2	1.08	95.93	0.707	0.4138
500	27.4	1.13	114.7	0.718	0.4945
600	27.6	1.14	136.6	0.751	0.5891
700	28.2	1.17	155.9	0.756	0.6727
800	28.4	1.17	176.9	0.773	0.7634
900	28.6	1.18	197.7	0.778	0.8528
1000	29.0	1.20	216.7	0.795	0.9345

Run No. 5
V_m = 30.85 ft/sec (9.4 m/sec) Elevation = 0.635 in. (1.61 cm)

Convective Frequency	Convective Velocity, fps (m/sec × 3.28)	V_f/V_o	K_f	V_f/V_m	$K_f\Delta W/2\pi$, cycles
All	21.7	1.00	0.00	0.703	0.0000
10	21.7	1.00	2.90	0.703	0.0125
100	21.7	1.00	28.95	0.703	0.1250
200	22.0	1.01	57.12	0.713	0.246
300	22.5	1.04	83.78	0.729	0.362
400	23.6	1.09	106.5	0.765	0.457
500	23.8	1.10	132.0	0.771	0.570
600	24.2	1.11	155.78	0.784	0.671
700	24.4	1.12	180.3	0.791	0.787
800	24.4	1.12	206.0	0.791	0.890
900	24.5	1.13	230.8	0.794	0.994
1000	24.5	1.13	256.5	0.794	1.106

TABLE 2. (Concluded)

Run No. 6
V_m = 25.5 ft/sec (7.8 m/sec) Elevation = 0.240 in. (0.61 cm)

Convective Frequency	Convective Velocity, fps (m/sec × 3.28)	V_f/V_o	K_f	V_f/V_m	$K_f\Delta W/2\pi$, cycles
All	17.1	1.00	0.00	0.671	0.000
10	17.1	1.00	3.67	0.671	0.016
100	17.1	1.00	36.74	0.671	0.158
200	17.1	1.00	73.49	0.671	0.317
300	17.1	1.00	110.0	0.671	0.475
400	17.2	1.01	146.1	0.671	0.631
500	17.2	1.01	182.7	0.671	0.788
600	17.3	1.01	212.1	0.671	0.915
700	17.3	1.01	254.2	0.671	1.098
800	17.3	1.01	290.6	0.671	1.253

TABLE 3. TEST III CONVECTIVE VELOCITY PARAMETERS

Run No. 1
ΔW = 0.002083 ft. (0.635 mm)
V_m = 35.7 ft/sec (10.9 m/sec) Elevation = 1.105 in. (2.81 cm)

Convective Frequency	Convective Velocity, fps (m/sec × 3.28)	V_f/V_o	K_f	V_f/V_m	$K_f\Delta W/2\pi$, cycles
All	7.44	1.000	0.00	0.208	0.0000
10	7.44	1.000	8.45	0.208	0.0028
100	7.44	1.000	84.45	0.208	0.0280
200	8.04	1.081	156.3	0.225	0.0530
300	8.67	1.165	217.4	0.243	0.0720
400	10.4	1.398	241.7	0.291	0.0800
500	13.0	1.747	241.7	0.364	0.0800

TABLE 3. (Continued)

Run No. 2
V_m = 30.5 ft/sec (9.3 m/sec) Elevation = 0.525 in. (1.33 cm)

Convective Frequency	Convective Velocity, fps (m/sec × 3.28)	V_f/V_o	K_f	V_f/V_m	$K_f\Delta W/2\pi$, cycles
All	8.0	1.000	0.000	0.262	0.0000
10	8.0	1.000	7.850	0.262	0.0026
100	8.0	1.000	78.54	0.262	0.0260
200	8.0	1.000	157.1	0.262	0.0520
300	8.5	1.063	221.8	0.278	0.0732
400	9.9	1.238	253.9	0.324	0.0838
500	11.6	1.450	270.8	0.380	0.0895

Run No. 3
V_m = 26.5 ft/sec (8.1 m/sec) Elevation = 0.265 in (0.673 cm)

Convective Frequency	Convective Velocity, fps (m/sec × 3.28)	V_f/V_o	K_f	V_f/V_m	$K_f\Delta W/2\pi$, cycles
All	7.4	1.000	0.000	0.279	0.0000
10	7.4	1.000	8.490	0.279	0.0028
100	7.4	1.000	85.91	0.279	0.0281
200	7.4	1.000	169.8	0.279	0.0562
300	8.3	1.122	227.1	0.313	0.0751
400	9.9	1.338	253.9	0.374	0.0838
500	11.6	1.568	270.8	0.437	0.0895

Run No. 4
V_m = 21.2 ft/sec (6.47 m/sec) Elevation = 0.080 in. (0.203 cm)

Convective Frequency	Convective Velocity, fps (m/sec × 3.28)	V_f/V_o	K_f	V_f/V_m	$K_f\Delta W/2\pi$, cycles
All	5.3	1.000	0.00	0.250	0.0000
10	5.3	1.000	11.86	0.250	0.0039
100	5.3	1.000	118.55	0.250	0.0393
200	5.3	1.000	237.1	0.250	0.0785
300	6.2	1.170	303.7	0.292	0.1005
400	6.9	1.302	364.2	0.325	0.1207

TABLE 3. (Concluded)

Run No. 5
V_m = 15.7 ft/sec (4.8 m/sec) Elevation = 0.020 in. (0.0508 cm)

Convective Frequency	Convective Velocity, fps (m/sec × 3.28)	V_f/V_o	K_f	V_f/V_m	$K_f\Delta W/2\pi$, cycles
All	5.5	1.000	0.00	0.350	0.0000
10	5.5	1.000	11.42	0.350	0.0038
100	5.5	1.000	114.2	0.350	0.0378
200	5.5	1.000	228.5	0.350	0.0756
300	5.8	1.055	324.9	0.370	0.1077

TABLE 4. TEST IV CONVECTIVE VELOCITY PARAMETERS

Run No. 1
ΔW = 0.0050 ft (15.3 mm)
V_m = 41.2 ft/sec (12.6 m/sec) Elevation = 2.708 in. (6.9 cm)

Convective Frequency	Convective Velocity, fps (m/sec × 3.28)	V_f/V_o	K_f	V_f/V_m	$K_f\Delta W/2\pi$, cycles
All	2.08	1.000	0.00	0.051	0.0000
10	2.27	1.091	27.68	0.0550	0.0221
50	2.63	1.264	119.5	0.0638	0.0950
75	3.45	1.659	136.6	0.0835	0.1083
100	3.84	1.846	163.6	0.0930	0.1300
150	5.26	2.529	179.2	0.1275	0.1472
200	6.25	3.005	201.1	0.1515	0.1600

TABLE 4. (Continued)

Run No. 2
V_m = 41.0 ft/sec (12.5 m/sec) Elevation = 1.848 in. (4.70 cm)

Convective Frequency	Convective Velocity, fps (m/sec × 3.28)	V_f/V_o	K_f	V_f/V_m	$K_f\Delta W/2\pi$, cycles
All	4.81	1.000	0.00	0.117	0.0000
10	4.90	1.019	12.80	0.119	0.0102
100	5.3	1.102	118.6	0.129	0.0945
200	5.8	1.206	216.7	0.141	0.172
300	7.2	1.497	261.8	0.175	0.208
400	8.6	1.788	292.2	0.210	0.232
500	9.8	2.037	320.6	0.238	0.255
600	12.2	2.536	309.0	0.336	0.246

Run No. 3
V_m = 35.6 ft/sec (10.8 m/sec) Elevation = 0.898 in. (2.28 cm)

Convective Frequency	Convective Velocity, fps (m/sec × 3.28)	V_f/V_o	K_f	V_f/V_m	$K_f\Delta W/2\pi$, cycles
All	10.0	1.000	0.000	0.280	0.0000
10	10.0	1.000	6.280	0.280	0.0050
100	10.0	1.000	62.83	0.280	0.0500
200	10.6	1.060	118.6	0.298	0.0943
300	11.6	1.160	162.5	0.326	0.1294
400	13.1	1.310	191.8	0.376	0.1527
500	13.9	1.390	227.0	0.390	0.1810
600	15.5	1.550	243.2	0.435	0.1935
700	16.7	1.670	263.3	0.469	0.209
800	17.5	1.750	287.2	0.491	0.228

TABLE 4. (Continued)

Run No. 4
V_m = 28.4 ft/sec (8.66 m/sec) Elevation = 0.388 in. (0.985 cm)

Convective Frequency	Convective Velocity, fps (m/sec × 3.28)	V_f/V_o	K_f	V_f/V_m	$K_f\Delta W/2\pi$, cycles
All	9.5	1.00	0.00	0.346	0.0000
10	9.5	1.00	6.55	0.346	0.0052
100	10.0	1.053	62.83	0.364	0.0500
200	10.4	1.095	120.83	0.379	0.0955
300	11.5	1.211	163.9	0.405	0.1297
400	12.6	1.326	199.5	0.444	0.1590
500	13.3	1.400	236.2	0.468	0.1880
600	14.7	1.547	249.7	0.517	0.1980
700	15.5	1.632	283.8	0.546	0.225

Run No. 5
V_m = 24.0 ft/sec (7.33 m/sec) Elevation = 0.158 in. (0.402 cm)

Convective Frequency	Convective Velocity, fps (m/sec × 3.28)	V_f/V_o	K_f	V_f/V_m	$K_f\Delta W/2\pi$, cycles
All	9.6	1.00	0.00	0.400	0.000
10	9.6	1.00	6.55	0.400	0.0052
100	9.6	1.00	65.45	0.400	0.0520
200	9.7	1.010	129.55	0.404	0.1030
300	10.4	1.083	181.25	0.433	0.1440
400	11.5	1.198	218.6	0.479	0.1735
500	12.75	1.328	246.4	0.531	0.1970
600	13.5	1.406	279.3	0.562	0.222
700	14.3	1.490	307.6	0.595	0.244
800	14.6	1.521	344.3	0.608	0.274
900	15.9	1.656	395.2	0.662	0.315

TABLE 4. (Concluded)

Run No. 6
V_m = 20.0 ft/sec (6.1 m/sec) Elevation = 0.033 in. (0.0839 cm)

Convective Frequency	Convective Velocity, fps (m/sec × 3.28)	V_f/V_o	K_f	V_f/V_m	$K_f\Delta W/2\pi$, cycles
All	8.3	1.00	0.00	0.415	0.0000
10	8.3	1.00	7.57	0.415	0.0060
100	8.3	1.00	75.7	0.415	0.0602
200	8.6	1.04	146.1	0.430	0.1163
300	9.3	1.120	202.7	0.464	0.161
400	10.4	1.253	241.7	0.520	0.192
500	11.6	1.398	370.8	0.580	0.215
600	12.8	1.542	294.5	0.640	0.234
700	13.1	1.578	335.7	0.655	0.267
800	13.5	1.627	372.3	0.675	0.296
1000	15.0	1.807	418.7	0.750	0.332

Run No. 7
V_m = 15.4 ft/sec (4.7 m/sec) Elevation = 0.008 in. (0.0215 cm)

Convective Frequency	Convective Velocity, fps (m/sec × 3.28)	V_f/V_o	K_f	V_f/V_m	$K_f\Delta W/2\pi$, cycles
All	5.9	1.00	0.00	0.383	0.0000
10	5.9	1.00	10.65	0.383	0.0085
100	5.9	1.00	106.5	0.383	0.0847
200	6.3	1.068	199.5	0.409	0.155
300	6.3	1.068	299.2	0.409	0.238
400	6.7	1.136	375.1	0.435	0.298
500	7.1	1.203	442.5	0.461	0.352

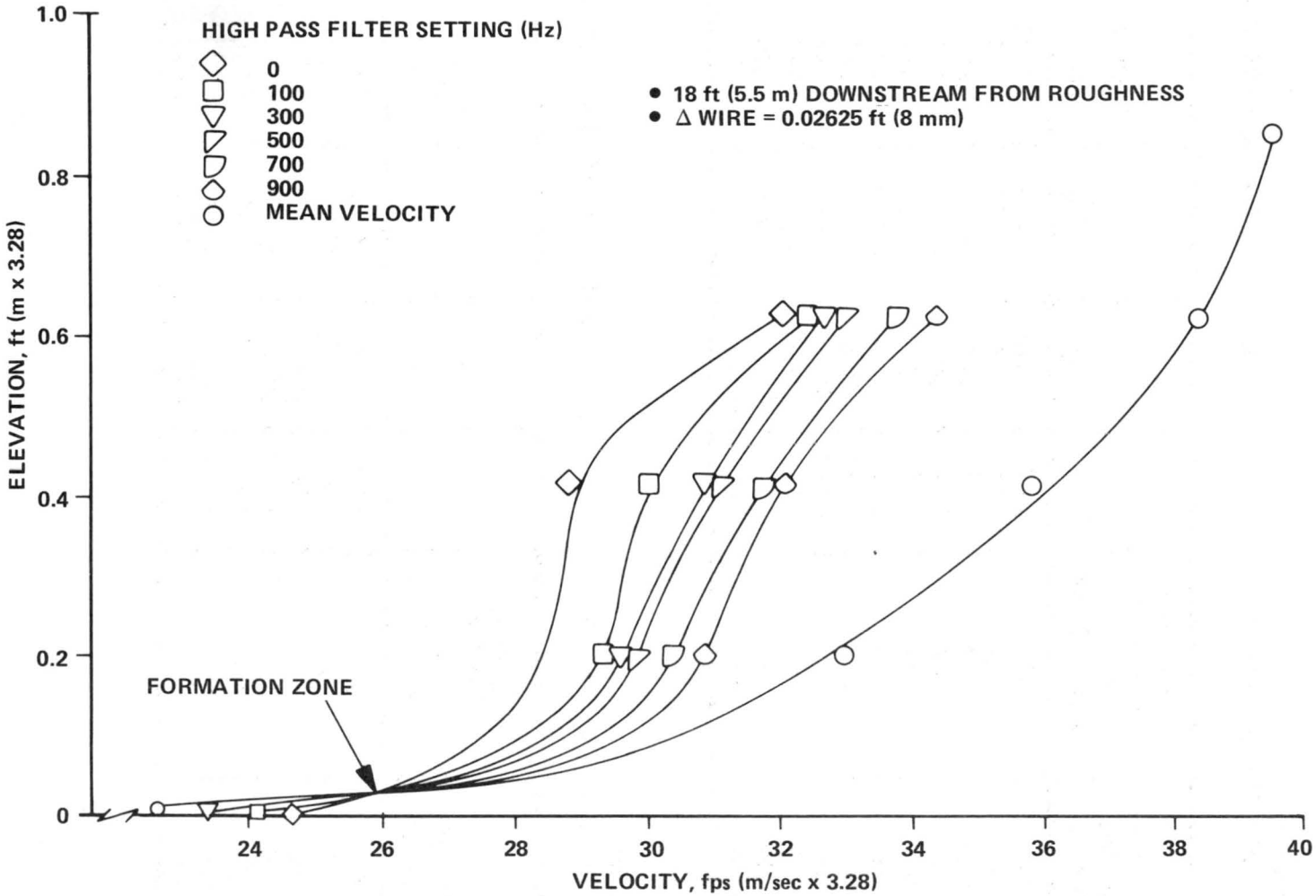

Figure 24. Convective velocities.

TABLE 5. CONVECTIVE VELOCITIES; X = 18 ft (5.5 m)

Station 18 ft (5.5 m) from roughness
U_∞ = 39.7 ft/sec (12.1 m/sec)
ΔW = 0.0275 ft (8.4 mm)

Elevation, in. (cm)	Mean Velocity, fps (m/sec × 3.28)	Convective Velocity, fps (m/sec × 3.28)								
		High Pass Filter Setting (Hz)								
		0	50	100	300	500	700	900	1100	1300
13.6 (34.5)	39.7	not sufficient information to obtain convective velocities								
10.214 (25.9)	39.5	34.7	34.7	34.7	34.7	34.7	34.7	34.7	34.7	34.7
7.527 (19.1)	38.4	32.1	32.3	32.4	32.7	33.1	33.9	34.4		
4.990 (12.7)	35.8	28.9		30.2	31.1	31.3	31.8	32.1	32.4	
2.444 (6.2)	33.1	28.4	28.9	29.3	29.6	29.9	30.4	30.9	31.3	31.5
0.050 (0.127)	22.7	24.7	24.6	24.2	23.4	22.9	22.9	22.9	22.9	

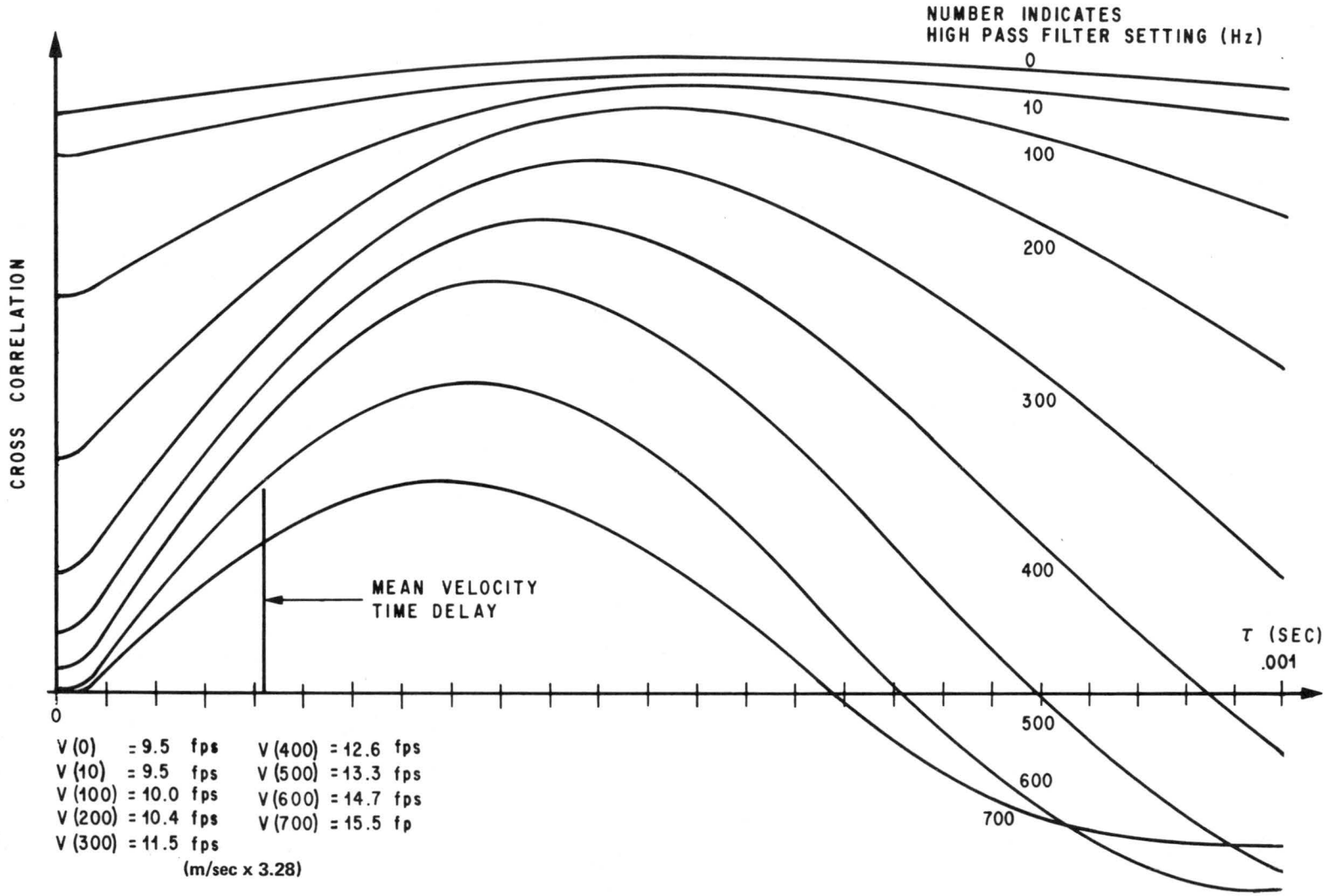

Figure 25. Correlation measurement of convective velocities as a function of frequency.

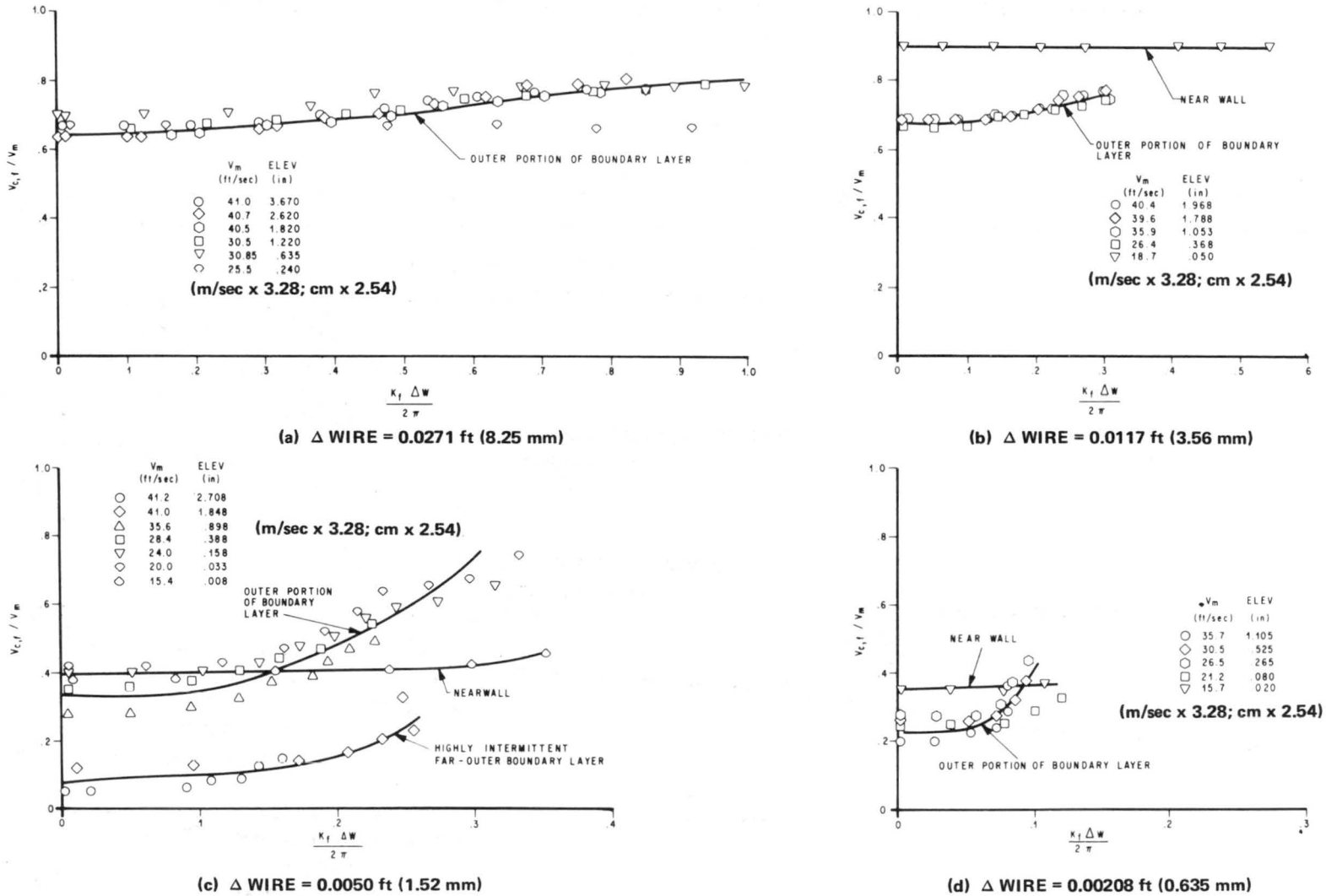

Figure 26. Ratio of convective velocity to mean velocity versus number of oscillations between sensors.

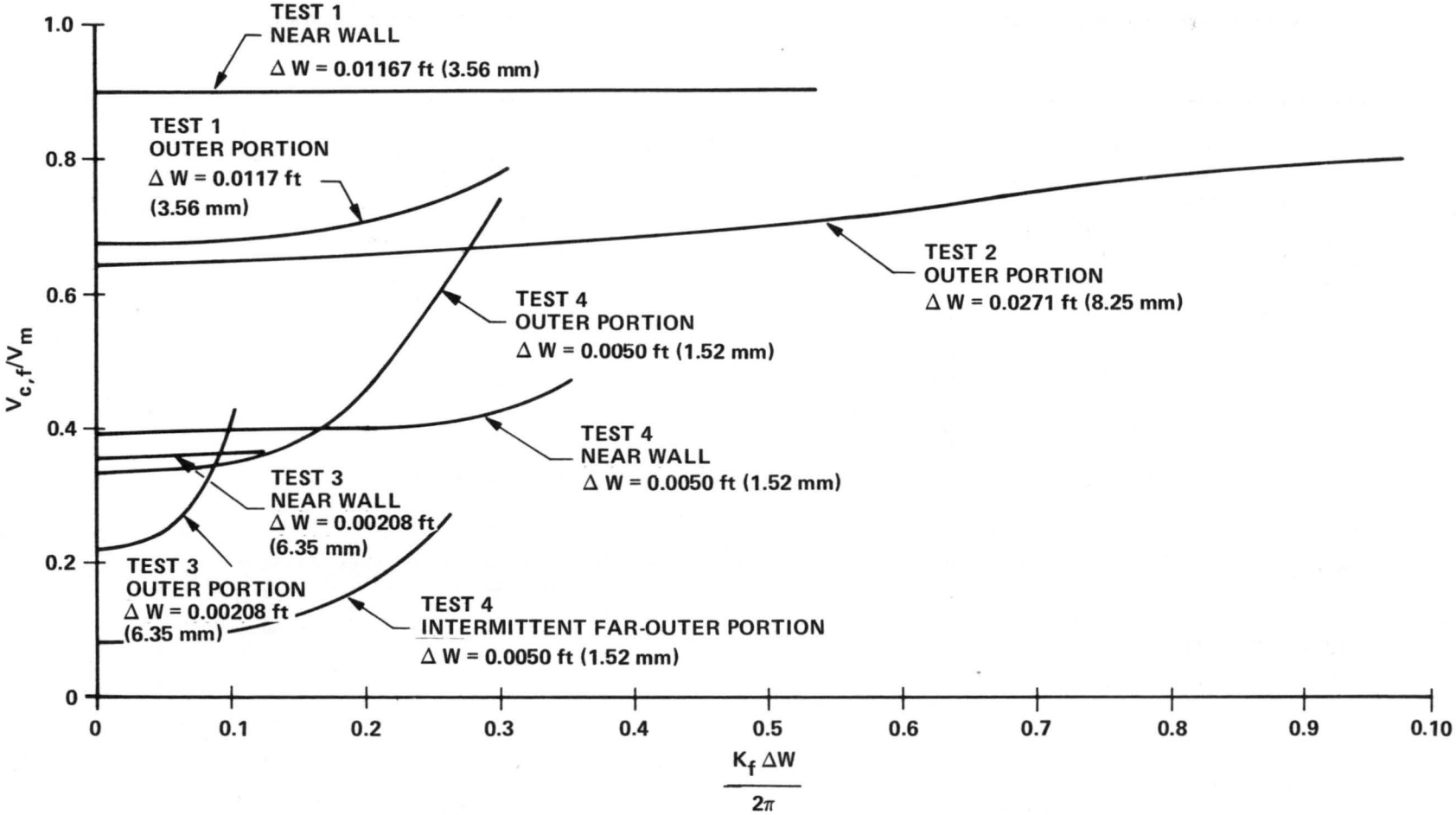

Figure 27. Composite of convective velocity versus number of oscillations between sensors.

Figure 27 is a composite of the four tests, the results of which are far from conclusive. Another possible explanation for the convective velocity being a function of spatial separation is that, for closely spaced sensors, a random walk phenomenon is occurring, and a conglomeration of many velocities is being measured. With longer and longer separations, only the trajectories moving directly in the direction of the two sensors would be correlated. The use of different separation distances might be a tool for measuring selected particle speed. Other authors have identified this problem [49, 57]. Before a firm explanation can be given, much more research needs to be done on this problem.

The convective velocity below the production zone was examined as a function of downstream distance. Figure 28 gives tabular and graphical results for the region near the surface. The model is consistent along the X-direction both above and below the production zone; that is, the smaller scale structures more nearly approach the mean velocity than do larger scale structures. The filtering of convective velocities is as predicted by the model.

D. Limiting Convective Velocities

The purpose of this section is to provide experimental evidence to support the postulate in Section III that the convective velocity must approach the mean velocity throughout the boundary layer after a sufficiently long dwell time.

Example 1 of Section III predicted that the convective velocity will approach the mean velocity for a boundary layer that had developed for approximately 28 ft (8.55 m) with a free-stream velocity of 20 ft/sec (6.1 m/sec). Since the meteorological wind tunnel is capable of producing the large growth lengths necessary to test the prediction, the convective velocity profiles were measured for a boundary layer developing for 30 ft (9.15 m) in length. A free-stream velocity of about 25 ft/sec (7.63 m/sec) was used for the study. Figure 29 shows the convective and mean velocity profiles at the 30-ft (9.15-m) station. The variation of convective velocity, as a function of frequency, was very small. A typical set of correlation curves is shown in Figure 30. Figure 30 indicates that all the frequencies are moving at very nearly the same velocity. According to Appendix D, paragraph F, one would expect a nearly symmetrical probability density distribution for the velocity fluctuations. This in turn would produce a symmetrical cross-correlation. Figure 30 shows very symmetrical correlation curves at all frequencies.

Since the formation zone exists along the entire boundary floor, there will be some packets being continually fed into the flow all along the boundary layer. This means that there will be a few packets that are somewhat newer to the flow than others. Thus, complete conformity between the convective velocity and the mean velocity may not ever be exactly obtained.

The present measurements again confirm the physical model. Table 6 gives the measurements of Figure 29 in tabular form.

Very near the floor, where the production zone is still active, one would still expect to see some difference between the convective and the mean velocity even at the large X-distances. The region near the floor at a test location 18 ft (5.5 m) downstream shows that the convective velocities near the floor are still very much different from the local mean velocity (Fig. 28).

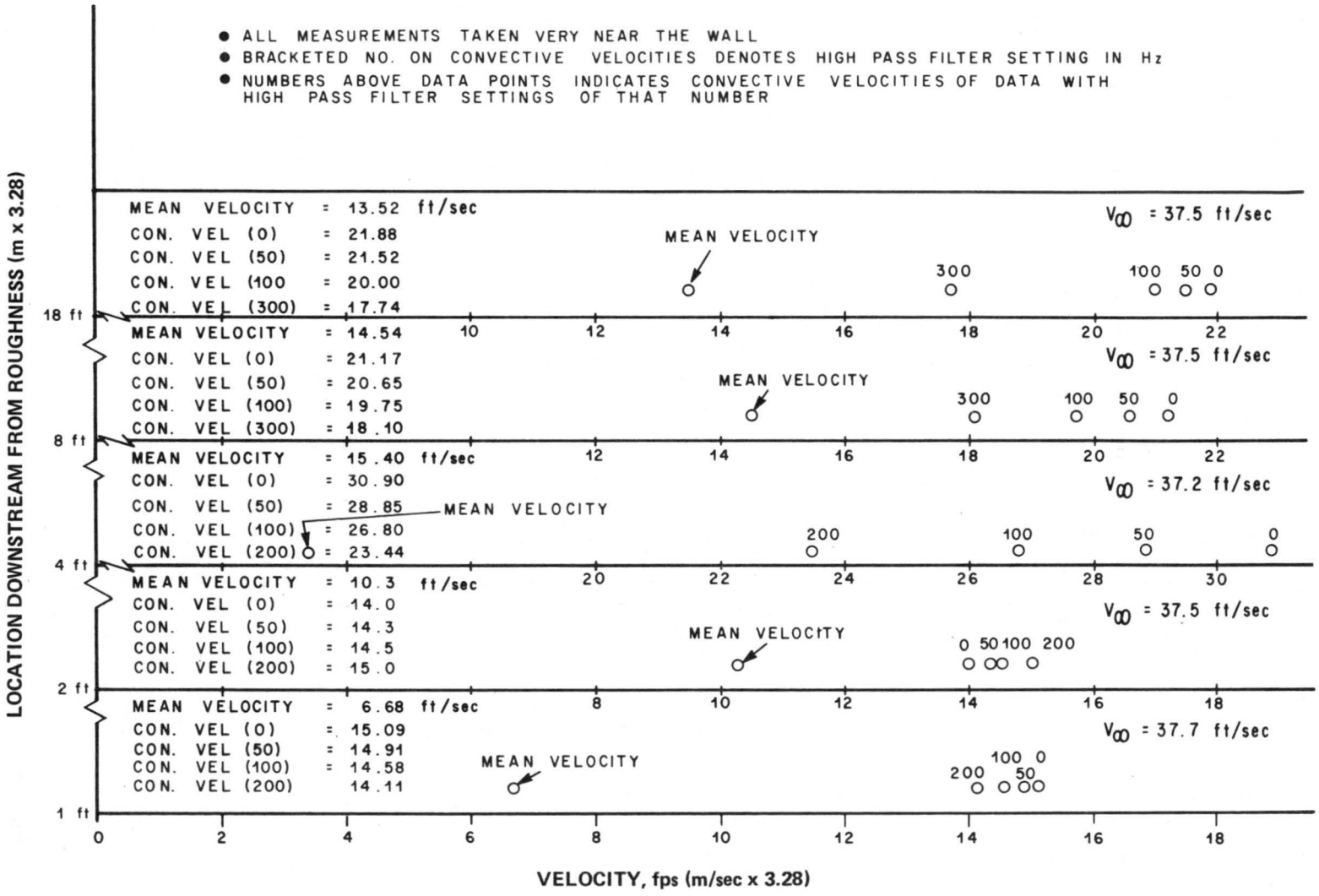

Figure 28. Convective velocities near the surface.

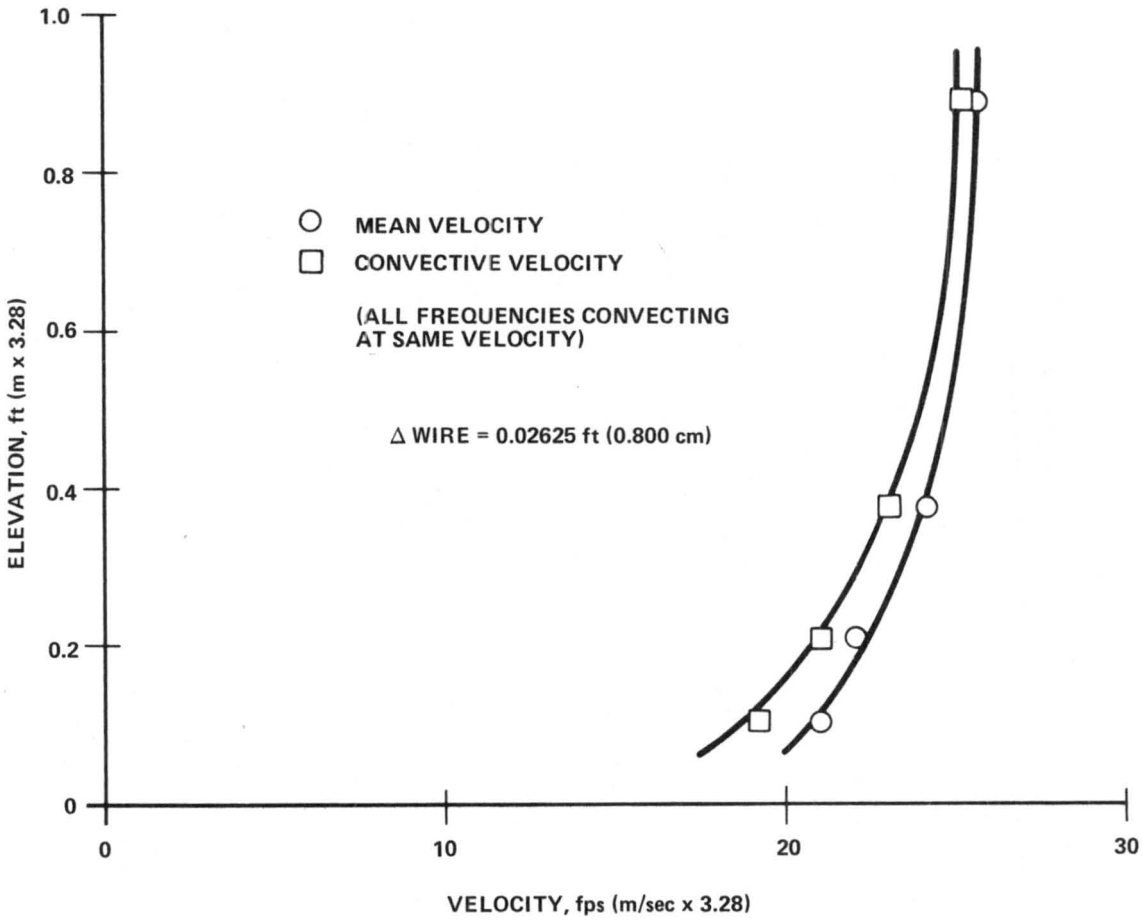

Figure 29. Convective velocities 30 ft (9.15 m) from roughness.

The limiting case of the convective velocity catching up with the mean velocity may give some insight into why similarity solutions do not exist except for very thick boundary layers.

E. Convective Velocity Measurements from the Phase Spectrum

This section gives a brief account of experimental data taken from the phase portion of the spectrum to determine transit times and convective velocities.

Appendix D, paragraph C, gives the theory which allows the phase spectrum to be used to evaluate convective velocities and transit times. Equation (D-50) shows the relation of transit time between sensors to the shift in phase. Figure 31 shows the phase spectrum and the calculation of transit time from the phase spectrum, $\theta = 2\pi f\tau$. The data are also given in tabular form in Figure 31. Equation (D-51) gives the necessary relation for determining the convective velocity from the phase spectrum,

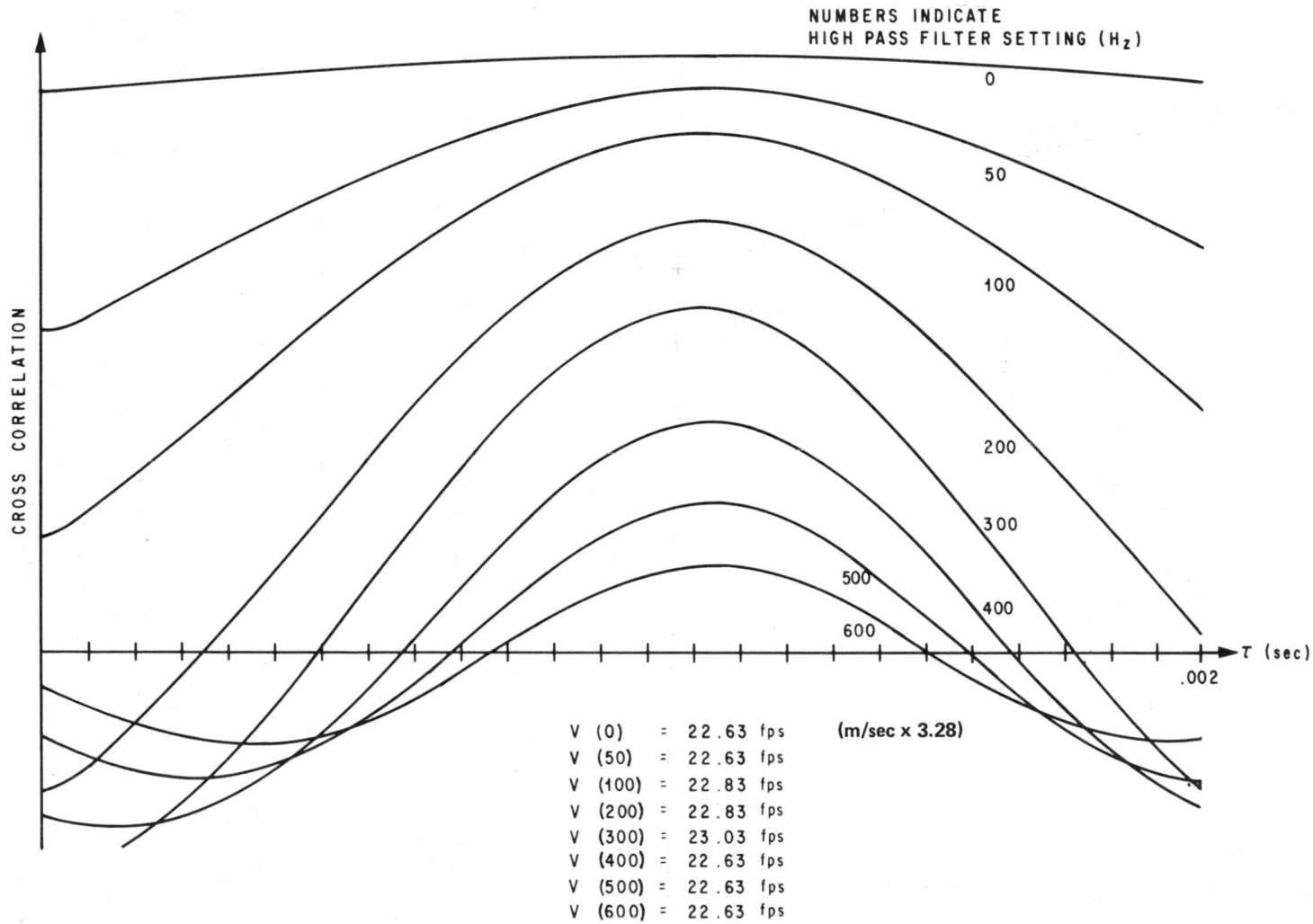

Figure 30. Correlation measurement of convective velocities.

TABLE 6. CONVECTIVE VELOCITIES; X = 30 ft (9.15 m)

Station 30 ft (9.15 m) from roughness
Meteorological wind tunnel
ΔW = 0.0275 ft (8.4 mm)

Elevation in. (cm)	Mean Velocity, fps (m/sec X 3.28)	Convective Velocity, fps (m/sec X 3.28)							
		High Pass Filter Setting (Hz)							
		0	50	100	200	300	400	500	600
10.35 (26.3)	25.5	25.2	25.2	24.1	24.3	25.2			
4.6 (11.7)	24.4	22.6	22.6	22.8	22.8	23.0	22.6	22.6	22.6
2.4 (6.1)	22.0	20.5	20.5	20.5	21.2	20.8	20.5	20.5	20.5
1.24 (3.15)	19.3	18.5	18.5	18.5	19.3	19.3	19.3	19.3	19.3

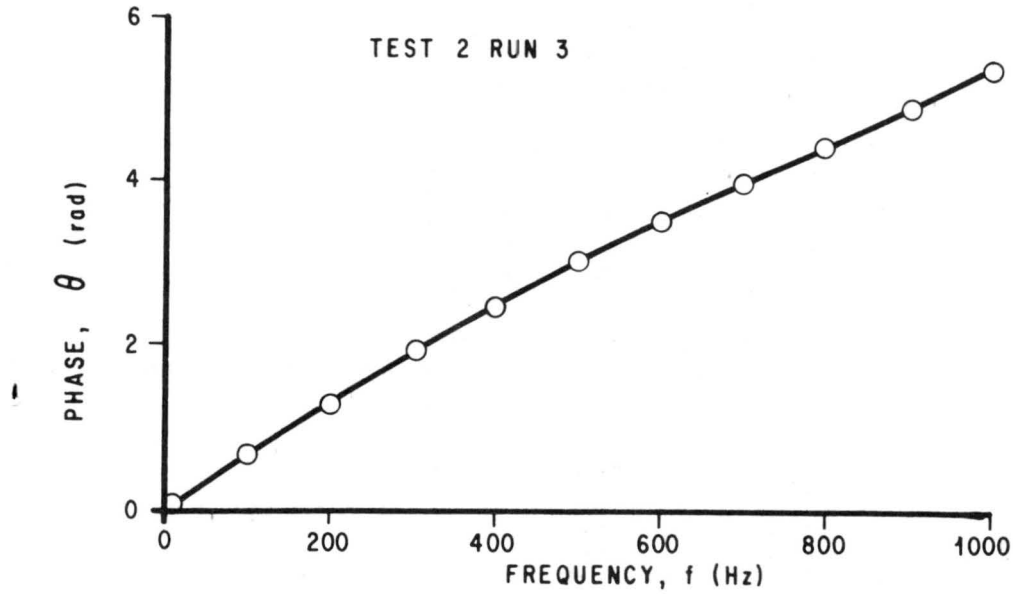

(a) PHASE ANGLE

θ (radians)	0	.654	1.298	1.883	2.44	3.02	3.50	3.97	4.42	4.88	5.38
f (Hz)	0	100	200	300	400	500	600	700	800	900	1000
τ (10^3 sec)	1.048	1.04	1.032	1.00	.976	.96	.928	.904	.880	.864	.856

$\tau = \theta_f / 2\pi f$

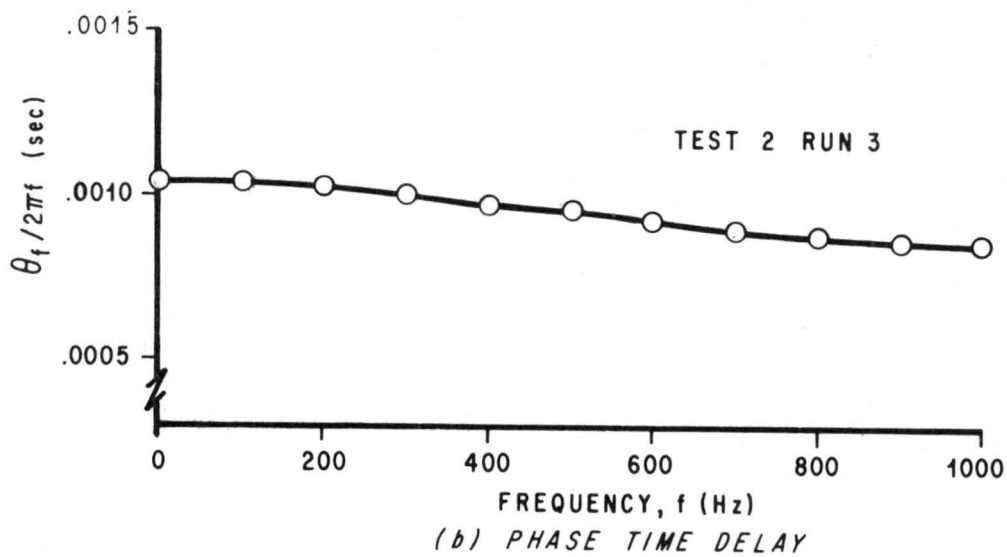

(b) PHASE TIME DELAY

Figure 31. Phase spectrum evaluation.

$$V_c = \frac{2\pi f\xi}{\theta_{c,n}} \quad .$$

Figure 32 gives a tabular and graphical result of one of the test runs.

This method is valuable for measuring the convective velocity because one can determine the bandwidth of the spectrum for which convective velocity measurements are meaningful. That is, only when the time delay determined by the phase spectrum is a smooth continuous function would the convective velocity measurement be significant. The graphical display of the phase spectrum, phase convective velocity, and phase time delay appears to be a useful and easy tool for determining the significance of a measurement for any particular frequency bandwidth.

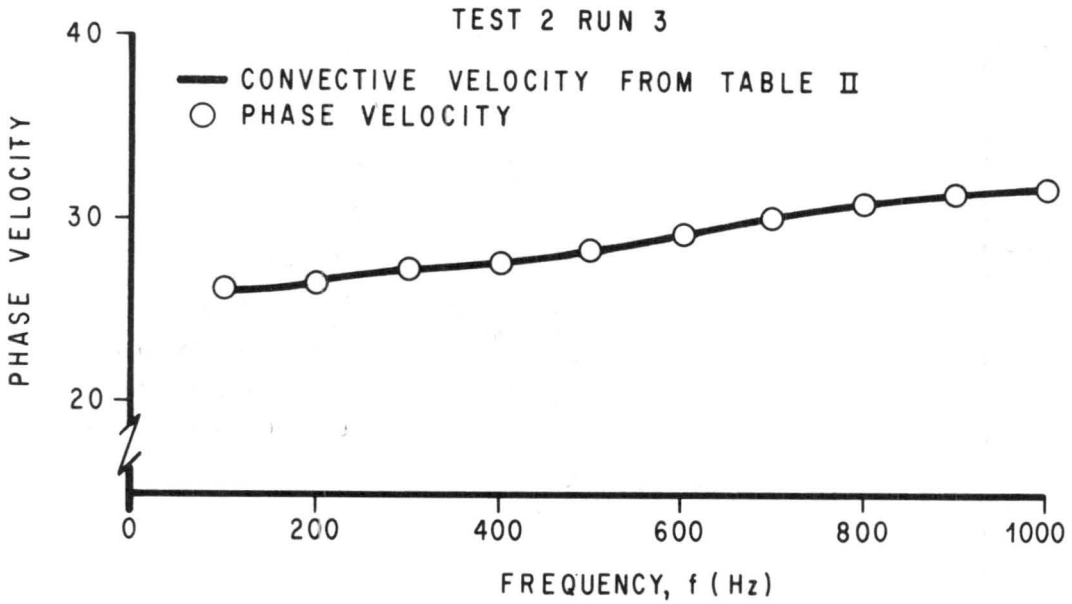

$\frac{2\pi f\xi}{\theta}$ (ft/sec)	26.0	26.2	27.1	27.8	28.2	29.2	30.0	30.8	31.4	31.6
f (Hz)	100	200	300	400	500	600	700	800	900	1000
CON. VEL. FROM TABLE 2, ft/sec (m x 3.28)	26.1	26.3	27.1	27.6	28.2	29.4	30.0	30.8	31.2	31.6

Figure 32. Phase velocity.

F. An Exploratory Test

Convective velocity profiles were taken at a station 1 ft (0.305 m) downstream of the roughness near the meteorological wind tunnel inlet. It was felt that inlet accelerations would have an effect at this location. The mean free-stream velocity in the test section was approximately 38 ft/sec (11.6 m/sec). Figure 33 shows the results of the measurements in the boundary layer. Figure 34 shows the correlation curves over the frequency range of interest for one location.

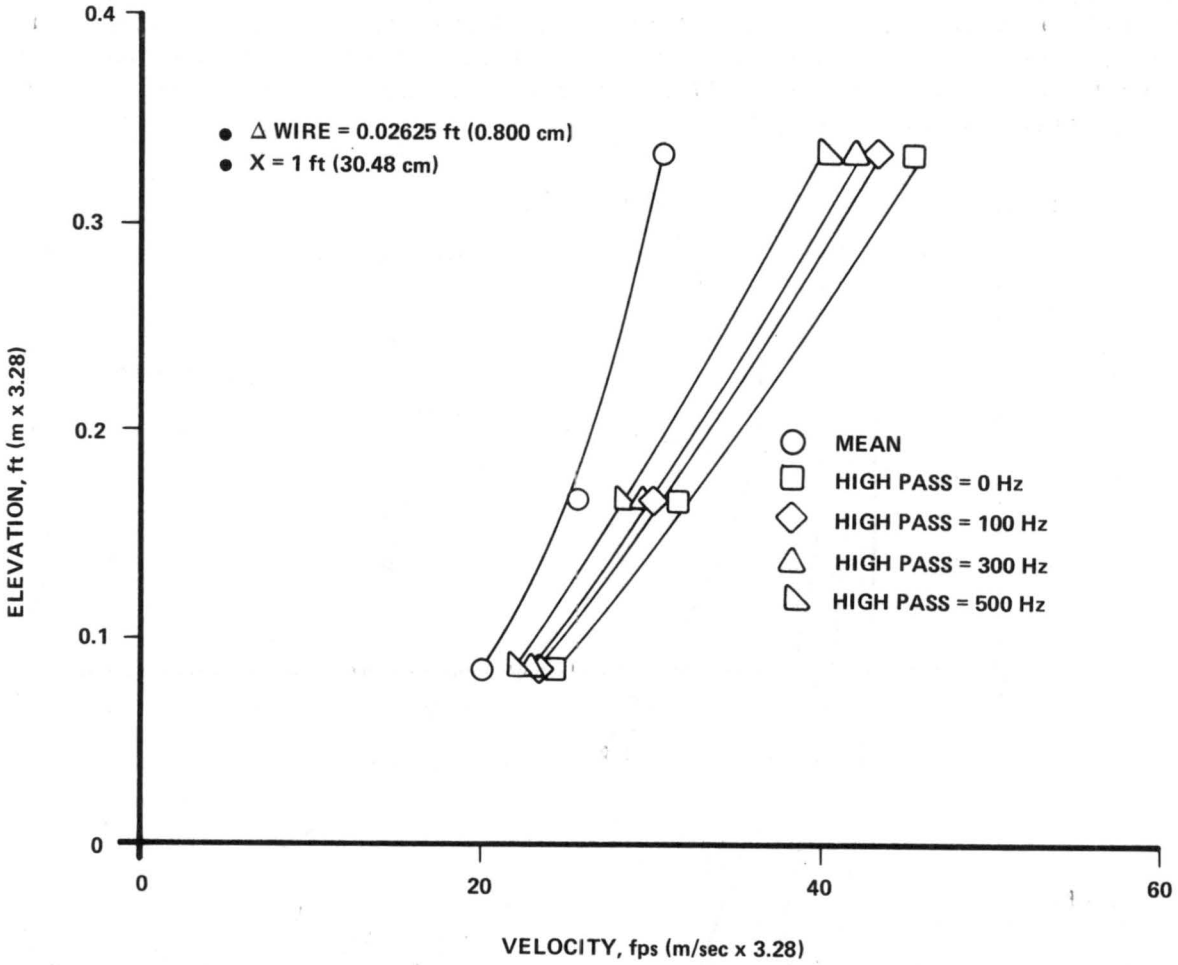

Figure 33. Convective velocities at entrance of meteorological wind tunnel.

It is seen that the convective velocities are larger than the local mean velocity. The higher the frequency is, the more nearly the convective velocity approaches the local mean velocity, as predicted by the model.

This test is presented as an exploratory case where not all of the phenomenological aspects of the inlet accelerations are known.

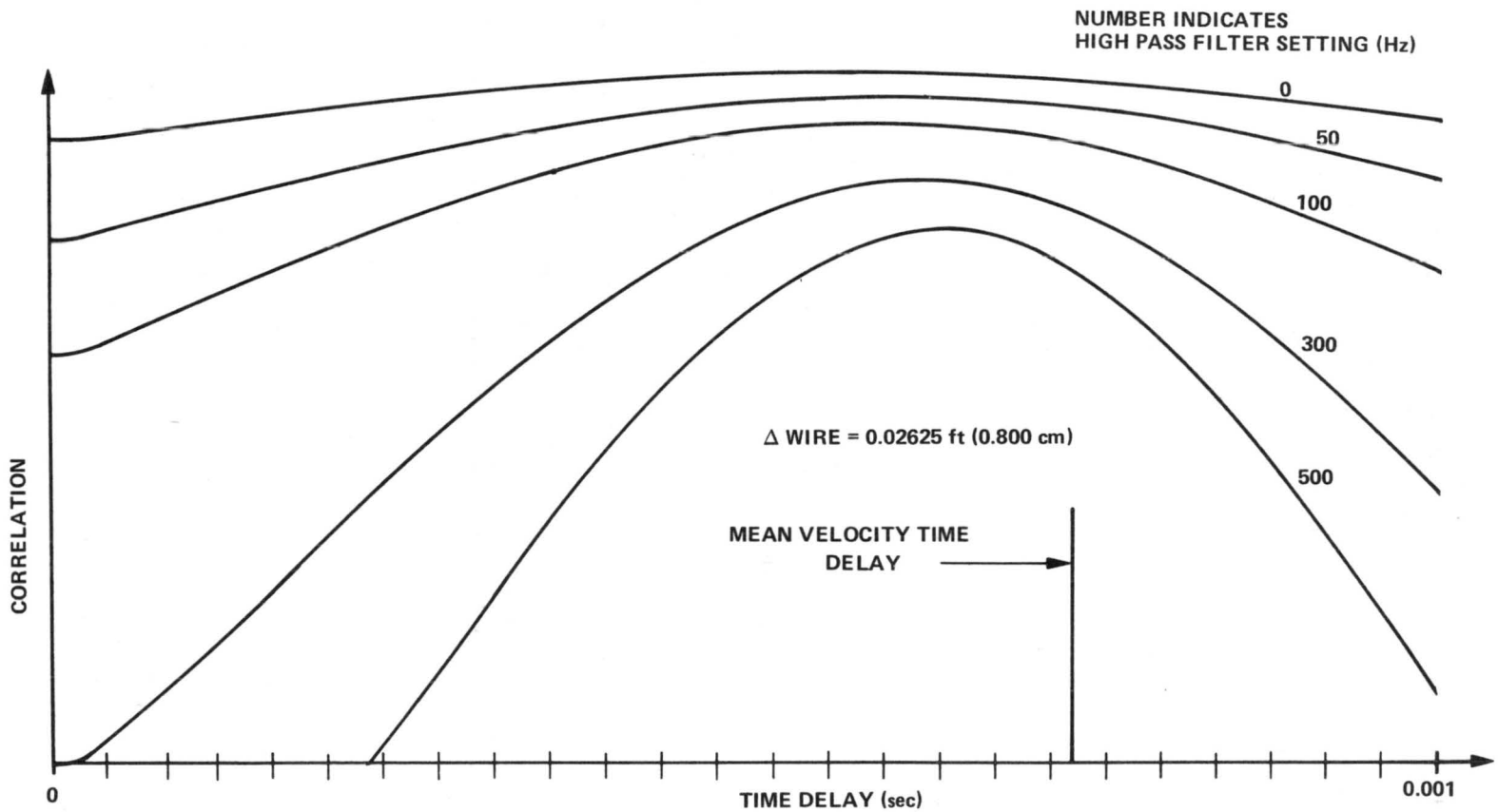

Figure 34. Correlation measurement of convective velocities at entrance of meteorological wind tunnel.

G. Some Thoughts Concerning Eddy Viscosity

Taylor stated, "It seems natural to suppose that eddies will transfer not only the heat and water vapour, but also the momentum of the layer in which they originated to the layer with which they mix" [17]. Similarly, it seems logical to describe a viscosity created by turbulent interactions by a velocity profile of the turbulent motion rather than the mean motion. One might think of this as macroscale interactions of turbulent packets, similar to the concept of dynamic viscosity of a gas being caused by collisions of molecules. Describing an eddy viscosity by

$$\tau = \epsilon \frac{dV_c}{dy} \quad ,$$

where ϵ is the eddy viscosity, seems realistic. Rotta notes that for nonequilibrium boundary layers, the concept of a constant eddy viscosity defined by

$$\tau = \epsilon \frac{dV}{dy}$$

becomes more realistic with distance downstream [72]. The results would be consistent with a constant eddy viscosity based on the convective velocity profile, because farther downstream the convective velocity profile more nearly approaches the mean velocity profile. At the distance downstream where the two profiles assume the same shapes, a constant eddy viscosity concept for the outer portions of the layer would be identical for both convective and mean velocity profiles. Rotta also points out that, for more accurate results, the effect of upstream history on the turbulent motion must be taken into account [72]. Both the mathematical model and the experimental results show that the convective velocity depends upon the upstream history. Since the mean velocity profile may not be representative of the turbulent interactions, the concept of eddy viscosity being defined by the convective velocity profile of the turbulence is presented as an alternative approach.

VII. CONCLUSIONS

A physical model is proposed to explain the formation and motion of packets of vorticity within the turbulent boundary layer. It is hypothesized that a production region exists where turbulent packets are formed. These packets migrate into that portion of the flow field which is above and into that portion of the flow which is below this formation zone. A mathematical model describing the above action was used to predict the convective velocity behavior across the turbulent boundary layer. Experiments were then devised to check certain of the conclusions derived from the model.

The three hypotheses of the model may be summarized as follows:

1. The undulating outer edge of the boundary layer is the driving function for the flow regime near the wall.

2. Packets of vorticity are produced in the region which correlate with the outer edge variation.

3. The packets migrate into the boundary layer with some initial vertical velocity, their horizontal velocity being that of the zone from which they are produced.

For the third hypothesis the mathematical model predicts the following:

1. Convective velocities outside the formation zone are different from the pointwise mean velocities.

2. Convective velocities are filtered by the boundary layer such that the higher frequencies are initially accelerated at a greater rate than the lower frequencies. Thus, initially, the boundary layer separates the various frequencies, allowing the higher frequencies to more closely approach the pointwise mean motion in the boundary layer. Convective velocities are functions of frequency.

3. The acceleration of the packet is a function of the square of the difference between its velocity and the velocity of the mean motion of the surrounding fluid.

4. The limiting boundary layer will have a growth that is linear with respect to the streamwise direction.

5. For fluid structures of all sizes, the convective velocity will approach the mean velocity profile for very long growth distances of boundary layers. This is because the mean velocity is the driving function on the fluid structures and, thus, will accelerate the packets and will be the asymptotic value for the convective velocities.

The conclusions of the experimental portion of the study may be summarized as follows:

1. There is a correlation between the velocity fluctuations of the highly intermittent outer edge of the boundary layer and those very close to the wall.

2. A production zone exists where fluid packets appear to be formed. Here the convective velocity is independent of wave number. The convective velocity equals the pointwise mean velocity for this region.

3. The convective velocity becomes a function of wave number outside the production zone. That is, the boundary layer appears to filter the various sizes. The smaller sizes are accelerated more than the large sizes. This may also be stated as follows: packets whose characteristic frequency are higher are convected at a rate more nearly the mean velocity than are packets with lower characteristic frequencies.

4. For boundary layers which have developed over long lengths, the convective velocity becomes independent of wave number in the outer regions due to the asymptotic relationship between the convective and mean velocities in the outer regions of the boundary layer.

5. The probability density distributions of the turbulent fluctuations are skewed when the convective velocity does not equal the local mean velocity.

6. The cross-phase spectrum may be used to determine the uniformity of convection velocity over wide bandwidths.

The experimental results are consistent with the requirements of the physical model.

APPENDIX A

SOLUTION OF EQUATIONS (10) AND (11)

The equation needed to solve the X-direction of motion of the packet of vorticity is equation (10). That is,

$$\frac{dV_x}{dt} = \frac{C_d V_x^2}{\lambda_1} - \frac{2C_d V_m V_x}{\lambda_1} + \frac{C_d V_m^2}{\lambda_1} \quad .$$

Noting that C_d , λ_1 , and V_m may all be functions of time, equation (10) becomes the generalized Riccati equation. This is a special case of the Abel equation [63, 64]. The Riccati equation is a differential equation of the form

$$y(t)' = h(t) + g(t)y + f(t)y^n \quad . \tag{A-1}$$

Kamke [63] states that the solution may be found, if suitably selected constants α and β may be found, where

$$\left(\frac{h(t)}{f(t)}\right)^{1/n} = e^{\int g(t)dt} \left[\beta + \alpha \int h(t) e^{-\int g(t)dt} \, dt\right] \quad , \tag{A-2}$$

such that $Z(t) = \left(\frac{h(t)}{f(t)}\right)^{1/n}$ is a solution of the linear differential equation,

$$Z(t)' - g(t)\, Z(t) = \alpha h(t) \quad . \tag{A-3}$$

Then, the solution of the original differential equation follows from

$$y(t) = \left(\frac{h(t)}{f(t)}\right)^{1/n} U(t) \quad , \tag{A-4}$$

where U(t) is determined by

$$\int \frac{dU}{U^2 - \alpha U + 1} + C = \int \left(\frac{f(t)}{h(t)}\right)^{1/n} h(t)\, dt \quad . \tag{A-5}$$

For equation (10), the constants α and β must be selected such that

$$V_m = e^{-\int \frac{2C_d V_m}{\lambda_1} dt} \left[\beta + \alpha \int \frac{C_d V_m^2}{\lambda_1} e^{\int \frac{2C_d V_m}{\lambda_1} dt} dt\right] \quad . \tag{A-6}$$

Equation (A-6) requires an explicit relationship for C_d, V_m, and λ_1 as functions of time. For many cases, these will not be known and approximations must be used. One may wish to consider C_d, λ_1, and V_m to be independent of time. The differential equation then becomes a special form of Abel's equation to which the solution is given below.

By equation (A-1),

$$h = \frac{C_d V_m^2}{\lambda_1} \quad ; \quad g = \frac{-2C_d V_m}{\lambda_1} \quad ; \quad f = \frac{C_d}{\lambda_1} \quad , \tag{A-7}$$

and

$$Z = \left(\frac{h}{f}\right)^{1/2} = V_m \quad . \tag{A-8}$$

Using (A-2)

$$V_m = e^{-\int \frac{2C_d V_m}{\lambda_1} dt} \left[\beta + \alpha \int \frac{C_d C_m^2}{\lambda_1} e^{\int \frac{2C_d V_m}{\lambda_1} dt} dt\right] \quad . \tag{A-9}$$

At $t = 0$, $V_m = V_m \Rightarrow \beta = V_m$. Differentiating equation (A-9) yields

$$0 = \frac{-2C_d V_m^2}{\lambda_1} + \frac{\alpha C_d V_m^2}{\lambda_1} \Rightarrow \alpha = 2 \quad . \tag{A-10}$$

From (A-5),

$$U' = \frac{C_d V_m}{\lambda_1}(U^2 - 2U + 1) \quad ,$$

and

$$\frac{dU}{U^2 - 2U + 1} = \frac{1}{1 - U} = \frac{V_m C_d t + C}{\lambda_1} \quad . \tag{A-11}$$

Equation (A-4) gives $V_x = ZU$, where $V_x = V_i$ at $t = 0$. The equation for velocity of the packet besomes

$$V_x = V_m - \frac{\lambda_1 (V_m - V_i)}{tC_d(V_m - V_i) + \lambda_1} \quad . \tag{A-12}$$

Integration of equation (A-12) yields the X-direction of motion for the packet:

$$X(t) = V_m t - \frac{\lambda_1 (V_m - V_i)}{C_d (V_m - V_i)} \ell n[\lambda_1 + tC_d (V_m - V_i)] + C \quad . \tag{A-13}$$

The initial condition that $X = 0$, at time $t = 0$, yields

$$X(t) = V_m t - \frac{\lambda_1}{C_d} \ell n[\lambda_1 + tC_d(V_m - V_i) + \frac{\lambda_1 \ell n \lambda_1}{C_d} \quad . \tag{A-14}$$

Thus, the equations of motion for the packet in the X-direction are as follows:

Acceleration

$$\frac{d^2 X(t)}{dt^2} = \frac{dV_x(t)}{dt} = \frac{C_d}{\lambda_1}[V_x^2 - 2V_m V_x + V_m^2] \quad . \tag{A-15}$$

Velocity

$$\frac{dX(t)}{dt} = V_x(t) = V_m - \frac{\lambda_1 (V_m - V_i)}{\lambda_1 + tC_d(V_m - V_i)} \quad . \tag{A-16}$$

Distance

$$X(t) = V_m t - \frac{\lambda_1}{C_d} \ell n[\lambda_1 + tC_d(V_m - V_i)] + \frac{\lambda_1 \ell n \lambda_1}{C_d} \quad . \tag{A-17}$$

The technique used to solve this equation was selected to give reference for general use. The following is given as proof that the previous approach will give a solution for the equation:

$$Y' = f(x)\, Y^n + g(x)\, Y + h(x) \quad , \tag{A-18}$$

where

$$Z = \left(\frac{h}{f}\right)^{1/n} = e^{\int g dx} \left[\beta + \alpha \int h e^{-\int g dx}\, dx\right] \tag{A-19}$$

and

$$\int \frac{dU}{U^n - \alpha U + 1} + C = \int \left(\frac{f}{h}\right)^{1/n} h dx \quad . \tag{A-20}$$

The hypothesis being that $Y = ZU$ is a solution of the differential equation, (A-18).

Proof

$$Z' = e^{\int g dx} g \quad Ze^{-\int g dx} + e^{\int g dx} \alpha h e^{-\int g dx} = gZ + \alpha h \tag{A-21}$$

$$U' = \frac{h}{Z}(U^n - \alpha U + 1) \quad . \tag{A-22}$$

From the hypothesis $Y = ZU$,

$$Y' = Z'U + U'Z \quad . \tag{A-23}$$

Equation (A-23), combined with equations (A-21) and (A-22), yields:

$$Y' = U(gZ + \alpha h) + Z\frac{h}{Z}(U^n - \alpha U + 1)$$

$$Y' = gZU + hU^n + h$$

$$Y' = hY^n + gY + h \quad . \tag{A-24}$$

Equation (A-24) is the original equation, and thus $Y = ZU$ is a solution to equation (A-18).*

The solution to equations (10) and (11), where C_d, V_m, and λ_1 are independent of time, may also be found by noting that equation (10) may be written as

$$\frac{dV_x}{dt} - C(V_x^2 + 2aV_x + b) = 0 \quad , \tag{A-25}$$

---

*Proof of existence thanks to Dr. H. G. Krause, NASA, MSFC.

where

$$C = -\frac{C_d}{\lambda_1} \; ; \; a = -V_m \; ; \text{ and } b = V_m^2 \quad .$$

Equation (A-25) is now a special form of Abel's equation [63] where the solution is known

$$V_x - V_m = 1/(-\frac{C_d T}{\lambda_1} + C) \quad . \tag{A-26}$$

Applying the initial conditions $V_x = V_i$ at time, $t = 0$,

$$V_m - V_x = \frac{\lambda_1 (V_m - V_i)}{tC_d(V_m - V_i) + \lambda_1} \quad , \tag{A-27}$$

which is the same as equation (A-12) derived earlier.

Equation (A-27) may now be viewed as a differential equation to describe the distance the packet moves in the X-direction.

$$\frac{dx}{dt} = \frac{\lambda_1 (V_m - V_i)}{-tC_d(V_m - V_i) - \lambda_1} + V_m \quad , \tag{A-28}$$

the solution being

$$x = \frac{-\lambda_1 (V_m - V_i)}{C_d(V_m - V_i)} \ell n[\lambda_1 + tC_d(V_m - V_i)] + V_m t + C \quad , \tag{A-29}$$

which is the solution to equation (11).

Applying the initial condition that $X = 0$ at time $t = 0$, we obtain

$$x(t) = \frac{-\lambda_1}{C_d} \ell n[\lambda_1 + tC_d(V_m - V_i)] + V_m t + \frac{\lambda_1 \ell n \lambda_1}{C_d} \quad , \tag{A-30}$$

equation (A-30) being identical to equation (A-17).

For easy reference the basic equations for the X-direction of motion of the packet are given. (Note: C_d, λ_1, and V_m are independent of time.)

Acceleration of the packet in the X-direction

$$A_x = \frac{dV_x}{dt} = \frac{C_d(V_m - V_i)^2}{\lambda_1} = \frac{C_d}{\lambda_1} [V_x^2 - 2V_m V_x + V_m^2] \quad . \tag{A-31}$$

Velocity of the packet in the X-direction

$$V_x = V_m - \frac{\lambda_1 (V_m - V_i)}{\lambda_1 + tC_d(V_m - V_i)} \quad . \tag{A-32}$$

Displacement of the packet in the X-direction

$$x(t) = V_m t - \frac{\lambda_1}{C_d} \ell n[\lambda_1 + tC_d(V_m - V_i)] + \frac{\lambda_1 \ell n \lambda_1}{C_d} \quad . \tag{A-33}$$

APPENDIX B

SOLUTION OF EQUATION (28)

The solution of equation (28),

$$\frac{dV_x}{dt} = \frac{C_d V_x^2}{\lambda_1} - \frac{2C_d}{\lambda_1}[C_v V_{yi} t + V_i] V_x + \frac{C_d}{\lambda_1}[C_v V_{yi} t + V_i]^2$$

$$= \frac{C_d}{\lambda_1}[V_x - (C_v V_{yi} t + V_i)]^2 \quad ,$$

is performed by using a change of variables. Let

$$Z = [V_x - (C_v V_{yi} t + V_i)] \quad . \tag{B-1}$$

Then,

$$\frac{dZ}{dt} = \frac{dV_x}{dt} - C_v V_{yi} \quad . \tag{B-2}$$

Equation (28) may now be written as

$$\frac{dZ}{dt} = \frac{C_d Z^2}{\lambda_1} - C_v C_{yi} \quad . \tag{B-3}$$

Solutions to this differential equation may be found in Reference 63, p. 296, no. 123, or Reference 64, p. 229, no. 55.

Murphy [64] gives for $y' = a + by^2$,

(i) $\quad ry = a \tan (C + rx) \; ; \; r = \sqrt{ab}$.

(ii) $sy = a \tanh (C + sx)$; $s = \sqrt{-ab}$.

(iii) $y(C - bx) = 1$; $a = 0$.

(iv) $y = ax + b$; $b = 0$.

For the case in question, $y = z$, $x = t$, $a = -C_v V_{yi}$, $b = C_d/\lambda_1$, and $ab = (-C_d C_v V_{yi})/\lambda_1$.

The velocity profile in question has velocity increasing with elevation; thus, $C_v > 0$. Also, $V_{yi} > 0$, $C_d > 0$, and $\lambda_1 > 0$. Equation (ii) must therefore be used.

$$sy = a \tanh (C + sx) \; ; \; s = \sqrt{-ab} \quad .$$

Therefore,

$$\left(\frac{C_d C_v V_{yi}}{\lambda_1}\right)^{1/2} (V_x - C_v V_{yi} t - V_i) = -C_v V_{yi} \tanh \left[C + \left(\frac{C_d C_v V_{yi}}{\lambda_1}\right)^{1/2} t\right] .$$

Solving for V_x , we obtain

$$V_x = \frac{-C_v V_{yi} \tanh \left[C + \left(\frac{C_d C_v V_{yi}}{\lambda_1}\right)^{1/2} t\right] + C_v V_y t + V_i}{\left(\frac{C_d C_v V_{yi}}{\lambda_1}\right)^{1/2}} .$$

At $t = 0$, $V_x = V_i \Rightarrow C = 0$. Thus, the equation for the velocity in the X-direction becomes

$$V_x = \frac{-C_v V_{yi}}{\left(C_d C_v V_{yi}/\lambda_1\right)^{1/2}} \tanh \left(\frac{C_d C_v V_{yi}}{\lambda_1}\right)^{1/2} t + C_v V_{yi} t + V_i$$

or (B-4)

$$V_x = V_m - \frac{C_v V_{yi}}{(C_d C_v V_{yi}/\lambda_1)^{1/2}} \tanh \left(\frac{C_d C_v V_{yi}}{\lambda_1}\right)^{1/2} t \quad .$$

Integration of equation (B-4) yields

$$x(t) = C_v V_{yi} \frac{t^2}{2} + V_i t - \frac{\lambda_1}{C_d} \ell n \cosh \left(\frac{C_d C_v V_{yi}}{\lambda_1}\right)^{1/2} t + C \quad .$$

At time $t = 0$, $x(0) = 0 \Rightarrow C = 0$, which makes the X-direction of motion become

$$x(t) = V_m t - \frac{\lambda_1}{C_d} \ell n \cosh \left(\frac{C_d C_v V_{yi}}{\lambda_1}\right)^{1/2} t \quad . \tag{B-5}$$

Since $V_m = C_v V_{yi} t + V_i$, $C_v V_{yi} = (V_m - V_i)/t$.

The equations for velocity and distance of the packet may now be written as follows:

Velocity of the Packet

$$V_x = -\left(\frac{\lambda_1}{C_d}\right)^{1/2} \left(\frac{V_m - V_i}{t}\right)^{1/2} \tanh \left[\frac{C_d}{\lambda_1}(V_m - V_i)\, t\right]^{1/2} + V_m \quad . \tag{B-6}$$

Translation of the Packet

$$x(t) = \frac{V_m + V_i}{2} t - \frac{\lambda_1}{C_d} \ell n \cosh \left[\frac{C_d}{\lambda_1}(V_m - V_i)\, t\right]^{1/2} \quad . \tag{B-7}$$

APPENDIX C

SOLUTION OF EQUATION (10)

Equation (10) for a velocity gradient of $V_m = (C_v y)^{1/7} + V_i$, where y(t) is described by $\dot{V}_{yi} t = y(t)$, will be solved by the Kamke approach outlined in Appendix A.

For the Kamke approach,

$$h = \frac{C_d V_m^2}{\lambda_1} \; ; \; g = \frac{-2C_d V_m}{\lambda_1} \; ; \; f = \frac{C_d}{\lambda_1} \; ; \text{ and } Z = \left(\frac{h}{f}\right)^{1/2} = V_m \quad .$$

Given the velocity gradient,

$$V_m = (C_v V_{yi} t)^{1/7} + V_i \quad , \tag{C-1}$$

Z′ becomes

$$Z' = \frac{1}{7}(C_v V_{yi} t)^{-6/7} \, C_v V_{yi} = \frac{1}{7}(V_m - V_i)^{-6} \, C_v V_{yi} \quad . \tag{C-2}$$

However Z′ also equals $gZ + \alpha h$; thus

$$Z' = \frac{1}{7}(V_m - V_i)^{-6} \, C_v V_{yi} = \frac{-2C_d V_m^2}{\lambda_1} + \alpha \frac{C_d V_m^2}{\lambda_1} \quad . \tag{C-3}$$

Solving for α , we obtain

$$\alpha = \left[\frac{1}{7}(V_m - V_i)^{-6}\, C_v V_{yi} + \frac{2C_d \dot{V}_m^2}{\lambda_1} \right] \frac{\lambda_1}{C_d V_m^2}$$

$$= \left\{ \frac{1}{7} \left[(C_v V_{yi} t)^{1/7} \right]^{-6/7} C_v V_{yi} + \frac{2C_d}{\lambda_1} \left[(C_v V_{yi} t)^{1/7} + V_i \right]^2 \right\} \frac{\lambda_1}{C_d [(C_v V_{yi} t) + V_i]^2} \quad .$$

At $t = 0$,

$$\alpha = +2 \; ; \quad \alpha^2 - 4 = 0 \quad .$$

Solving for U, we obtain

$$\int \frac{dU}{U^2 - \alpha U + 1} + C = \int \frac{dU}{(1-U)^2} + C = \frac{1}{1-U} + C \quad .$$

From equation (A-5)

$$\frac{1}{1-U} + C = \frac{C_d}{\lambda_1} \int [(C_v V_{yi} t)^{1/7} + V_i]\, dt \quad .$$

Integrating and solving for U;

$$U = 1 - \frac{1}{\frac{C_d}{\lambda_1} \left[\frac{7}{8} C_v V_{yi} t^{8/7} + V_i t \right] - C} \quad .$$

Using equation (A-4)

$$V_x = V_m - \frac{V_m}{\frac{C_d}{\lambda_1} \left[\frac{7}{8} C_v V_{yi} t^{8/7} + V_i t \right] - C} \quad . \qquad \text{(C-4)}$$

Using the initial conditions that $V_x = V_i$ at $t = 0$, equation (C-4) may be solved for the constant c yielding

$$c = -\frac{V_m}{(V_m - V_i)} \quad .$$

Equation (C-4) for the velocity in the X-direction becomes

$$V_x = V_m - \frac{V_m(V_m - V_i)}{\frac{C_d}{\lambda_1}(V_m - V_i)\left[\frac{7}{8} C_v V_{yi} t^{8/7} + V_i t\right] + V_m} \quad . \qquad \text{(C-5)}$$

APPENDIX D

SIGNAL ANALYSIS

A. General Analysis

The objective of this section is to establish the analysis which will be used to extract information from time series of finite duration. For convenience, it may be supposed that the signal is coming from a hot wire anemometer, since this is the type of signal used in the experimental portion of this paper. The figure below is given for illustration.

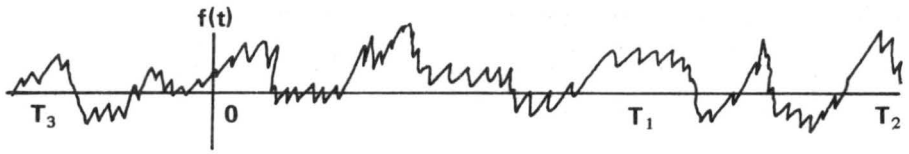

The recorded signal is of some given finite length, (T_3, T_2). The present examination will concern itself with less than the total record length; for example, $0 \leqslant T \leqslant T_1$.

Common statistical parameters that may be used to analyze such a function are generally based on the first four moments of the function:

1. Mean value, $M_{f(T)}$:

$$M_{f(t)} = \overline{f(t)} = \frac{1}{T_1} \int_0^{T_1} f(t)dt \quad . \tag{D-1}$$

2. rms value, $\sigma_{f(t)}$:

$$\sigma_{f(t)} = \left[\frac{1}{T_1} \int_0^{T_1} \left(f(t) - M_{f(t)}\right)^2 dt \right]^{1/2} \quad . \tag{D-2}$$

3. Skewness factor, $S_{f(t)}$:

$$S_{f(t)} = \frac{\frac{1}{T_1}\int_0^{T_1}\left[f(t) - M_{f(t)}\right]^3 dt}{\left[\frac{1}{T_1}\int_0^{T_1}\left(f(t) - M_{f(t)}\right)^2 dt\right]^{3/2}} \quad . \tag{D-3}$$

4. Kurtosis factor, $k_{f(t)}$:

$$k_{f(t)} = \frac{\frac{1}{T_1}\int_0^{T_1}\left(f(t) - M_{f(t)}\right)^4 dt}{\left[\frac{1}{T_1}\int_0^{T_1}\left(f(t) - M_{f(t)}\right)^2 dt\right]^2} \quad . \tag{D-4}$$

5. Auto-correlation, $R_{ff}(\tau)$:

$$R_{ff}(\tau) = \frac{1}{T_1}\int_0^{T_1} f(t)\, f(t+\tau)\, dt \quad . \tag{D-5}$$

6. Auto-covariance, $c_{ff}(\tau)$:

$$c_{ff}(\tau) = \frac{1}{T_1}\int_0^{T_1} \left[f(t) - M_{f(t)}\right]\left[f(t+\tau) - M_{f(t+\tau)}\right] dt \quad . \tag{D-6}$$

It is easily shown that only one of the mean values need be used to calculate the auto-covariance function; that is, one of the mean values may be set at zero or any convenient constant value while using the true mean for the other mean value.

7. Normalized auto-covariance, $C_{ff}(\tau)$:

$$C_{ff}(\tau) = \frac{c_{ff}(\tau)}{\sigma_{f(t)}\,\sigma_{f(t)}} \tag{D-7}$$

The above expressions give meaningful statistical values in either the time domain or time-delay domain. It will also be important to know certain statistical values of the original function in the frequency domain. Taylor [13] elucidates on work by Simmons in 1938 to show the formal beginning of the importance of the frequency domain.

The simplest approach for basic understanding is to examine the function f(t) and find the best-fit sine wave with n periods in time T_1 . A least-square fit from 0 to T_1 , for n oscillations gives

$$\frac{d}{dB_n} \int_0^{T_1} \left[B_n \sin \frac{2\pi nt}{T_1} - f(t) \right]^2 dt = 0 \quad . \tag{D-8}$$

Using the Leibniz theorem for differentiation of an integral in equation (D-8) yields

$$\int_0^{T_1} \left[2B_n \sin^2 \frac{2\pi nt}{T_1} - 2 \sin \frac{2\pi nt}{T_1} f(t) \right] dt = 0 \quad . \tag{D-9}$$

Integration of equation (D-9) gives

$$B_n T_1 - 2 \int_0^{T_1} \sin \frac{2\pi nt}{T_1} f(t)\, dt = 0 \quad . \tag{D-10}$$

Solving for B_n , we obtain

$$B_n = \frac{1}{T_1/2} \int_0^{T_1} \sin \frac{2\pi nt}{T_1} f(t)\, dt \quad . \tag{D-11}$$

B_n is now recognized as being the nth Fourier coefficient of the sine terms of f(t) . The above procedure may also be used for all cosine terms with integer oscillations over the interval $(0,T_1)$.

A more satisfying approach is to assume that f(t) over $(0,T_1)$ may be represented by a series of harmonic components, such as

$$f(t) = \sum_{i=0}^{\infty} A_n \cos \frac{2\pi nt}{T_1} + B_n \sin \frac{2\pi nt}{T_1} \quad . \tag{D-12}$$

To solve for any A_n or B_n, multiply both sides of the equation by the sine or cosine function which accompanies the A_n or B_n, and then integrate both sides over the interval $(0,T_1)$. The integration is solved, leaving

$$A_n = \frac{1}{T_1/2} \int_0^{T_1} \cos \frac{2\pi nt}{T_1} f(t)\, dt \tag{D-13}$$

and

$$B_n = \frac{1}{T_1/2} \int_0^{T_1} \sin \frac{2\pi nt}{T_1} f(t)\, dt \quad . \tag{D-14}$$

Using the above equations leads the right-hand side of equation (D-12) to converge absolutely and uniformly to f(t) over the prescribed interval if f(t) is continuous and f'(t) is at least sectionally continuous over the interval $(0,T_1)$. The only exception is at the end points where the right-hand side of equation (D-12) yields $\frac{1}{2}[f(0) + f(T_1)]$. The above restrictions are applicable since the functions that are dealt with are both continuous and continuously differentiable. Thus, the Fourier series will converge within any given error with a finite number of terms.

Equation (D-12) may be written in the form:

$$f(t) = \sum_{n=-\infty}^{\infty} C_n e^{\frac{i2\pi nt}{T_1}} \quad , \tag{D-15}$$

where

$$C_n = \frac{1}{T_1} \int_0^{T_1} f(t)\, e^{\frac{-i2\pi nt}{T_1}}\, dt \quad . \tag{D-16}$$

Noting

$$\omega = \frac{2\pi n}{T_1}, \quad n = \frac{\omega T_1}{2\pi}, \quad \text{and} \quad \Delta\omega = \frac{2\pi}{T_1}[(n+1) - n] = \frac{2\pi}{T_1},$$

equation (D-16) becomes

$$f(t) = \sum_{n=-\infty}^{\infty} C_n \frac{T_1}{2\pi} e^{i\omega t}\, \Delta\omega \quad .$$

If the time period becomes long, $\Delta\omega$ approaches $d\omega$ with

$$f(t) = \int_{-\infty}^{\infty} \frac{T_1 C_n}{2\pi} e^{i\omega t}\, d\omega = \frac{1}{2\pi} \int_{-\infty}^{\infty} g(\omega) e^{i\omega t}\, d\omega \tag{D-17}$$

and

$$g(\omega) = T_1 C_n = \int_0^{T_1} f(t)\, e^{-i\omega t}\, dt \quad . \tag{D-18}$$

Cross-channel manipulations require the following statistical concepts:

1. Cross correlation of f(t) and g(t) :

$$R_{fg}(\tau) = \frac{1}{T_1} \int_0^{T_1} f(t)g(t+\tau)\,dt \quad . \tag{D-19}$$

2. Covariance of f(t) and g(t) :

$$c_{fg}(\tau) = \frac{1}{T_1} \int_0^{T_1} [f(t) - M_{f(t)}][g(t+\tau) - M_g(t+\tau)]\,dt \quad . \tag{D-20}$$

3. Normalized covariance of f(t) and g(t) :

$$C_{fg}(\tau) = \frac{c_{fg}(\tau)}{\sigma_{f(t)}\,\sigma_{g(t+\tau)}} \quad . \tag{D-21}$$

It is permissible that the functions of f(t) and g(t) be moments of functions, such as $f(t) = h(t)^n$.

B. Restrictions Caused by Physical Limitations

The previous section on signal analysis provides the mathematical tools with which to analyze real time functions. This section shows the feasibility of defining turbulent flow structure with the preceding statistical quantities in view of physical restrictions placed on the flow. It is also an objective of this section to show how restrictions placed on a single time function propagate the function's restrictions into moments and cross-moments with other functions.

For the purpose of analysis, consideration will be placed on a finite flow field with finite velocities.

Consider two points in the finite flow field domain: A at (x_1, y_1, z_1) and B at (x_2, y_2, z_2). Consider also the velocity of the fluid at point A in the direction a and the velocity of the fluid at point B in the direction b. For simplicity, it is assumed that the mean flow is in the direction of the X-axis with a constant mean value. Then,

$$U_a(t) = \overline{U}_x e_{ax} + u_a(t) \text{ at } A \tag{D-22}$$

and

$$U_b(t) = \overline{U_x}\, e_{bx} + u_b(t) \text{ at } B \quad , \tag{D-23}$$

where the e_{ij}'s are the direction cosines of the ith direction with the jth direction.

The cross-correlation becomes

$$R_{u_a u_b}(\tau) = \overline{U_a(t)\, U_b(t+\tau)} = U_x^2\, e_{ax}\, e_{bx} + \overline{u_a(t)\, u_b(t+\tau)} \quad . \tag{D-24}$$

If the signals are ac-coupled, that is, if only the fluctuating portion of the signal is of concern, then,

$$R_{u_a u_b} = \overline{u_a(t)\, u_b(t+\tau)} \quad . \tag{D-25}$$

Since $u_a(t)$ is the fluctuation portion only, i.e., $u_a(t) = 0$, the Fourier representation of $u_a(t)$ over the interval $(0,T_1)$ may be written as

$$u_a(t) = \sum_{n=1}^{\infty} \left(a_n \cos \frac{2\pi nt}{T_1} + b_n \sin \frac{2\pi nt}{T_1} \right) \quad , \tag{D-26}$$

where

$$a_n = \frac{2}{T_1} \int_0^{T_1} u_a(t) \cos \frac{2\pi nt}{T_1}\, dt \tag{D-27}$$

and

$$b_n = \frac{2}{T_1} \int_0^{T_1} u_b(t) \sin \frac{2\pi nt}{T_1} dt \quad . \tag{D-28}$$

Similarly,

$$u_b(t+\tau) = \sum_{n=1}^{\infty} \left(a'_n \cos \frac{2\pi n(t+\tau)}{T_1} + b'_n \sin \frac{2\pi n(t+\tau)}{T_1} \right) \tag{D-29}$$

with

$$a'_n = \frac{2}{T_1} \int_{\tau}^{T_1+\tau} u_b(t+\tau) \cos \frac{2\pi n(t+\tau)}{T_1} dt \tag{D-30}$$

and

$$b'_n = \frac{2}{T_1} \int_{\tau}^{T_1+\tau} u_b(t+\tau) \sin \frac{2\pi n(t+\tau)}{T_1} dt \quad . \tag{D-31}$$

Letting $t' = t - \tau$ for any τ, dt' equals dt,

$$a'_n = \frac{2}{T_1} \int_0^{T_1} u_b(t') \cos \frac{2\pi nt'}{T_1} dt \quad , \tag{D-32}$$

and

$$b'_n = \frac{2}{T_1} \int_0^{T_1} u_b(t') \sin \frac{2\pi nt'}{T_1} dt \quad . \tag{D-33}$$

For any given τ

$$\overline{u_a(t)\, u_b(t+\tau)} = \frac{1}{T_1} \int_0^{T_1} \sum_{n=1}^{\infty} \left[\left(a_n \cos \frac{2\pi nt}{T_1} + b_n \sin \frac{2\pi nt}{T_1} \right) \right]$$

$$\left[\sum_{n=1}^{\infty} \left(a'_n \cos \frac{2\pi n(t+\tau)}{T_1} + b'_n \sin \frac{2\pi n(t+\tau)}{T_1} \right) \right] dt$$

$$= \frac{1}{T_1} \int_0^{T_1} \left[\sum_{n=1}^{\infty} \left(a_n \cos \frac{2\pi nt}{T_1} + b_n \sin \frac{2\pi nt}{T_1} \right) \right]$$

$$\left[\sum_{n=1}^{\infty} \left(a'_n \cos \frac{2\pi nt}{T_1} \cos \frac{2\pi nt}{T_1} - a'_n \sin \frac{2\pi nt}{T_1} \sin \frac{2\pi nt}{T_1} \right. \right.$$

$$\left. \left. + b'_n \sin \frac{2\pi nt}{T_1} \cos \frac{2\pi nt}{T_1} + b'_n \cos \frac{2\pi nt}{T_1} \sin \frac{2\pi nt}{T_1} \right) \right] dt \qquad \text{(D-34)}$$

Orthogonality of the function is noted and the integration is performed:

$$\overline{u_a(t)\, u_b(t+\tau)} = \frac{1}{T_1} \sum_{n=1}^{\infty} \left(\frac{T_1}{2} a_n a'_n \cos \frac{2\pi n\tau}{T_1} + \frac{T_1}{2} a_n b'_n \sin \frac{2\pi n\tau}{T_1} \right.$$

$$\left. - \frac{T_1}{2} b_n a'_n \sin \frac{2\pi n\tau}{T_1} + \frac{T_1}{2} b_n b'_n \cos \frac{2\pi n\tau}{T_1} \right)$$

$$= \frac{1}{2} \sum_{n=1}^{\infty} \left(a_n a'_n \cos \frac{2\pi n\tau}{T_1} + a_n b'_n \sin \frac{2\pi n\tau}{T_1} \right.$$

$$\left. - b_n a'_n \sin \frac{2\pi n\tau}{T_1} + b_n b'_n \cos \frac{2\pi n\tau}{T_1} \right) . \qquad \text{(D-35)}$$

The average value of the correlation over the τ region of interest becomes

$$\overline{{}_{\tau}u_a(t)\,u_b(t+\tau)} = \frac{1}{2\tau_m}\int_{-\tau_m}^{\tau_m} \frac{1}{2}\sum_{n=1}^{\infty}\left(a_n a'_n \cos\frac{2\pi n\tau}{T_1} + a_n b'_n \sin\frac{2\pi n\tau}{T_1}\right.$$

$$\left. - b_n a'_n \sin\frac{2\pi n\tau}{T_1} + b\,b'_n \cos\frac{2\pi n\tau}{T_1}\right) d\tau \quad . \tag{D-36}$$

Integration over symmetrical limits eliminates all odd functions, and integration of even functions over symmetrical limits yields twice the value integrated over half limits.

The average value may now be written (where the presubscript, τ, denotes averaging over τ) as

$$\overline{{}_{\tau}u_a(t)\,u_b(t+\tau)} = \frac{1}{2\tau_m}\int_{0}^{\tau_m} \sum_{n=1}^{\infty}\left(a_n a'_n \cos\frac{2\pi n\tau}{T_1}\right.$$

$$\left. + b_n b'_n \cos\frac{2\pi n\tau}{T_1}\right) d\tau \quad . \tag{D-37}$$

Letting $(a_n a'_n + b_n b'_n) = 2\,a'_n$, equation (D-37) becomes

$$\overline{{}_{\tau}u_a(t)\,u_b(t+\tau)} = \frac{1}{\tau_m}\int_{0}^{\tau_m} \sum_{n=1}^{\infty} a''_n \cos\frac{2\pi n\tau}{T_1}\,dt \tag{D-38}$$

or

$$\overline{{}_{\tau}u_a(t)\,u_b(t+\tau)} = \sum_{n=1}^{\infty} \frac{a''_n}{\tau_m}\frac{T_1}{2\pi n}\sin\frac{2\pi n\tau_m}{T_1} \quad . \tag{D-39}$$

Each term of equation (D-39) is identically zero whenever

$$m = \frac{m}{2} T_1 \quad , \quad m = 1, 2, 3, 4, \ldots \quad .$$

This zero value indicates that for structures defined within a finite time, their correlations are also defined within an identical finite time.

In equation (D-35), by letting

$$(a_n a'_n + b_n b'_n) = 2a''_n \text{ and } (a_n b'_n - b_n a'_n) = 2b''_n \quad .$$

the cross-covariance becomes

$$R_{u_a u_b}(\tau) = \overline{u_a(t)\, u_b(t+\tau)} = \sum_{n=1}^{\infty} \left(a''_n \cos \frac{2\pi n \tau}{T_1} + b''_n \sin \frac{2\pi n \tau}{T_1} \right) . \tag{D-40}$$

Equation (D-40) is identical to equation (D-26) except for the notation τ and t . Thus, any restrictions of a physical nature imposed upon the original functions are propagated invariantly to the correlation function.

If physical limitations allow the time series to be considered stationary through i moments, it is now proposed that products of moments will retain the original degree of stationarity.

Consider $U_a(t)$ and $U_b(t + \tau)$ stationary functions through their ith and jth moments, respectively; that is, the moments of $U_a(t)$ and $U_b(t+\tau)$ are independent of the placement of the interval to be analyzed as long as the length of the interval stays constant. Expressed mathematically, using the Leibnitz theorem,

$$\frac{\partial}{\partial \alpha} \int_{\alpha}^{\alpha+T_o} U_a^n(t)\, dt = 0 = U_a^n(\alpha + T_o) - U_a^n(\alpha) \tag{D-41}$$

and

$$\frac{\partial}{\partial \alpha} \int_{\alpha}^{\alpha+T_0} U_b^m (t+\tau)\, dt = 0 = U_b^m (\alpha + T_0 + \tau) - U_b^m (\alpha + \tau) , \quad \text{(D-42)}$$

where n and m represent any stationary moments of $u_a(t)$ and $U_b(t+\tau)$, respectively.

Examining the product of stationary time series for stationarity, the Leibnitz theorem becomes

$$\frac{\partial}{\partial \alpha} \int_{\alpha}^{\alpha+T_0} U_a^n(t)\, U_b^m(t+\tau)dt = U_a^n(\alpha + T_0)\, U_b^m(\alpha + T_0 + \tau)$$

$$- U_a^n(\alpha)\, U_b^m(\alpha + \tau)$$

$$= U_a^n(\alpha)\, U_b^m(\alpha + \tau)$$

$$- U_a^n(\alpha)\, U_b^m(\alpha + \tau) \quad . \quad \text{(D-43)}$$

A corollary of equation (D-43) could be expressed as follows: "The product of any number of stationary functions is also stationary." Thus, equation (D-43) would be

$$\frac{\partial}{\partial \alpha} \int_{\alpha}^{\alpha+T_0} U_a^n(t)\, U_b^m(t) \ldots U_i^j\, dt = U_a^n(\alpha + T_0)\, U_b^m(\alpha + T_0) \ldots U_i^j(\alpha + T_0)$$

$$- U_a^n(\alpha)\, U_b^m(\alpha) \ldots U_i^j(\alpha) \quad . \quad \text{(D-44)}$$

However from equation (D-41), $U_i^j(\alpha + T_0)$ equals $U_i^j(\alpha)$. Equation (D-44) now becomes identically equal to zero, and thus the product of moments of stationary functions is also stationary. This corollary may be expressed as follows: "The product of moments of two or more stationary functions is independent of the placement of the integral interval." Thus, by definition, the products of moments of two or more stationary time functions are themselves stationary.

The above analysis indicates that the product of stationary functions is only stationary to the degree that each individual function is stationary.

The conclusions of this section may be expressed as follows:

1. Any structure or function described in a finite time may also be described by correlation functions with finite time delays. Expressly, the time-delay range must be of the extent of the structure or function for a complete correlation description.

2. The average value of the correlation function is a function of the correlation's upper time delay and is only zero at prescribed time-delay values, equation (D-39), excluding, of course, the trivial case where all Fourier coefficients are zero.

3. The product of moments of two or more stationary time functions is also stationary to the degree of the least stationary component. That is to say, the degree of stationarity of a product of stationary functions is the same as that of the least stationary of its components. If any moment of any component is not stationary, this product will also be nonstationary.

4. A structure defined in a length of time T_1 can only be described fully in the time-delay domain if $\tau_{max} - \tau_{min} \geqslant T_1$.

C. A Physical Interpretation of the Fourier Phase Spectrum

Harmonic analysis is one tool which may be used to present data in such a way that their full meaning may be easier or better understood. Phase shifts of individual harmonics may be used to ascertain convective velocities. The phase spectrum is treated mathematically in this section, along with its physical interpretation.

Consider two time functions and their respective Fourier transforms:

$$x(t) = \frac{a_0}{2} + \sum_{n=1}^{\infty} a_n \cos \frac{2\pi nt}{T} + b_n \sin \frac{2\pi nt}{T}$$

$$= \frac{a_0}{2} + \sum_{n=1}^{\infty} (a^2{}_n + b^2{}_n)^{1/2} \cos\left(\frac{2\pi nt}{T} - \theta_{x,n}\right) \qquad \text{(D-45)}$$

and

$$y(t) = \frac{c_0}{2} + \sum_{n=1}^{\infty} c_n \cos \frac{2\pi nt}{T} + d_n \sin \frac{2\pi nt}{T}$$

$$= \frac{c_0}{2} + \sum_{n=1}^{\infty} (c^2_n + b^2_n)^{1/2} \cos\left(\frac{2\pi nt}{T} - \theta_{y,n}\right) \quad . \tag{D-46}$$

Where $\theta_{x,n}$ and $\theta_{y,n}$ represent the phase shift of each harmonic at the origin, $\theta_{x,n}$ equals $\tan^{-1} b_n/c_n$ and $\theta_{y,n}$ equals $\tan^{-1} d_n/c_n$. The correlation of x(t) and y(t) becomes

$$R_{xy}(\tau) = \frac{1}{T} \int_0^T \left[x(t)\, y(t+\tau) dt = \frac{a_0 c_0}{4} + \frac{1}{2} \sum_{n=1}^{\infty} a_n c_n \cos \frac{2\pi n\tau}{T} \right.$$

$$\left. + a_n d_n \sin \frac{2\pi n\tau}{T} - b_n c_n \sin \frac{2\pi n\tau}{T} + b_n d_n \cos \frac{2\pi n\tau}{T} \right] \quad . \tag{D-47}$$

The correlation may also be thought of as a function, without regard to the functions involved in its formation. The Fourier transform of the correlation function could be written as

$$R_{xy}(\tau) = \frac{e_0}{2} + \sum_{n=1}^{\infty} e_n \cos \frac{2\pi n\tau}{T} + f_n \sin \frac{2\pi n\tau}{T}$$

$$= \frac{e_0}{2} + \sum_{n=1}^{\infty} (e^2_n + f^2_n)^{1/2} \cos\left(\frac{2\pi n\tau}{T} - \theta_{c,n}\right) \quad , \tag{D-48}$$

where $\theta_{c,n}$ is the phase shift from the origin of the nth harmonic, $\theta_{c,n} = \tan^{-1} f_n/e_n$. Substituting from equation (D-47) for f_n and e_n we obtain

$$\theta_{c,n} = \tan^{-1}\frac{f_n}{e_n} = \tan^{-1}\frac{a_n d_n - b_n c_n}{a_n c_n + b_n d_n} = \tan^{-1}\frac{\frac{d_n}{c_n} - \frac{b_n}{a_n}}{1 + \frac{b_n}{a_n}\frac{d_n}{c_n}}$$

$$= \tan^{-1}\frac{\tan\theta_{y,n} - \tan\theta_{x,n}}{1 + \tan\theta_{y,n}\tan\theta_{x,n}} = \tan^{-1}\left[\tan\left(\theta_{y,n} - \theta_{x,n}\right)\right] \quad . \qquad \text{(D-49)}$$

Thus,

$$\theta_{c,n} = \theta_{y,n} - \theta_{x,n} \quad . \qquad \text{(D-50)}$$

The physical interpretation of equation (D-50) may be stated as follows: "The phase of the nth harmonic of the correlation is equal to the difference of the starting phases of the nth harmonics of the original time series which were used to calculate the correlation." A special case of this result occurs when $x(t) = y(t)$; thus, $\theta_{y,n}$ equals $\theta_{x,n}$. This means that $\theta_{c,n}$ must be equal to zero from equation (D-50); that is, the phase spectrum for the auto-correlation must equal zero for all frequencies. That the phase spectrum is equal to zero for the auto-correlation is well known and may also be arrived at by considering the evenness of the autocorrelation.

The correlation receives its major contribution from the nth harmonic when

$$\cos\left(\frac{2\pi n\tau}{T} - \theta_{c,n}\right) = 1 \quad ;$$

that is, when

$$\theta_{c,n} = \frac{2\pi n\tau}{T} = 2\pi f\tau \quad . \qquad \text{(D-51)}$$

If all waves travel such that they peak at approximately the same time delay, the correlation curve will have a pronounced maximum. The calculation of the convective velocity of any harmonic is then the separation distance between the sensors divided by $\theta_{c,n}/2\pi f$:

$$V_c = \frac{2\pi f\xi}{\theta_{c,n}} \quad . \tag{D-52}$$

Equations (D-51) and (D-52) show that the time delay may also be calculated from the phase spectrum; i.e., $\tau = \theta_{c,n}/2\pi f$. Figure 31 gives the phase spectrum and time-delay spectrum as functions of frequency for a given test.

The conclusions of this section are as follows:

1. The phase of a particular harmonic describing the correlation function equals the difference between the starting phases of the two functions used to calculate the correlation; i.e.,

$$\theta_{c,n} = \theta_{y,n} - \theta_{x,n} \quad .$$

2. The optimum time delay for a particular harmonic to convect from one sensor to another is given by the equation

$$\tau_p = \theta_{c,n}/2\pi f \quad .$$

3. The convective velocity of particular portions or individual harmonics may be calculated from the equation

$$V_c = 2\pi f\xi/\theta \quad .$$

These relations describe the convective phenomena in terms of phase and frequency.

D. Special Properties of Correlations of Time Functions

The time functions used to describe physical models must be of finite duration as a matter of practicality. Thus, for the following derivations the Fourier series is used rather than the more familiar Fourier integral. The time length analyzed in all cases will be of total length T_1 . The following cases will be examined:

1. Auto-correlation of function f(t) .

2. Cross-correlation of function f(t) with g(t) .

3. Cross-correlation of a function, f(t) , with its first time derivative.

4. Cross-correlation of a function, f(t), with a second function's first time derivative.

5. The derivative of the auto-correlation with respect to τ, time delay.

6. The derivative of the cross-correlation with respect to τ, time delay.

7. The derivative of an auto-correlation with respect to time.

8. The derivative of a cross-correlation with respect to time.

9. The second derivative of a cross-correlation with respect to time delay, τ.

1. Auto-Correlation of Function f(t). The auto-correlation will be examined considering the spectral content of the function to be auto-correlated.

$$f(t) = \frac{A_0}{2} + \sum_{n=1}^{\infty} A_n \cos \frac{2\pi nt}{T_1} + B_n \sin \frac{2\pi nt}{T_1} \tag{D-53}$$

$$A_n = \frac{2}{T_1} \int_0^{T_1} f(t) \cos \frac{2\pi nt}{T_1} \, dt \tag{D-54}$$

$$B_n = \frac{2}{T_1} \int_0^{T_1} f(t) \sin \frac{2\pi nt}{T_1} \, dt \tag{D-55}$$

$$f(t+\tau) = \frac{A'_0}{2} + \sum_{n=1}^{\infty} A'_n \cos \frac{2\pi n(t+\tau)}{T_1} + B'_n \sin \frac{2\pi n(t+\tau)}{T_1} \tag{D-56}$$

$$A'_n = \frac{2}{T_1} \int_0^{T_1} f(t+\tau) \cos \frac{2\pi n(t+\tau)}{T_1} \, dt \tag{D-57}$$

$$B'_n = \frac{2}{T_1} \int_0^{T_1} f(t+\tau) \sin \frac{2\pi n(t+\tau)}{T_1} \, dt \tag{D-58}$$

The auto-correlation may now be written as

$$\overline{f(t)\,f(t+\tau)} = \frac{1}{T_1}\int_0^{T_1} f(t)\,f(t+\tau)dt = \frac{1}{T_1}\int_0^{T_1}\left[\frac{A_0}{2} + \sum_{n=1}^{\infty}\left(A_n\cos\frac{2\pi nt}{T_1}\right.\right.$$

$$\left.\left. + B_n\sin\frac{2\pi nt}{T_1}\right)\right]\left[\frac{A'_0}{2} + \sum_{n=1}^{\infty}\left(A'_n\cos\frac{2\pi n(t+\tau)}{T_1}\right.\right.$$

$$\left.\left. + B'_n\sin\frac{2\pi n(t+\tau)}{T_1}\right)\right]\,dt = \frac{1}{T_1}\int_0^{T_1}\left[\frac{A_0}{2}\right.$$

$$\left. + \sum_{n=1}^{\infty}\left(A_n\cos\frac{2\pi nt}{T_1} + B_n\sin\frac{2\pi nt}{T_1}\right)\right]\left[\frac{A'}{2}\right.$$

$$\left. + \sum_{n=1}^{\infty}\left(A'_n\cos\frac{2\pi nt}{T_1}\cos\frac{2\pi n\tau}{T_1} - A'_n\sin\frac{2\pi nt}{T_1}\sin\frac{2\pi n\tau}{T_1}\right.\right.$$

$$\left.\left. + B'_n\sin\frac{2\pi nt}{T_1}\cos\frac{2\pi n\tau}{T_1} + B'_n\cos\frac{2\pi nt}{T_1}\sin\frac{2\pi n\tau}{T_1}\right)\right]\,dt \qquad \text{(D-59)}$$

Upon integration of equation (D-59), the auto-correlation becomes

$$\overline{f(t)\,f(t+\tau)} = \frac{A_0A'_0}{4} + \sum_{n=1}^{\infty}\left(\frac{A_nA'_n}{2}\cos\frac{2\pi n\tau}{T_1} + \frac{A_nB'_n}{2}\sin\frac{2\pi n\tau}{T_1}\right.$$

$$\left. - \frac{A'_nB_n}{2}\sin\frac{2\pi n\tau}{T_1} + \frac{B_nB'_n}{2}\cos\frac{2\pi n\tau}{T_1}\right) . \qquad \text{(D-60)}$$

Equation (D-60) may be rewritten as

$$\overline{f(t)\,f(t+\tau)} = \frac{A_0 A'_0}{4} + \sum_{n=1}^{\infty} \left(\frac{(A_n A'_n + B_n B'_n)}{2} \cos \frac{2\pi n\tau}{T_1} \right.$$

$$\left. + \frac{(A_n B'_n - A'_n B_n)}{2} \sin \frac{2\pi n\tau}{T_1} \right) . \qquad \text{(D-61)}$$

If the function f(t) is stationary,

$$A_n = A'_n \quad \text{and} \quad B_n = B'_n .$$

Thus, for a stationary function,

$$\frac{(A_n B'_n - A'_n B_n)}{2} = 0 .$$

The auto-correlation of f(t) is

$$\overline{f(t)\,f(t+\tau)} = \frac{A_0 A'_0}{4} + \sum_{n=1}^{\infty} \left(\frac{A_n A'_n + B_n B'_n}{2} \cos \frac{2\pi n\tau}{T_1} \right.$$

$$\left. + \frac{A_n B'_n - A'_n B_n}{2} \sin \frac{2\pi f\tau}{T_1} \right) . \qquad \text{(D-62)}$$

And, if the function f(t) is stationary, the auto-correlation becomes

$$\overline{f(t)\,f(t+\tau)} = \frac{A_0^2}{4} + \sum_{n=1}^{\infty} \frac{A_n^2 + B_n^2}{2} \cos \frac{2\pi n\tau}{T_1} . \qquad \text{(D-63)}$$

The spectra of f(t) and $\overline{f(t)\,f(t+\tau)}$ are seen to be related because $A_0^2/4$ equals $(A_0/2)^2$, and $(A_n^2 + B_n^2)/2$ equals one-half of the power spectrum of f(t) at the respective frequencies.

2. Cross-Correlation of Functions f(t) with g(t) . The functions of f(t) , A_n , and B_n are described by equations (D-53), (D-54), and (D-55), respectively. $g(t+\tau)$ is described by equations (D-56), (D-57), and (D-58), where $f(t+\tau)$ is replaced by $g(t+\tau)$.

The cross-correlation may thus be written as

$$\overline{f(t)\,g(t+\tau)} = \frac{1}{T_1}\int_0^{T_1} f(t)\,g(t+\tau)\,dt \quad . \tag{D-64}$$

The correlation in terms of its Fourier components becomes

$$\overline{f(t)\,g(t+\tau)} = \frac{A_0 A_0'}{4} + \sum_{n=1}^{\infty}\left(\frac{A_n A'_n + B_n B'_n}{2}\cos\frac{2\pi n\tau}{T_1}\right.$$

$$\left. + \frac{A_n B'_n - A'_n B_n}{2}\sin\frac{2\pi n\tau}{T_1}\right) \quad . \tag{D-65}$$

If the spectrum of f(t) is considered as $A_n + i\,B_n$ and the spectrum of $g(t+\tau)$ is considered as $A'_n + i\,B'_n$, where $i = \sqrt{-1}$ means a phase shift of 90 degrees, the spectrum of equation (D-65) may be obtained by multiplying the spectrum of $g(t+\tau)$ by the complex conjugate of the spectrum of f(t) .

3. Cross-Correlation of a Function, f(t) , with its First Time Derivative. Differentiating equation (D-53),

$$\frac{\partial f(t+\tau)}{\partial t} = \frac{2\pi}{T_1}\sum_{n=1}^{\infty} - A'_n\,n\sin\frac{2\pi n(t+\tau)}{T_1} + B'_n\,n\cos\frac{2\pi n(t+\tau)}{T_1} \quad . \tag{D-66}$$

where A'_n and B'_n are defined by equations (D-57) and (D-58), respectively. Thus,

$$\overline{f(t)\frac{\partial f(t+\tau)}{\partial t}} = \frac{1}{T_1}\int_0^{T_1} f(t)\frac{\partial f(t+\tau)}{\partial t}\,dt = \frac{1}{T_1}\int_0^{T_1}\left[\frac{A_0}{2}\right.$$

$$\left.+\sum_{n=1}^{\infty}\left(A_n\cos\frac{2\pi nt}{T_1}+B_n\sin\frac{2\pi nt}{T_1}\right)\right]\left[\frac{2\pi}{T_1}\sum_{n=1}^{\infty}\right.$$

$$\left.\left(-A'_n\,n\sin\frac{2\pi n(t+\tau)}{T_1}+B'_n\,n\cos\frac{2\pi n(t+\tau)}{T_1}\right)\right]\,dt$$

$$=\frac{1}{T_1}\int_0^{T_1}\left[\frac{A_0}{2}+\sum_{n=1}^{\infty}\left(A_n\cos\frac{2\pi nt}{T_1}+B_n\sin\frac{2\pi nt}{T_1}\right)\right]$$

$$\left[\frac{2\pi}{T_1}\sum_{n=1}^{\infty}\left(-A'_n\,n\sin\frac{2\pi nt}{T_1}\cos\frac{2\pi n\tau}{T_1}\right.\right.$$

$$+\,-A'_n\,n\cos\frac{2\pi nt}{T_1}\sin\frac{2\pi n\tau}{T_1}+B'_n\,n\cos\frac{2\pi nt}{T_1}\cos\frac{2\pi n\tau}{T_1}$$

$$\left.\left.+\,-B'_n\,n\sin\frac{2\pi nt}{T_1}\sin\frac{2\pi n\tau}{T_1}\right)\right]\,dt\quad. \tag{D-67}$$

Upon integration term by term,

$$\overline{f(t)\frac{\partial f(t+\tau)}{\partial t}} = \frac{\pi}{T_1}\sum_{n=1}^{\infty}\left(-A_nA'_n\,n\sin\frac{2\pi n\tau}{T_1}+A_nB'_n\,n\cos\frac{2\pi n\tau}{T_1}\right.$$

$$\left.-B_nA'_n\,n\cos\frac{2\pi n\tau}{T_1}-B_nB'_n\,n\sin\frac{2\pi n\tau}{T_1}\right)$$

$$=\frac{\pi}{T_1}\sum_{n=1}^{\infty}\left(n(A_nB'_n-B_nA'_n)\cos\frac{2\pi n\tau}{T_1}\right. \tag{D-68}$$

$$- n(A_n A'_n + B_n B'_n) \sin \frac{2\pi n\tau}{T_1} \Bigg) \quad . \qquad \text{(D-68) (Concluded)}$$

If the function f(t) is stationary, $A_n = A'_n$ and $B_n = B'_n$. Equation (D-68) then becomes

$$\overline{f(t) \frac{\partial f(t+\tau)}{\partial t}} = \frac{-\pi}{T_1} \sum_{n=1}^{\infty} n(A^2{}_n + B^2{}_n) \sin \frac{2\pi n\tau}{T_1} \quad . \qquad \text{(D-69)}$$

Equation (D-69) evaluated at $\tau = 0$ yields

$$\overline{f(t) \frac{\partial f(t+\tau)}{\partial t}} = 0 \quad , \quad \text{for } \tau = 0 \quad . \qquad \text{(D-70)}$$

4. Cross-Correlation of a Function, f(t), with a Second Function's First Time Derivative. f(t) is defined by equation (D-53), and $g(t+\tau)$ is defined by equation (D-56). The term $\frac{\partial g(t+\tau)}{\partial t}$ is defined by equation (D-66), where $f(t+\tau)$ is replaced by $g(t+\tau)$. Equation (D-68) now may be written to define $\overline{f(t) \frac{\partial g(t+\tau)}{\partial t}}$ as

$$\overline{f(t) \frac{\partial g(t+\tau)}{\partial t}} = \frac{-\pi}{T_1} \sum_{n=1}^{\infty} \Bigg(n(A_n B'_n - B_n A'_n) \cos \frac{2\pi n\tau}{T_1}$$

$$- n(A_n A'_n + B_n B'_n) \sin \frac{2\pi n\tau}{T_1} \Bigg) \quad . \qquad \text{(D-71)}$$

5. The Derivative of the Auto-Correlation with Respect to τ, Time Delay. Differentiating the auto-correlation with respect to time delay yields

$$\frac{\partial R_{ff}(\tau)}{\partial \tau} = \overline{\frac{\partial f(t)\, f(t+\tau)}{\partial \tau}} = \overline{f(t) \frac{\partial f(t+\tau)}{\partial \tau}} = \overline{f(t) \frac{\partial f(t+\tau)}{\partial (t+\tau)} \frac{\partial (t+\tau)}{\partial \tau}}$$

$$= \overline{f(t) \frac{\partial f(t+\tau)}{\partial (t+\tau)}} \quad . \qquad \text{(D-72)}$$

Note that

$$\frac{\partial f(t+\tau)}{\partial t} = \frac{\partial f(t+\tau)}{\partial (t+\tau)} \frac{\partial (t+\tau)}{\partial t} = \frac{\partial f(t+\tau)}{\partial (t+\tau)} = \frac{\partial f(t+\tau)}{\partial \tau} \quad . \tag{D-73}$$

From equations (D-72) and (D-73),

$$\frac{\partial R_{ff}(\tau)}{\partial \tau} = \overline{f(t) \frac{\partial f(t+\tau)}{\partial t}} \quad . \tag{D-74}$$

Therefore, from equation (D-70), the auto-correlation must have a maximum at $\tau = 0$; i.e., the slope at $\tau = 0$ must equal 0. The spectrum of equation (D-74) would follow from equation (D-68).

6. The Derivative of a Cross-Correlation with Respect to τ, Time Delay. In equation (D-72), replacing $f(t+\tau)$ by $g(t+\tau)$ gives

$$\frac{\partial R_{fg}\tau}{\partial \tau} = \overline{f(t) \frac{\partial g(t+\tau)}{\partial t}} \quad . \tag{D-75}$$

The spectrum of the above follows from equation (D-71).

7. The Derivative of an Auto-Correlation with Respect to Time. Taking the time derivative of the auto-correlation function gives

$$\frac{\partial R_{ff}(\tau)}{\partial t} = 0 = \overline{f(t) \frac{\partial f(t+\tau)}{\partial t}} + \overline{\frac{\partial f(t)}{\partial t} f(t+\tau)} \quad . \tag{D-76}$$

Since $R_{ff}(\tau)$ is not a function of time, its time derivative is zero. This does, however, give

$$\overline{f(t) \frac{\partial f(t+\tau)}{\partial t}} = -\overline{\frac{\partial f(t)}{\partial t} f(t+\tau)} \quad . \tag{D-77}$$

Therefore the spectrum of $\overline{\frac{\partial f(t)}{\partial t}\ f(t+\tau)}$ would follow from the negative of equation (D-68).

8. The Derivative of a Cross-Correlation with Respect to Time. Replacing $f(t+\tau)$ by $g(t+\tau)$ in equations (D-76) and (D-77) gives

$$\frac{\partial R_{fg}(\tau)}{\partial t} = 0 \tag{D-78}$$

and

$$\overline{f(t)\frac{\partial g(t+\tau)}{\partial t}} = -\overline{\frac{\partial f(t)}{\partial t}\, g(t+\tau)} \quad . \tag{D-79}$$

The spectrum of $\overline{\frac{\partial f(t)}{\partial t}\ g(t+\tau)}$ follows from the negative of equation (D-71).

9. The Second Derivative of a Cross-Correlation with Respect to Time Delay, τ. Using equations (D-72), (D-73), (D-75), and (D-79), the second derivative of the cross-correlation with respect to time delay becomes

$$\frac{\partial^2 R_{fg}(\tau)}{\partial \tau^2} = \overline{\frac{\partial^2 f(t)}{\partial \tau^2}\, g(t+\tau)} \tag{D-80}$$

$$= \overline{f(t)\,\frac{\partial^2 g(t+\tau)}{\partial t^2}} \tag{D-81}$$

$$= \overline{-\frac{\partial f(t)}{\partial t}\,\frac{\partial g(t+\tau)}{\partial t}} \quad . \tag{D-82}$$

To consider the auto-correlation, merely replace $g(t+\tau)$ by $f(t+\tau)$.

The spectral content of equations (D-80), (D-81), and (D-82) may be expressed as

$$\frac{\partial^2 R_{fg}(\tau)}{\partial \tau^2} = \frac{2\pi^2}{T_1^2} \sum_{n=1}^{\infty} n^2 (A_n A'_n + B_n B'_n) \cos \frac{2\pi n \tau}{T_1}$$

$$+ n^2 (A_n B'_n - A'_n B_n) \sin \frac{2\pi n \tau}{T_1} \quad . \tag{D-83}$$

For an auto-correlation of a stationary function, equation (D-83) becomes

$$\frac{\partial^2 R_{ff}(\tau)}{\partial \tau^2} = \frac{1}{2} \sum_{n=1}^{\infty} \frac{2\pi n^2}{T_1} (A^2_n + B^2_n) \cos \frac{2\pi n \tau}{T_1} \quad . \tag{D-84}$$

Notice that equation (D-83) gives the spectral content for equations (D-80), (D-81), and (D-82). Notice also that the spectra of equations (D-83) and (D-84) are identical with the spectra of equations (D-65) and (D-63) except that each term is multiplied by the square of its angular frequency. Equation (D-80) gives the relationship of the correlation of two functions to the correlation of the derivatives of the two functions.

E. The Effect of Space and Frequency Weighting Functions on the Normalized Cross-Covariance

Let f(t) be the fluctuating portion of the signal which first senses the flow phenomena. Let g(t) be the fluctuating portion of the signal which then senses the same flow phenomena at some later time, the separation between the sensors being ξ .

Assume for the moment that f(t) is changed only due to spacing and frequency before it becomes g(t) . Then,

$$f(t) = \sum_{n=1}^{\infty} \left(a_n \cos n\omega t + b_n \sin n\omega t\right) \tag{D-85}$$

and

$$g(t) = F(\xi,f)\, f(t - \tau_n) = F(\xi,f) \sum_{n=1}^{\infty} \left[a_n \cos n\omega (t - \tau_n)\right.$$

$$\left. + b_n \sin n\omega (t - \tau_n)\right] \quad , \tag{D-86}$$

where $F(\xi,f)$ is the above weighting function in space and frequency and τ_n is the time it takes for the nth harmonic to reach the second sensor. The correlation of f(t) and g(t) becomes

$$\overline{f(t)\,g(t+\tau)} = \frac{1}{T}\int_0^T \sum_{n=1}^{\infty} (a_n \cos n\omega t + b_n \sin n\omega t)$$

$$F(\xi,f) \sum_{n=1}^{\infty} \left[a_n \cos n\omega(t-\tau_n+\tau) + b_n \sin n\omega(t-\tau_n+\tau)\right] dt$$

$$= F(\xi,f) \sum_{n=1}^{\infty} \frac{a^2_n + b^2_n}{2} \cos n\omega(\tau - \tau_n) \quad . \qquad \text{(D-87)}$$

The rms values of f(t) and g(t) are

$$\left(\overline{f(t)^2}\right)^{1/2} = \left[\sum_{n=1}^{\infty} \left(\frac{a^2_n + b^2_n}{2}\right)\right]^{1/2} \qquad \text{(D-88)}$$

and

$$\left[\overline{g(t)^2}\right]^{1/2} = F(\xi,f) \left[\sum_{n=1}^{\infty} \frac{a^2_n + b^2_n}{2}\right]^{1/2} \quad . \qquad \text{(D-89)}$$

Thus, the normalized cross-covariance becomes

$$C_{fg}(\tau) = \frac{\overline{f(t)\,g(t+\tau)}}{\left[\overline{f(t)^2}\right]^{1/2}\left[\overline{g(t)^2}\right]^{1/2}} = \frac{\sum_{n=1}^{\infty} \frac{a^2_n + b^2_n}{2} \cos n\omega(\tau - \tau_n)}{\sum_{n=1}^{\infty} \frac{a^2_n + b^2_n}{2}} \quad . \qquad \text{(D-90)}$$

The peak value occurs for each harmonic when $\tau = \tau_n$. If all harmonics travel at the same rate, τ_n = constant, the maximum for the cross-covariance occurs at τ_n and its value is 1. Thus for convective velocities that are independent of frequency, the value of the normalized cross-correlation is unchanged by space and frequency weighting functions.

The point to be made is that, assuming decay in time is negligible, weighting in space or frequency does not change the value of the normalized covariance. Thus, a decrease in the normalized covariance must come as a result of a nonlinear phase shift as a function of frequency for each harmonic. This may be expressed as a shifting transit time for individual harmonics to travel between two sensors. In the case of a nonlinear phase shift as a function of frequency, the peak value would be less than one, and the curve would have a greater width.

Since in many constant fluid flows, the turbulent intensity does not significantly decrease between closely spaced sensors (i.e., the power spectrum is not a function of the spacing along the stream tube.

$$\overline{x(t)^2} = \frac{1}{\sqrt{2\pi}} \sum_{-\infty}^{\infty} A(\omega)\, d\omega \quad),$$

the decrease and spreading of the correlation curve as a function of the separation distance will be a result of varying phase shifts of the harmonics and thereby varying convective velocities as a function of frequency.

F. A Physical Look at Space-Time Covariance Computations

The space-time covariance has been defined by equation (D-20) as

$$c_{fg}(\tau) = \frac{1}{T_1} \int_0^{T_1} [f(t) - M_{f(t)}]\, [g(t+\tau) - M_{g(t+\tau)}]\, dt \quad , \tag{D-91}$$

where the points of origin of the time functions $f(t)$ and $g(t+\tau)$ are spatially separated by some finite length ξ, M_i being the time mean of the function i.

Generally speaking, only the fluctuating component, ac, is used to preserve information on the structure of turbulence for correlation processes. The dc components only raise or lower the value of the correlation by a uniform amount.

A typical example is a hot wire anemometer signal. The emf representing the mean motion of the fluid particles at the location of the wire is the mean value of the signal. Equation (D-91) states that the mean value is subtracted from each representative signal. Thus, the space-time covariance has rejected the basic method of measuring mean flow velocities.

The remaining portion of the signal, which is used for analysis, is the fluctuations about the mean. Probability statistics tell something about the nature of what is being measured with the space-time correlation. A perturbation from the mean of $\pm\Delta f(t)$, that has traversed the separation of the two probes in time, τ_m, with some attenuation or modification, A, now becomes $g(t+\tau) = \pm A\Delta f(t)$. The product of f(t) and $g(t+\tau)$ becomes equal to $A\Delta f(t)_1^2$. If the perturbation is over a period of time, Δt_1, the contribution to the covariance will be

$$\Delta t_1 f(t)_1 \; g(t+\tau)_1 = A\Delta f(t)_1^2 \Delta t_1 \quad . \tag{D-92}$$

Since the average value of f(t) is zero (the means have been subtracted out) and since the perturbation, $\Delta f(t)_1$, acted over a time, Δt_1, a cancelling oscillation of $\Delta f(t)_2$ acting over a time Δt_2 must exist such that $\Delta f(t)_1 \Delta t_1 + \Delta f(t)_2 \Delta t_2 = 0$. The contribution to the covariance by $\Delta f(t)_2$ would be $A\Delta f(t)_2^2 \Delta t_2$. Thus, $A\Delta f(t)_1^2 \Delta t_1 = A\Delta f(t)_2^2 \frac{\Delta t_2^2}{\Delta t_1}$, which is the contribution to the correlation by the perturbation $\Delta f(t)_1$, the contribution by $\Delta f(t)_2$ being $A\Delta f(t_2)^2 \Delta t_2$. If $\Delta f(t)_1 > \Delta f(t)_2$, then $\Delta t_1 < \Delta t_2$. The ratio of the contributions becomes

$$\frac{A\Delta f(t)_1^2 \Delta t_1}{A\Delta f(t)_2^2 \Delta t_2} = \frac{\Delta t_2}{\Delta t_1} > 1 \quad . \tag{D-93}$$

Therefore, the larger perturbations are more heavily weighted in the covariance computation even though they exist for a shorter duration.

Equation (D-92) states that the space-time covariance of temporal signals is related to the probability density distribution through the square of the signal from the mean.

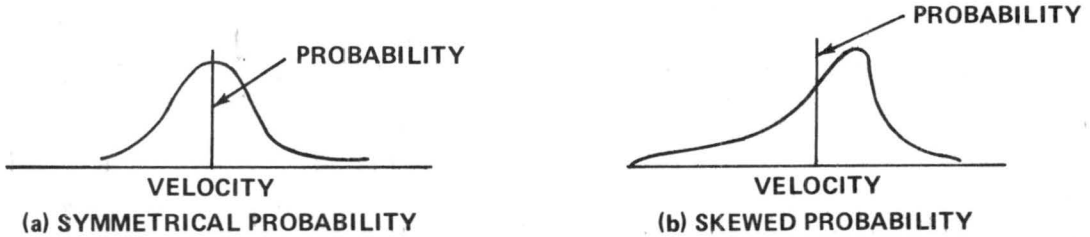

(a) SYMMETRICAL PROBABILITY

(b) SKEWED PROBABILITY

Therefore, there is a weighting of the wings of the probability distribution. If the probability of the velocity distribution is symmetrical, speeds moving faster than the mean velocity are weighted equally to those of a lesser velocity. The correlation would then build equally at the corresponding time delays, the average value being the mean velocity indicated by the mean value of the probability density distribution. If, however, the velocity distribution is skewed (Fig. (b) above), the longer wing is weighted much more heavily. The covariance would indicated a speed commensurate with those associated with the long wing.

Therefore, either natural skewness of the distribution or the effects of two separate flows would give an indication of a velocity other than the mean. Intermittency of the boundary layer is just such a situation. In the outer poriton of the boundary layer, the model presented indicates that wave packets propagate to the outer region and are travelling well below the mean velocity. These wave packets are then the tails of the probability curve. The velocity measured from the space-time covariance calculation would indicate the packet's speed rather than the mean velocity, as indicated above. In fact, there appears to be no reason at this time to expect the measured convective velocity to be near the mean velocity except at the point of production where the probability distribution will be symmetrical and at the location where the turbulent packets are in equilibrium with the surrounding flow.

G. Conclusions

The values which determine the mean statistical averages of a signal are eliminated from covariance computations, and thus the ability to measure mean values is coincident, rising from the shape of the probability distribution. Eddy motion and intermittency both affect the shape of the distribution and thus affect the measured value of convective velocity.

George C. Marshall Space Flight Center
National Aeronautics and Space Administration
Marshall Space Flight Center, Alabama, March 30, 1973

REFERENCES

1. Klebanoff, P.S.: Characteristics of Turbulence in a Boundary Layer with Zero Pressure Gradient. NACA Report 1247, 1954.

2. Kline, S.J.; Reynolds, W.C.; Schraub, F.A.; and Rundstadler, P.W.: The Structure of Turbulent Boundary Layers. JFM, vol. 30, part 4, 1967, pp. 741-773.

3. Grant, H.L.: The Large Eddies of Turbulent Motion. JFM, part 2, June 1958, pp. 149-190.

4. Taylor, G.I.: The Spectrum of Turbulence. Proceedings of the Royal Society, A, vol. CLXIV, 1938, pp. 476-90.

5. Comte-Bellot, G.; and Corrsin, S.: Simple Eulerian Time Correlation of Full and Narrow-Band Velocity Signals in Grid-Generated "Isotropic" Turbulence. JFM, vol. 48, part 2, 1971, pp. 273-337.

6. Wills, J.A.B.: On Convective Velocities in Turbulent Shear Flows. JFM, vol. 20, part 3, 1964, pp. 417-432.

7. Wills, J.A.B.: Convective Velocities in a Viscous Sublayer. NPL AERO Report 1251, November 1967.

8. Wills, J.A.B.: On Convective Velocities in Turbulent Shear Flows. NPL AERO Report 1050, January 1963.

9. Wills, J.A.B.: Measurements of the Wave-Number/Phase Velocity Spectrum of Wall Pressure Beneath a Turbulent Boundary Layer. JFM, vol. 45, part 1, 1970, pp. 65-90.

10. Favre, A.; Gaviglio, J.; and Dumas, R.: Some Measurements of Time and Space Correlation in a Wind Tunnel. NACA TM 1370, February 1955.

11. Favre, A.J.; Gaviglio, J.J.; and Dumas, R.: Space-time Correlations and Spectra in a Turbulent Boundary Layer. JFM, part 3, May 1957, pp. 313-342.

12. Favre, A.J.; Gaviglio, J.J.; and Dumas, R.J.: Further Space-Time Correlations of Velocity in a Turbulent Boundary Layer. JFM, part 3, December 1957, pp. 344-356.

13. Favre, A.; and Gaviglio, J.: Spectral Distributions of Space Time Correlations of Speed in the Case of a Turbulent Boundary Layer. Office National D'Etudes et de Recherches Aerospatiales, Paris, France, 1964.

14. Dumas, R.; Favre, A.; and Gaviglio, J.: Structure of Velocity Space-Time Correlations in a Boundary Layer. Physics of Fluids, vol. 10, part 2, 1967, pp. s138-s145.

REFERENCES (Continued)

15. Dumas, R.; Favre, A.; and Verollet, E.: Celerities of Temperature and Velocity Turbulent Fluctuations in a Boundary Layer. Presented at the 12th International Congress of Applied Mechanics, Stanford, California, August, 1968, pp. 26-31.

16. Reynolds, Osborn.: On the Dynamical Theory of Incompressible Viscous Fluids and the Determination of the Criteria. Phil. Trans. Royal Society, vol. 186, 1895, pp. 123-164.

17. Taylor, G.I.: Eddy Motion in the Atmosphere. Phil. Trans. of the Royal Society, A, vol. CCSV, 1915, pp. 1-26.

18. Taylor, G.I.: Observations and Speculations on the Nature of Turbulent Motion. Reports & Memoranda of the Advisory Committee for Aeronautics, No. 345, 1917.

19. Taylor, G.I.: On the Dissipation of Eddies. Reports & Memoranda of the Advisory Committee for Aeronautics, No. 598, 1918.

20. Taylor, G.I.: Diffusion by Continuous Movements. Proceedings of the London Mathematical Society, ser. 2, vol. XX, 1921, pp. 196-212.

21. Taylor, G.I.: The Decay of Eddies in a Fluid. Paper written for the Aeronautical Research Committee, 1923.

22. Taylor, G.I.: Effect of Variation in Density on the Stability of Superposed Streams of Fluid. Proceedings of the Royal Society, A, vol. CXXXII, 1931, pp. 499-523.

23. Taylor, G.I.: Statistical Theory of Turbulence, Part I. Proceedings of the Royal Society, A, vol. CLI, 1935, pp. 421-44.

24. Taylor, G.I.: Statistical Theory of Turbulence, Part II. Proceedings of the Royal Society, A, vol. CLI, 1935, pp. 444-54.

25. Taylor, G.I.: Statistical Theory of Turbulence, Part III: Distribution of Dissipation of Energy in a Pipe over Its Cross-Section. Proceedings of the Royal Society, A, vol. CLI, 1935, pp. 455-64.

26. Taylor, G.I.: Statistical Theory of Turbulence, Part IV: Diffusion in a Turbulent Air Stream. Proceedings of the Royal Society, A, vol. CLI, 1935, pp. 465-78.

27. Taylor, G.I.: Statistical Theory of Turbulence, Part V: Effect of Turbulence on Boundary Layer, and Theoretical Discussion of Relationship Between Scale of Turbulence and Critical Resistance of Spheres. Proceedings of the Royal Society, A, vol. CLVI, 1936, pp. 307-17.

REFERENCES (Continued)

28. Dryden, H.L.; Schubauer, G.B.; Mock, W.C.; and Skramstad, H.K.: Measurements of Intensity and Scale of Wind Tunnel Turbulence and Their Relation to the Critical Reynold's Number of Spheres. NACA Report 581, 1937.

29. Townsend, A.A.: The Measurement of Double and Triple Correlation Derivatives in Isotropic Turbulence. Proceedings of the Cambridge Philosophical Society, vol. 43, part 4, October 1947, pp. 560-570.

30. Batchelor, K.G.: Kolmogoroff's Theory of Locally Isotropic Turbulence. Proceedings of the Cambridge Philosophical Society, vol. 43, 1947, pp. 533-559.

31. Van Atta, C.W.; and Chen, W.Y.: Correlation Measurements in Grid Turbulence Using Digital Harmonic Analysis. JFM, vol. 34, part 3, 1968, pp. 497-515.

32. Snyder, W.H.; and Lumley, J.L.: Some Measurement of Particle Velocity Autocorrelation Functions in a Turbulent Flow. JFM, vol. 48, part 1, 1917, pp. 41-71.

33. Kline, S.J.: Observed Structure Features in Turbulent and Transitional Boundary Layers. In Fluid Mechanics of Internal Flow, ed. by G. Sovran, Elsevier Publishing Co., 1967, pp. 27-68.

34. Kibens, V.; and Kovasznay, L.S.G.: The Intermittent Region of a Turbulent Boundary Layer. Department of Mechanics, The Johns Hopkins University, Baltimore, Maryland, Report No. 1, 1969, U.S. Army, DA-31-124-ARO-D-313.

35. Kuo, A.Y.: Experiments on the Internal Intermittency in Turbulent Flow. Dissertation, Department of Mechanics, The Johns Hopkins University, Baltimore, Maryland, April 1970.

36. Corrsin, S.J.; and Kistler, A.L.: Free-Stream Boundaries of Turbulent Flows. NACA Report 1244, 1954.

37. Fiedler, H.; and Head, M.R.: Intermittency Measurements in the Turbulent Boundary Layer. JFM, vol. 25, part 4, 1966. pp. 719-735.

38. Sandborn, V.A.: Measurement of Intermittency of Turbulent Motion in a Boundary Layer. JFM, vol. 6, part 2, 1959, pp. 221-40.

39. Roa, K.N.; Narasimha, R.; and Narayanan, M.A.B.: The 'Bursting' Phenomenon in a Turbulent Boundary Layer. JFM, vol. 48, part 2, 1971, pp. 339-352.

40. Corino, E.R.; and Brodkey, R.S.: A Visual Investigation of the Wall Region in Turbulent Flow. JFM, vol. 37, part 1, 1969, pp. 1-36.

REFERENCES (Continued)

41. Tu, B.J.; and Willmarth, W.W.: Structures of Turbulence in the Boundary Layer near the Wall. Physics of Fluids, vol. 10, part 2, 1967, pp. S134-S137.

42. Kovasznay, L.S.G.: The Turbulent Boundary Layer. In Annual Review of Fluid Mechanics, ed. by M. V. Dyke, W. G. Vincenti, and J.V. Weh, vol. 2, 1970, pp. 95-112.

43. Kovasznay, L.S.G.; and Nee, V.W.: Simple Phenomenological Theory of Turbulent Shear Flows. Physics of Fluids, vol. 12, 1969, pp. 473-484.

44. Kim, H.T.; Kline, S.J.; and Reynolds, W.C.: An Experimental Study of Turbulence Production near a Smooth Wall in a Turbulent Boundary Layer with Zero Pressure Gradient. Stanford University, Thermosciences Division, Report MD-20, January 1968.

45. Batchelor, G.K.: The Dynamics of Homogeneous Turbulence. In the Mechanics of Turbulence, Gordon & Breach Science Publishers, New York, 1964, pp. 85-97.

46. Wygnanski, I.; and Fiedler, H.E.: The Two-Dimensional Mixing Region. JFM, vol. 41, part 2, 1970, pp. 327-361.

47. Kovasznay, L.S.G.; Kibens, V.; and Blackwelder, R.F.: Large-Scale Motion in the Intermittent Region of a Turbulent Boundary Layer. JFM, vol. 41, part 2, 1970, pp. 283-325.

48. Corcos, G.M.: The Structure of the Turbulent Pressure Field in Boundary-Layer Flows. JFM, part 3, March 1964, pp. 353-379.

49. Bradshaw, P.: 'Inactive' Motion and Pressure Fluctuations in Turbulent Boundary Layers. JFM, vol. 30, part 2, 1967, pp. 241-258.

50. Blake, W.K.: Turbulent Boundary-Layer Wall-Pressure Fluctuations in Smooth and Rough Walls. JFM, vol. 44, part 4, 1970, pp. 637-660.

51. Willmarth, W.W.; and Roos, F.W.: Resolution and Structure of the Wall Pressure Field beneath a Turbulent Boundary Layer. JFM, vol. 22, part 1, 1965, pp. 81-94.

52. Willmarth, W.W.; and Wooldridge, C.E.: Measurements of the Fluctuating Pressure at the Wall beneath a Thick Turbulent Boundary Layer. JFM, vol. 4, part 2, October 1962, pp. 187-210.

53. Tritton, D.J.: Some New Correlation Measurements in a Turbulent Boundary Layer. JFM, vol. 28, part 3, 1967, pp. 439-462.

REFERENCES (Continued)

54. Kline, S.J.; and Lahey, R.T., Jr.: Representation of Space-Time Velocity and Pressure Fluctuation Correlations by a Tentative Phenomenological Model. Scientific Interim Report, Stanford University, California, 1968.

55. Fisher, M.J.; and Davies, P.O.A.L.: Correlation Measurements in a Non-Frozen Pattern of Turbulence. JFM, part 1, January 1964, pp. 97-117.

56. Sternberg, J.: On the Interpretation of Space-Time Correlation Measurements in Shear Flow. Physics of Fluids, vol. 10, part 2, pp. 5146-5152.

57. Bull, M.K.: Space Time Correlations of the Boundary Layer Pressure Field in Narrow Frequency Bands. Technical Report, January 1960 – November 1961, Wright Patterson AFB, Ohio, AF Flight Dynamics Lab, November 1963.

58. Poreh, M.: Accelerations, Turbulent Trajectories and Space Time Correlations in Turbulent Shear Flow. Israel Journal of Technology, vol. 6, 1968, pp. 95-100.

59. Laufer, J.; and Narayanan, M.A.B.: Mean Period of the Turbulent Production Mechanism in a Boundary Layer. Physics of Fluids, vol. 14, no. 1, January 1971, pp. 182-183.

60. Cliff, W.C.: Visualization of Turbulent Mixing, Master's Thesis, Colorado State University, 1968.

61. Weber, H.E.: Turbulent and Transition Boundary Layer Based on Mixing Length and Intermittency. General Electric Co., Philadelphia, Pennsylvania, June 1967.

62. Sabersky, R.H.; and Acosta, A.J.: Fluid Flow. The Macmillan Company, New York, 1964, p. 144.

63. Kamke, E.: Differentialgleichungen Lösungsmethoden und Lösungen. Akademische Verlagsgesellschaft, Geest & Portig, vol. 1, 1959, pp. 302, 303.

64. Murphy, G.M.: Ordinary Differential Equations and Their Solutions. D. Van Nostrand Company, Inc., New York, 1960, p. 15.

65. Schlichting, H.: Boundary-Layer Theory. 6th Edition. McGraw-Hill Book Company, New York, 1968, p. 17.

66. Tieleman, H.W.: Viscous Region of Turbulent Boundary Layer. Colorado State University, CER67-68HWT21, December 1967.

67. Zoric, D.L.: Approach of Turbulent Boundary Layer to Similarity. Colorado State University, CER68-69DLZ9, September 1968.

REFERENCES (Concluded)

68. Plate, E.J.; and Cermak, J.E.: Micrometeorological Wind Tunnel Facility, Description & Characteristics. Colorado State University, Report CER63EJP-JEC9, February 1963.

69. Sandborn, V.A.; Tieleman, H.W.; and Liu, C.Y.: The Similarity of Large Scale Turbulent Boundary Layers. Colorado State University, Report CEM68-69VAS-HWT-CYL12, July 1968.

70. Finn, C.L.; and Sandborn, V.A.: The Design of a Constant Temperature Hot-Wire Anemometer. Advances in Hot-Wire Anemometry, Proceedings of the International Symposium on Hot-Wire Anemometry, University of Maryland, March 20-21, 1967.

71. Sandborn, V.A.: Hot Wire Anemometer Measurements in Large-Scale Boundary Layers. Proceedings of the International Symposium on Hot-Wire Anemometry, University of Maryland, March 20-21, 1967.

72. Rotta, J.C.: Critical Review of Existing Methods for Calculating Development of Turbulent Boundary Layers. In Fluid Mechanics of Internal Flow, ed. by G. Sovran, Elsevier Publishing Co., 1967, pp. 80-101.

☆U.S. GOVERNMENT PRINTING OFFICE: 1973-739-153/48